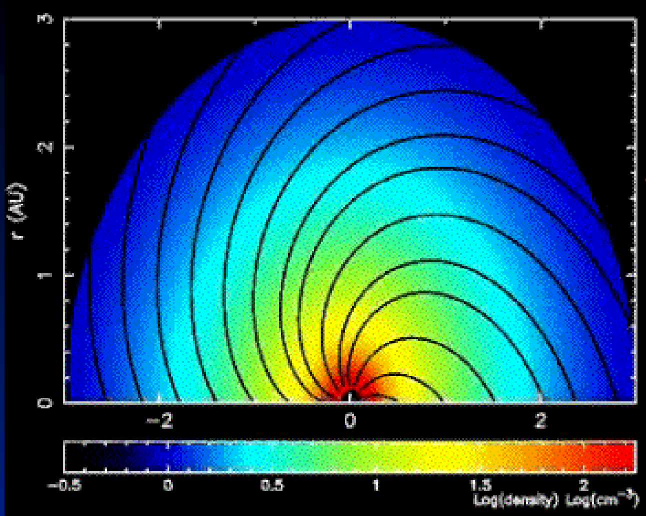

Particle Acceleration in Cosmic Plasmas

G.P. Zank
Institute of Geophysics and Planetary Physics (IGPP)
University of California, Riverside

Gang Li, Vladimir Florinski, Olga Verkhoglyadova Nick Pogorelov, Jacob Heerikhuisen, Kobus le Roux, Garry Webb, Hans Mueller, Brian Wood, Priscilla Frisch, Ian Axford, H. Washimi

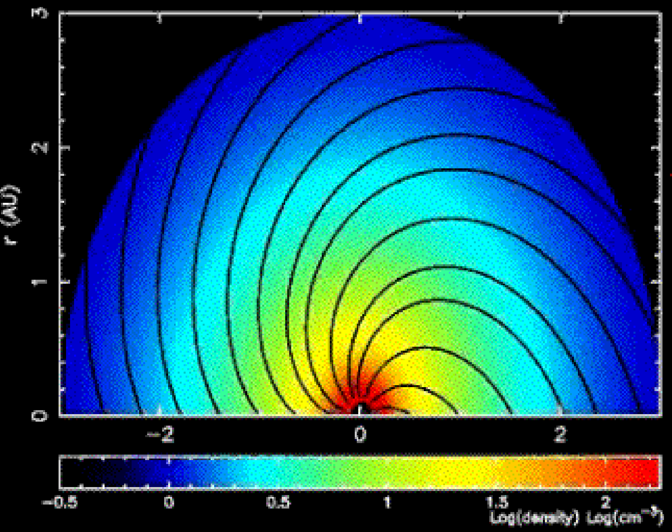

Particle Acceleration in Cosmic Plasmas

Three fundamental questions can be regarded as motivating this work:

1. *Explain the origin of energetic particle power-law spectra (e.g., the galactic cosmic ray spectrum).*
2. *Understand the origin and evolution of matter throughout the galaxy and universe.*
3. *Understand the origin of energetic particles at the Sun and their impact on the geospace environment.*

1. Explain the origin of energetic particle power law spectra (e.g., the universal galactic cosmic ray spectrum).

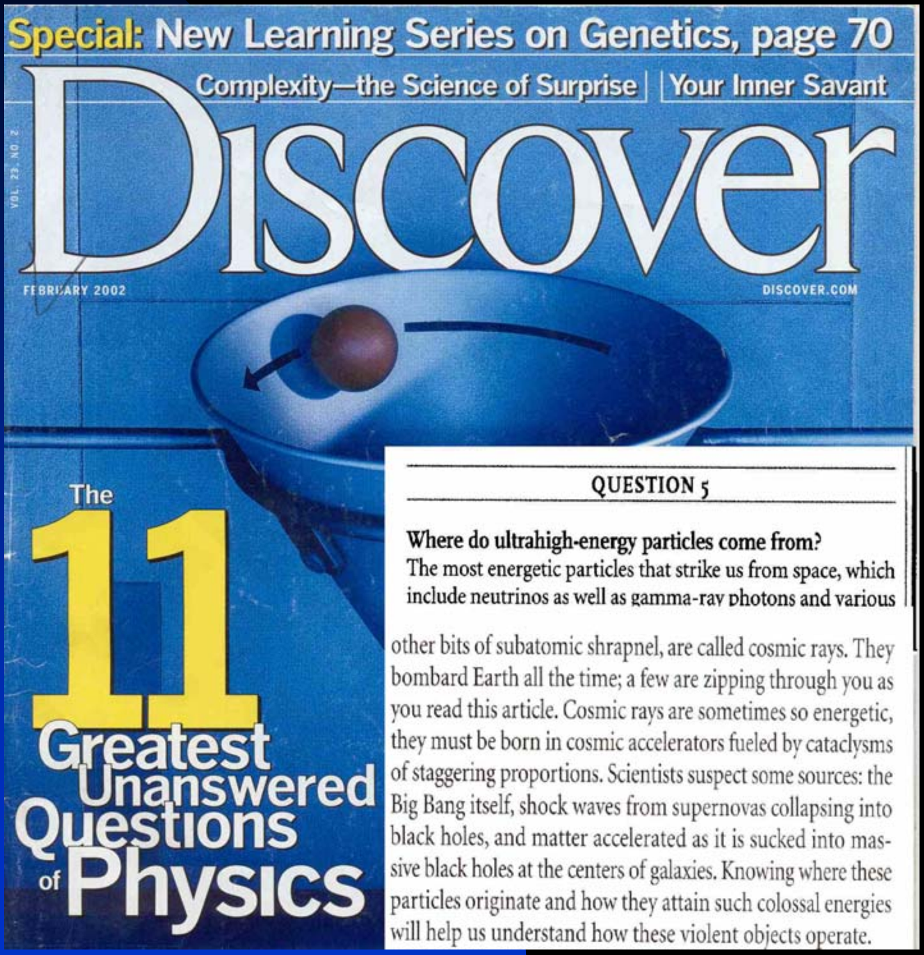

QUESTION 5

Where do ultrahigh-energy particles come from? The most energetic particles that strike us from space, which include neutrinos as well as gamma-ray photons and various other bits of subatomic shrapnel, are called cosmic rays. They bombard Earth all the time; a few are zipping through you as you read this article. Cosmic rays are sometimes so energetic, they must be born in cosmic accelerators fueled by cataclysms of staggering proportions. Scientists suspect some sources: the Big Bang itself, shock waves from supernovas collapsing into black holes, and matter accelerated as it is sucked into massive black holes at the centers of galaxies. Knowing where these particles originate and how they attain such colossal energies will help us understand how these violent objects operate.

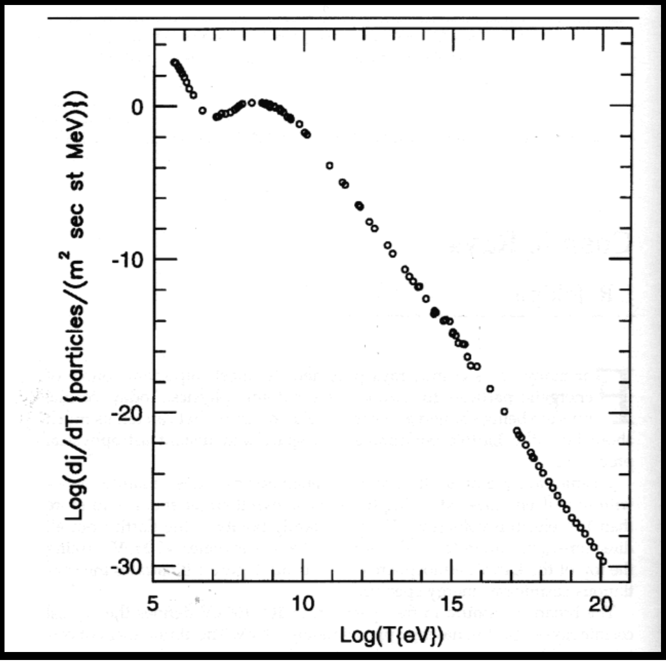

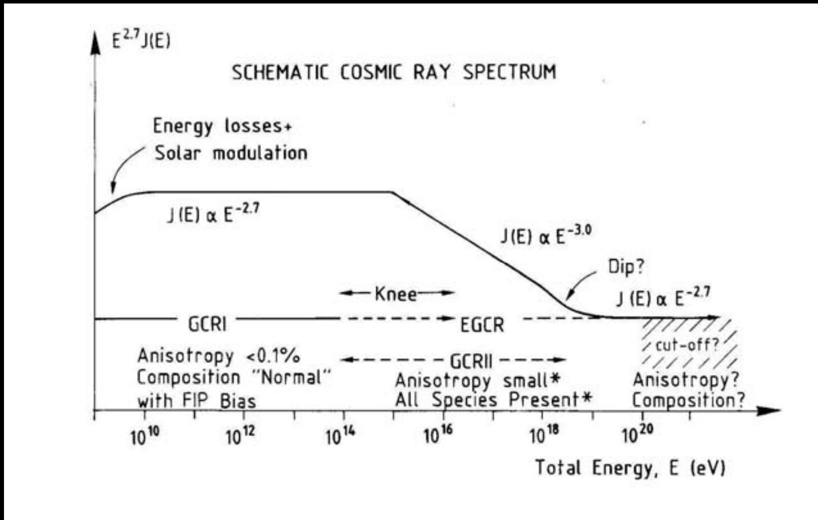

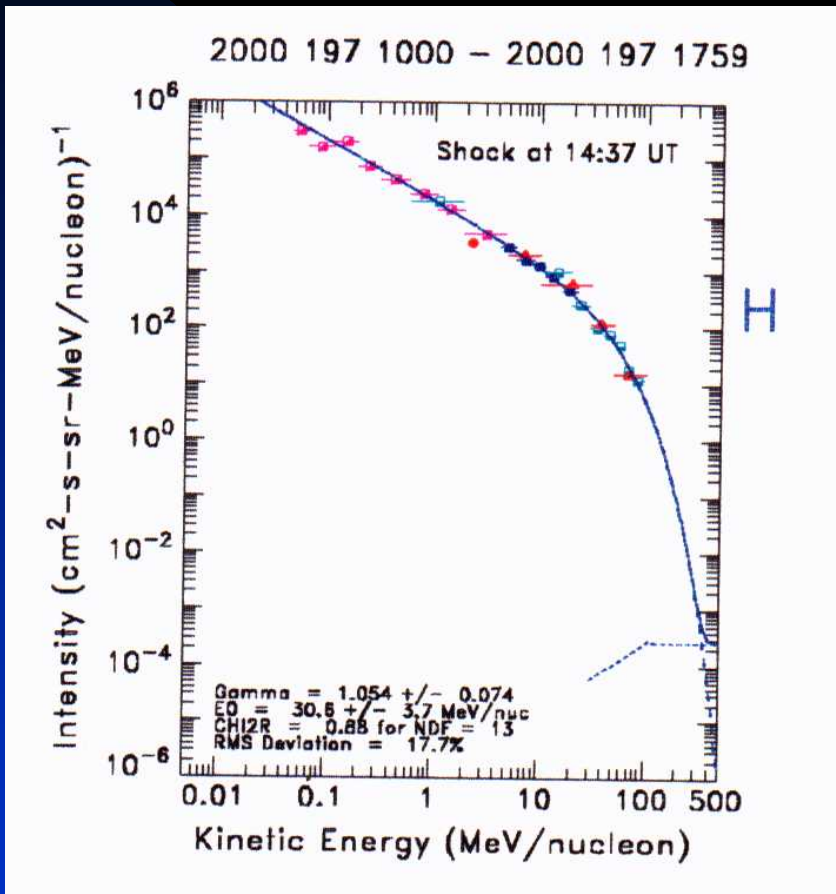

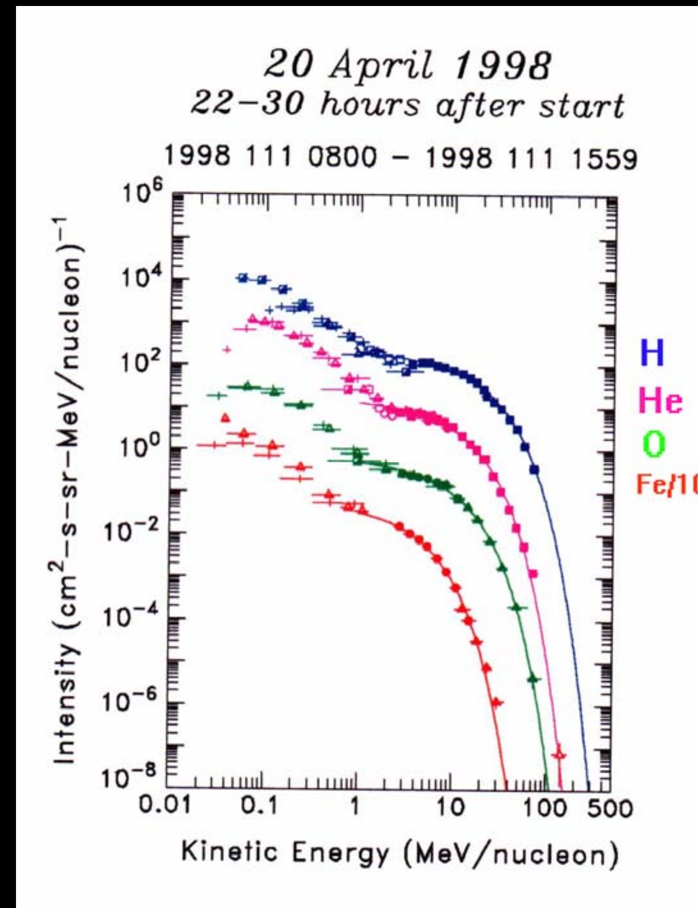

1AU data from WIND and IMP-8
courtesy of A.J. Tylka

2. Understand the origin and evolution of matter throughout the galaxy and universe: energetic particles as probes

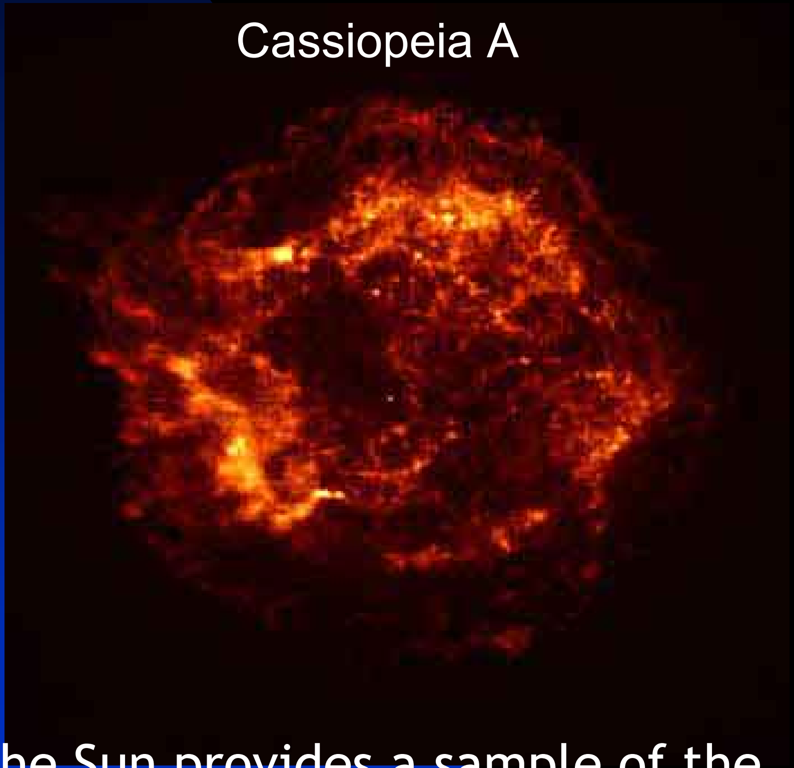

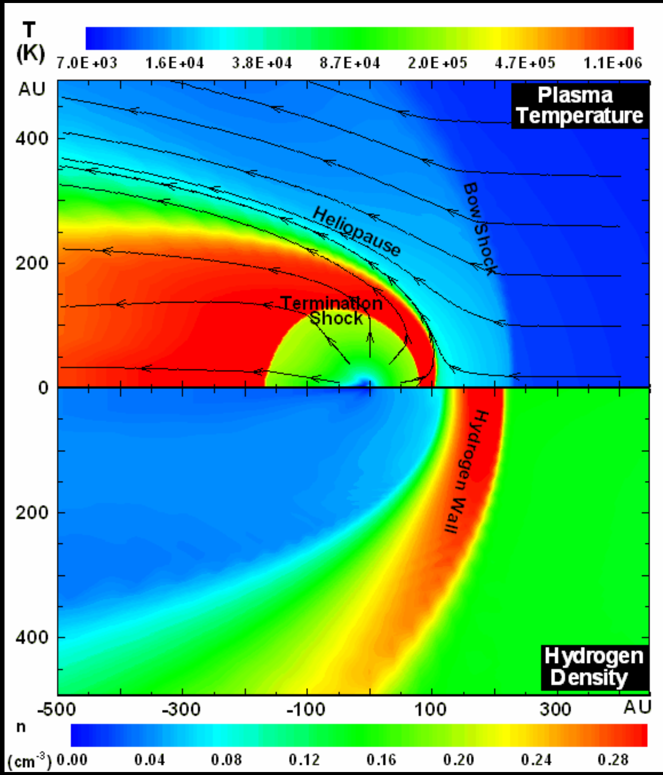

- The Sun provides a sample of the proto-solar nebula
- The Local Interstellar Cloud is a contemporary sample.

- The Sun & LIC are both accessible to in situ studies
- Supernovae provide samples of both stellar and ISM material

3. Understand the origin of energetic particles at the Sun and their impact on the geospace environment.

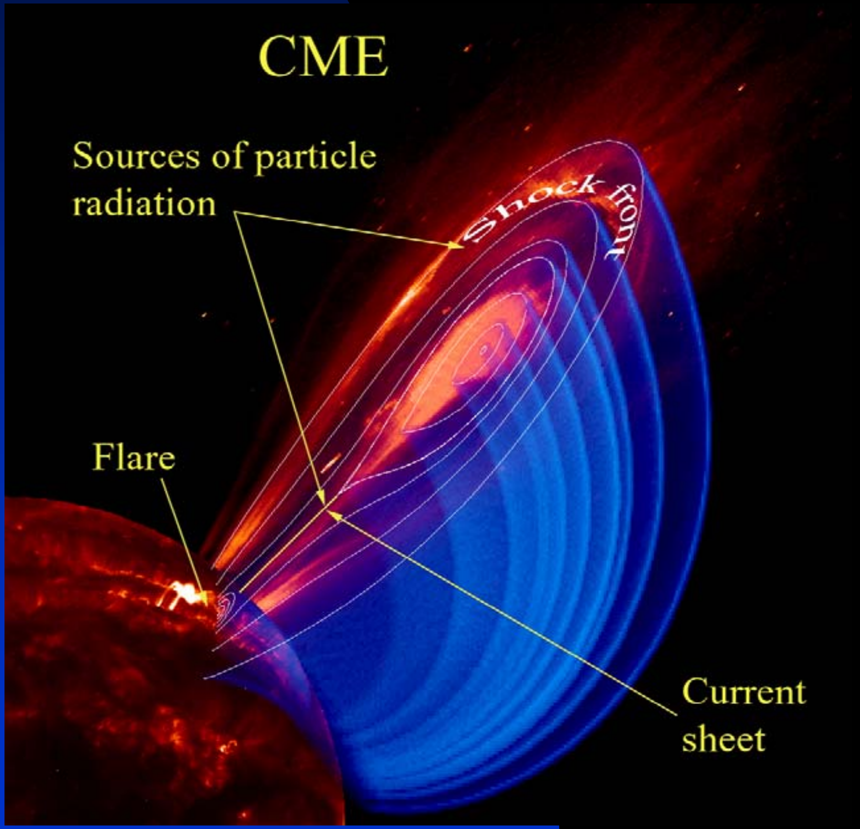

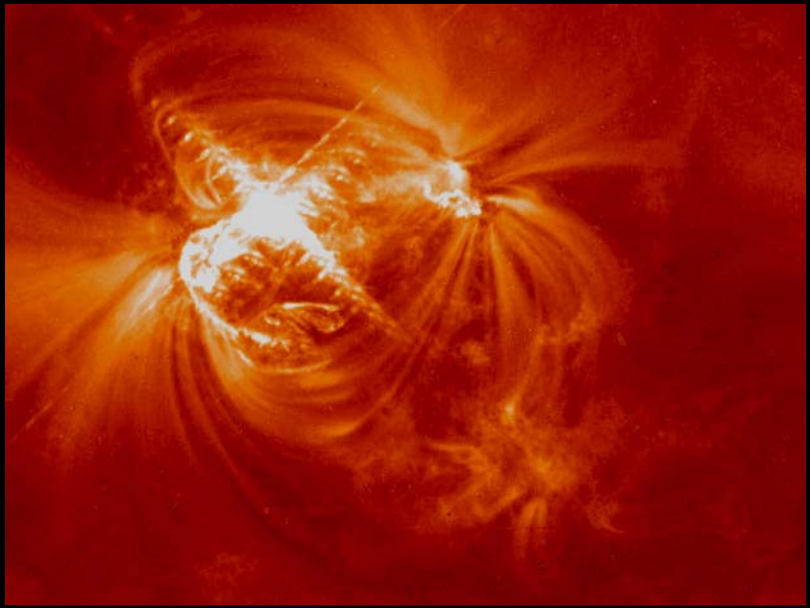

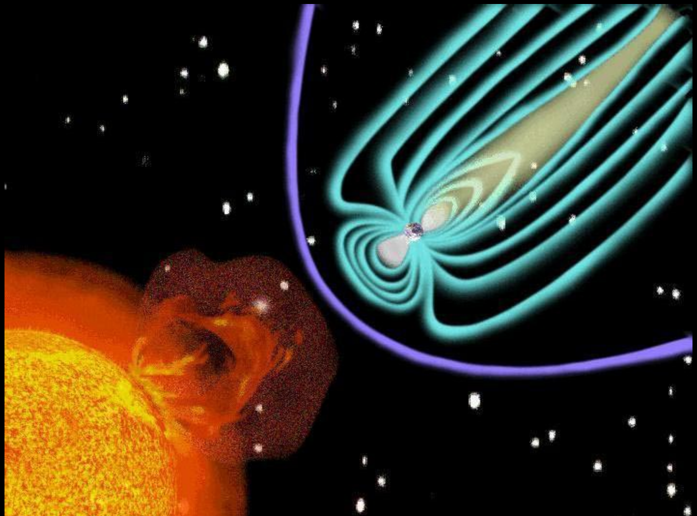

3. Understand the origin of energetic particles at the Sun and their impact on the geospace environment.

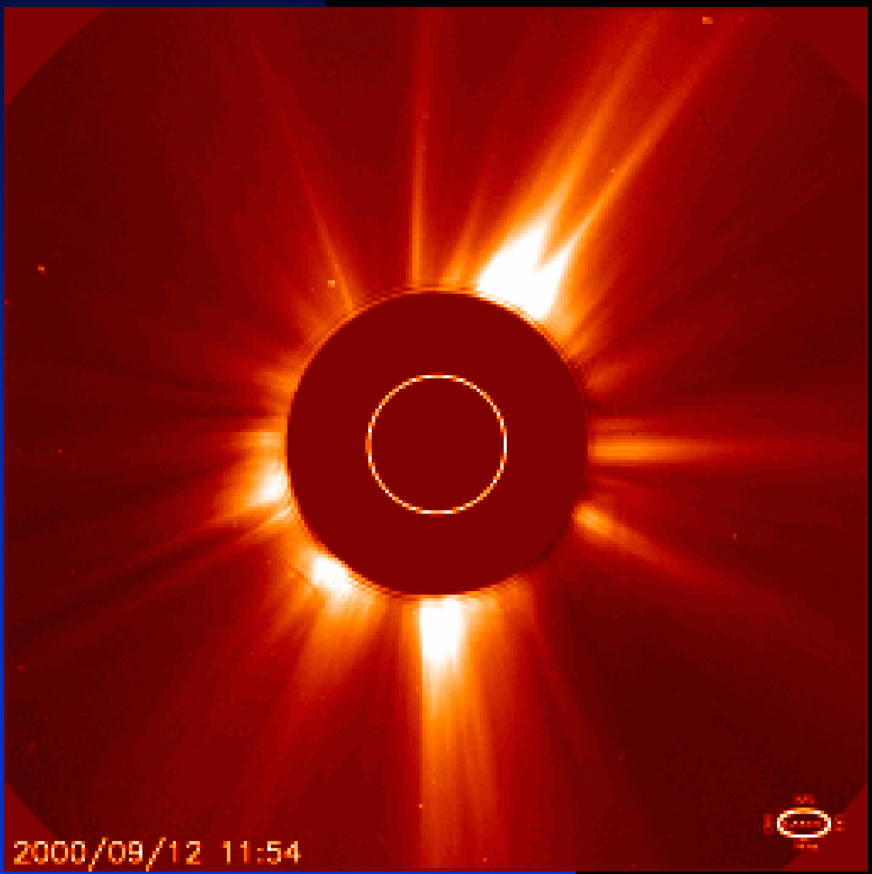

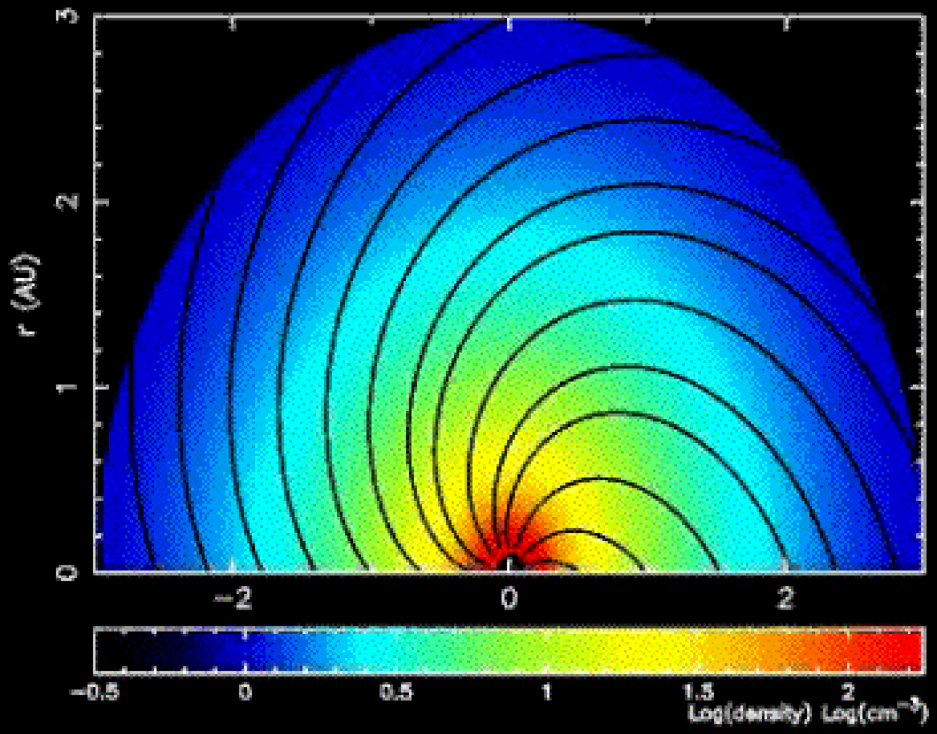

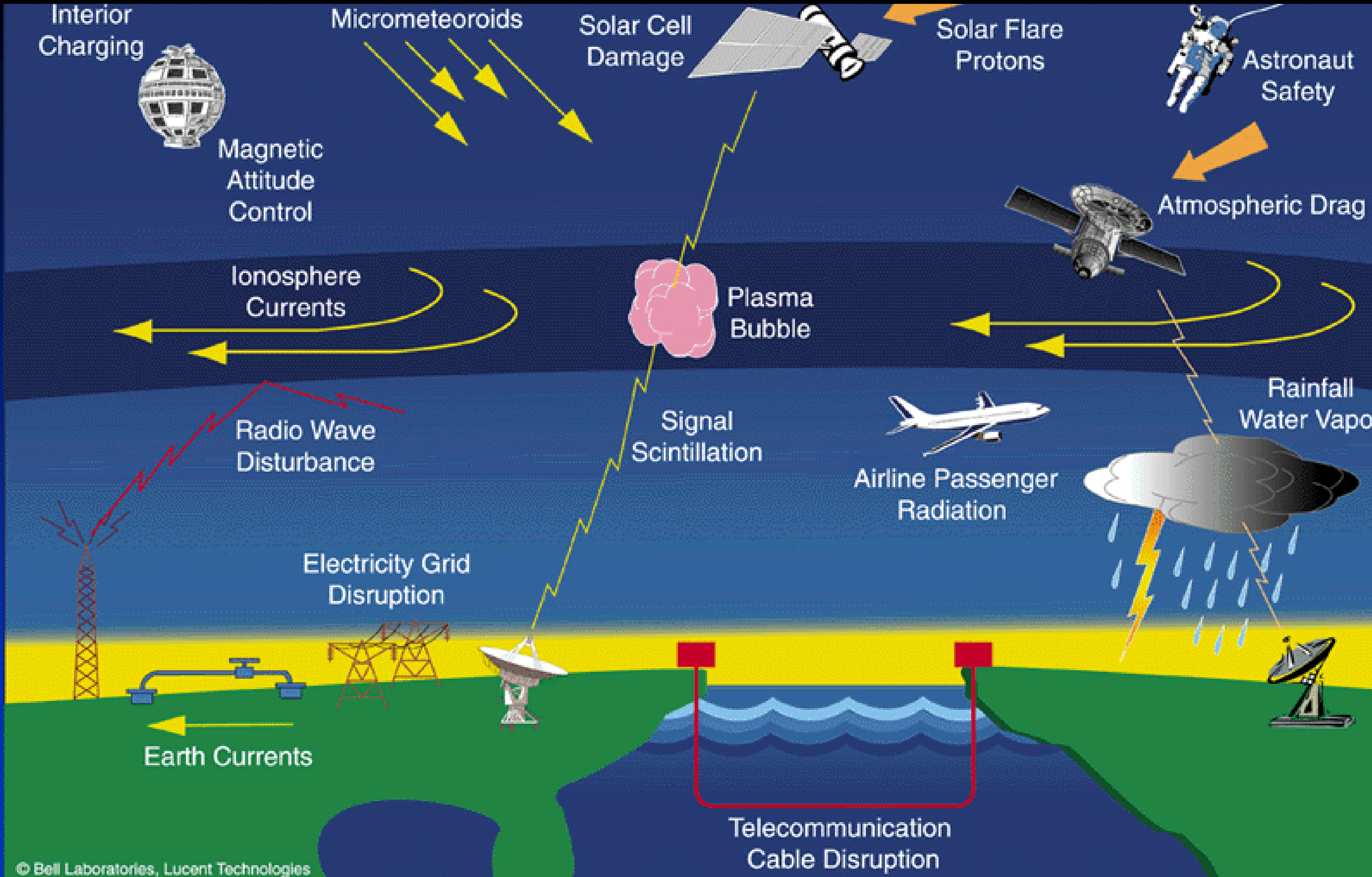
Interior Charging
Micrometeoroids
Solar Cell Damage
Solar Flare Protons
Astronaut Safety
Magnetic Attitude Control
Atmospheric Drag
Ionosphere Currents
Plasma Bubble
Radio Wave Disturbance
Signal Scintillation
Rainfall Water Vapor
Airline Passenger Radiation
Electricity Grid Disruption
Earth Currents
Telecommunication Cable Disruption
© Bell Laboratories, Lucent Technologies

Shock waves and energetic particles: observations

Ground Level Enhancements: 1/20/2005 example

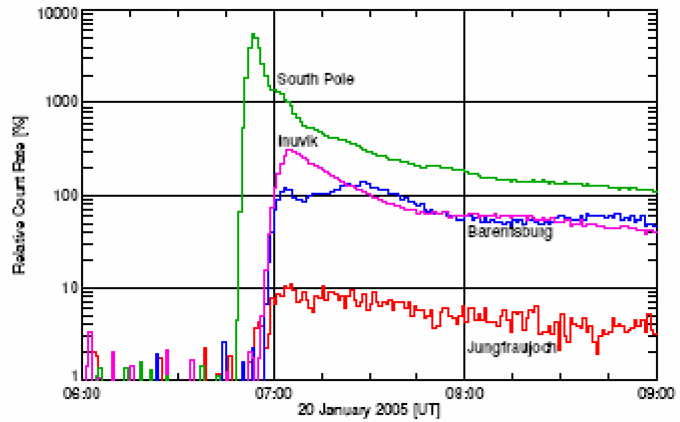

Figure 2. Relative neutron monitor count rates for January 20, 2005, 0600–0900 UT.

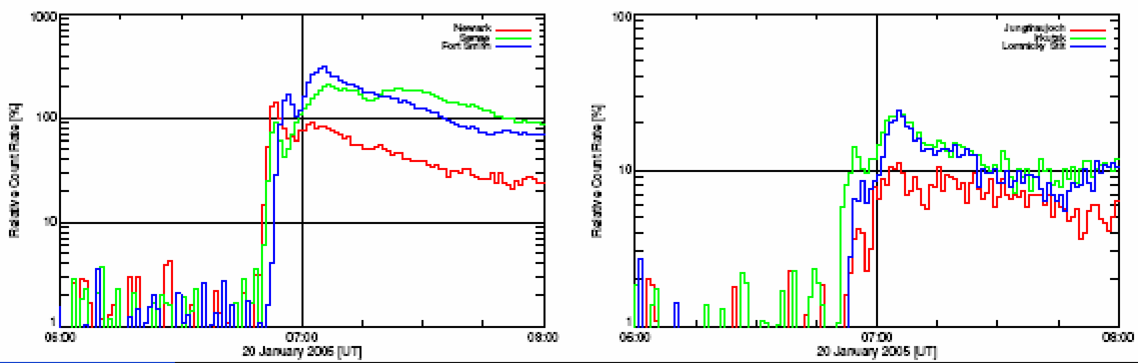

Flares – Coronal Mass Ejections (CMEs) – Energetic particles: A case study 5/13/2005

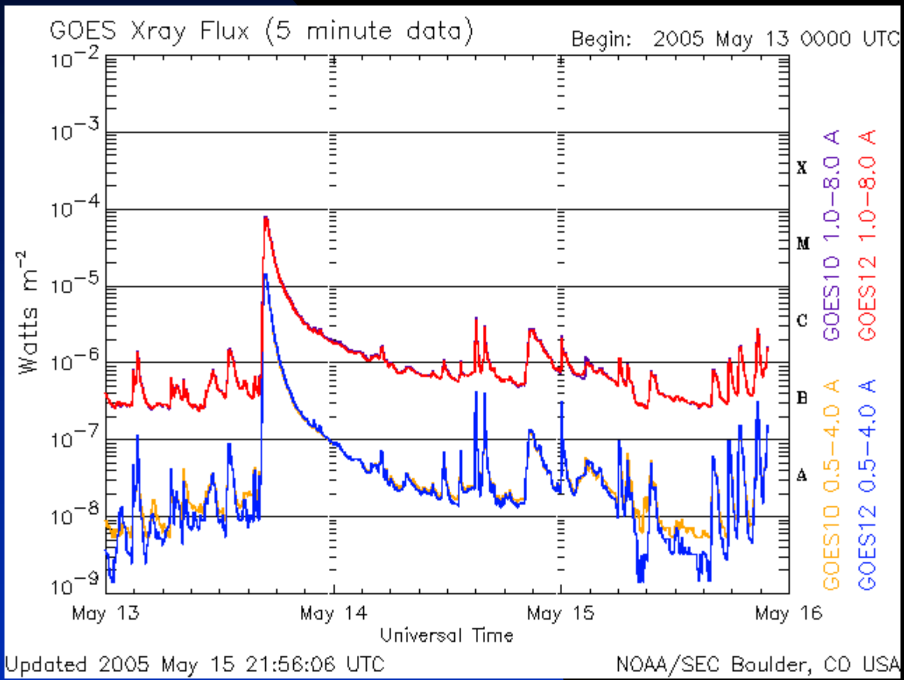

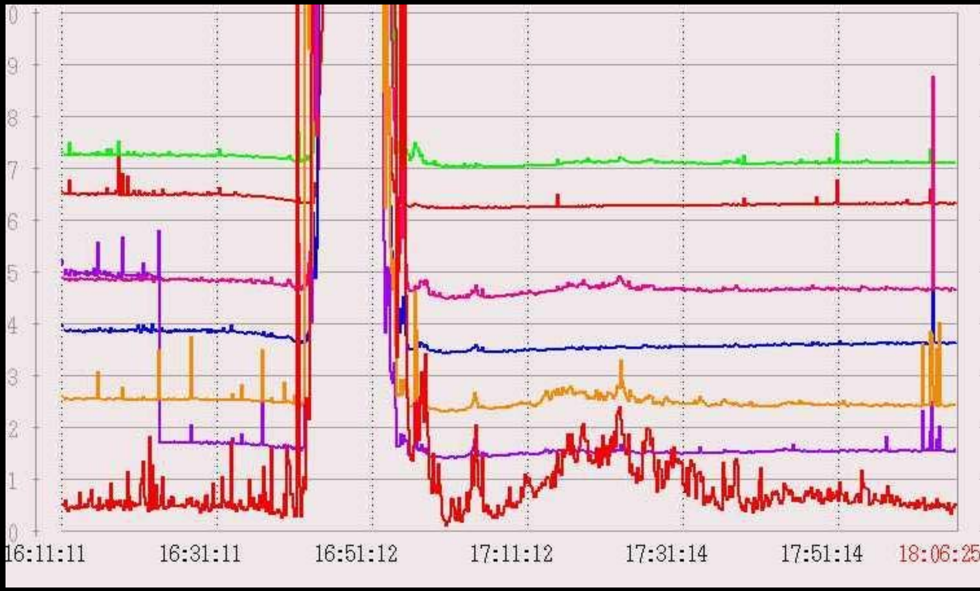

On May 13th, 2005 there was a huge flare on Sun, which produced emissions of various kinds. First the flare was detected in the X-ray (left) and radio range (right) at frequencies between 18 and 28 MHz

A case study 5/13/2005

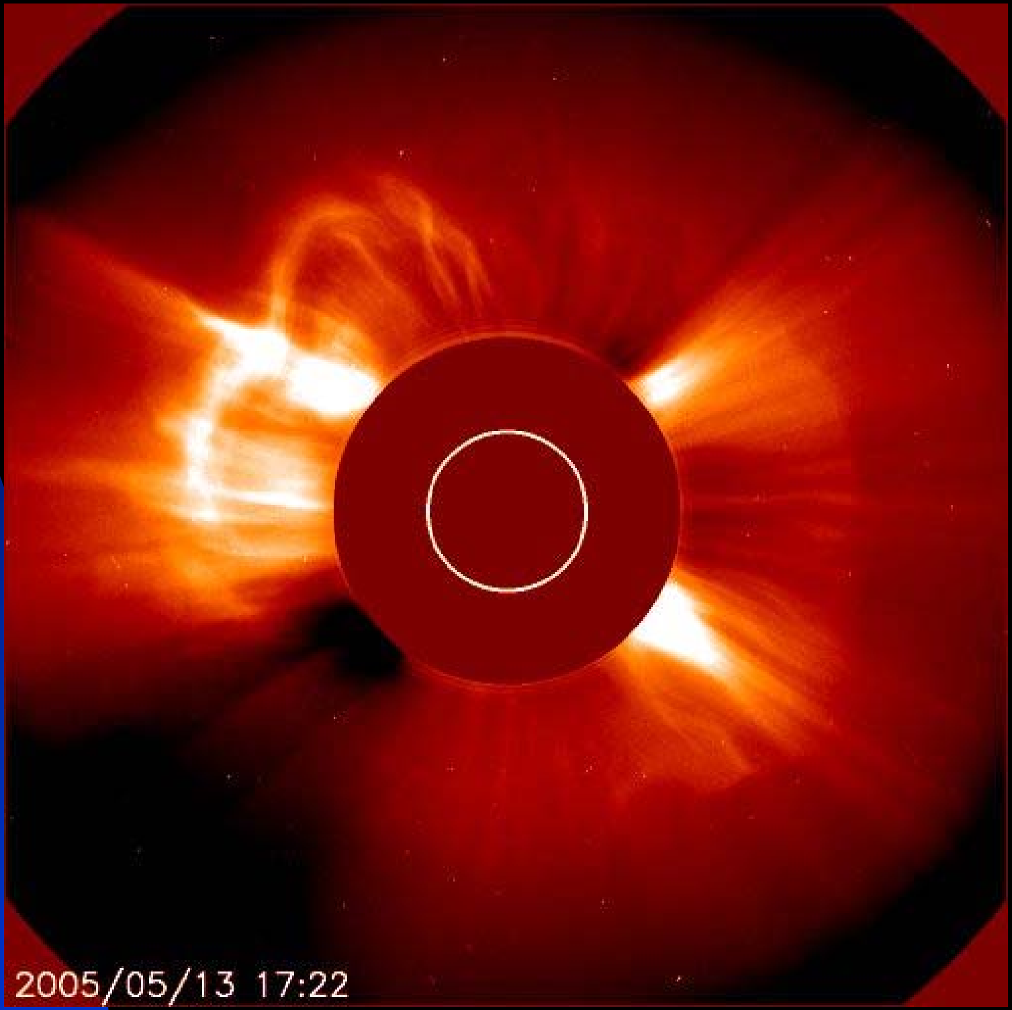

About half an hour later, the Coronal Mass Ejection (CME) was visible in this SOHO image (structures on the left in the image).

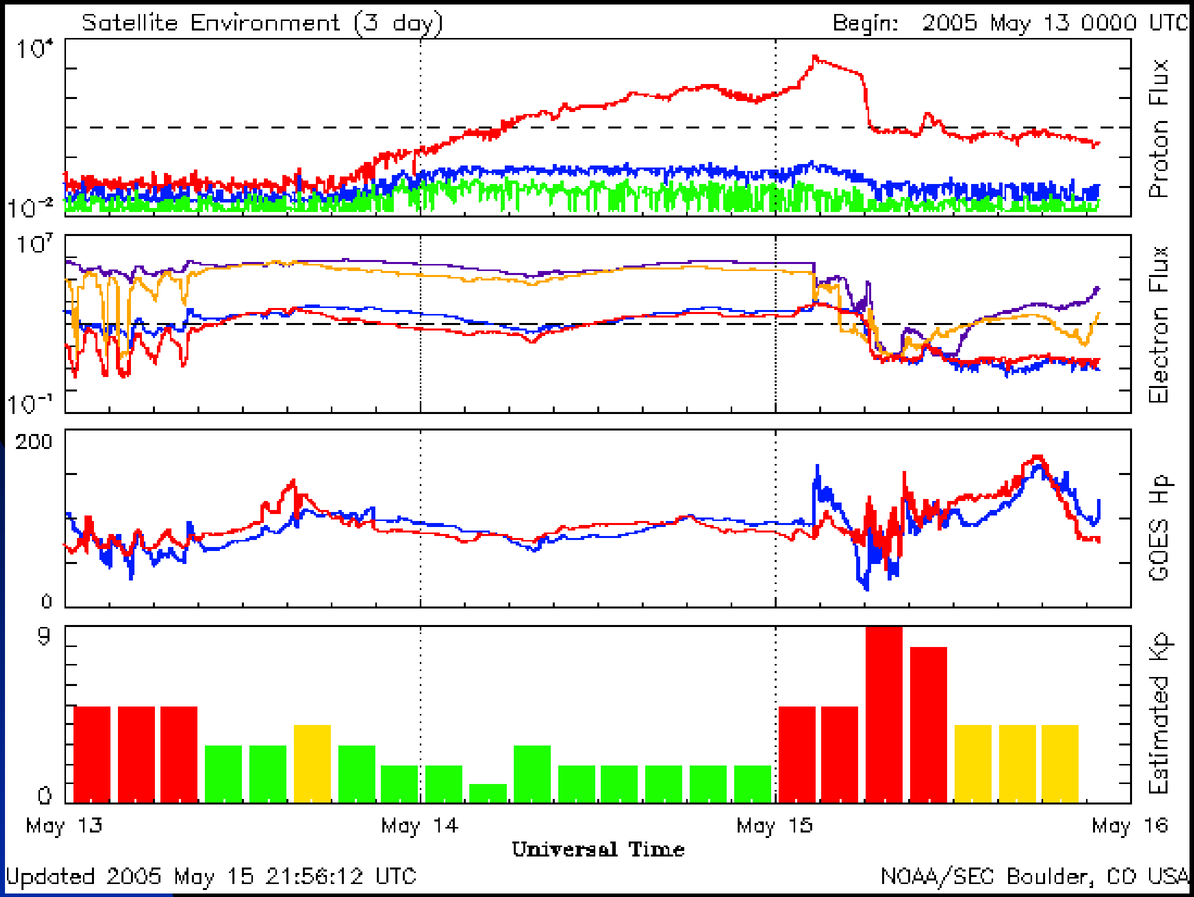

The CME propagated towards the Earth and hit Earth's atmosphere 33 hours later.

The proton and electron flux recorded by the GOES satellites, as well as the magnetic field of Earth recorded by these satellites and the calculated "planetary index" Kp.

When the shock wave hit Earth's atmosphere, the proton flux peaked, the electron flux and of course the magnetic field of Earth became highly distorted. The Aurora was visible at much lower latitudes than usual.

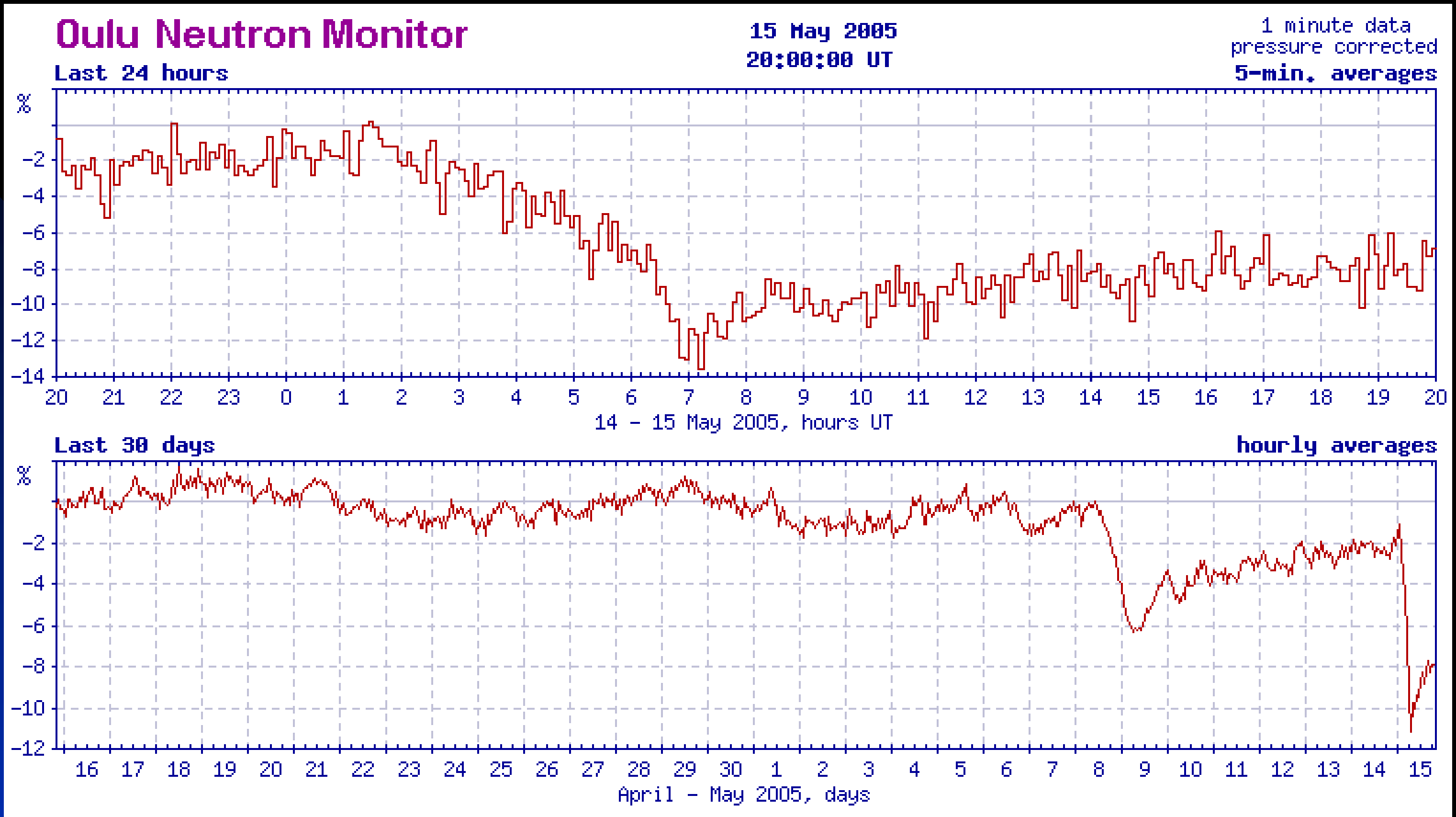

Another side-effect of the CME passing Earth is a decrease in cosmic ray flux or Forbush Decrease – clearly visible in the Oulu Neutron Monitor graph: The magnetic field of the CME deflect the Galactic Cosmic Rays and the secondary particle flux (Neutrons) decreases. Note another Forbush decrease is visible, which was caused by another, not that very powerful flare, which CME passed Earth a few days before this event.

Two Classes of Solar Energetic Particle Events

CME-Associated (Gradual Event)

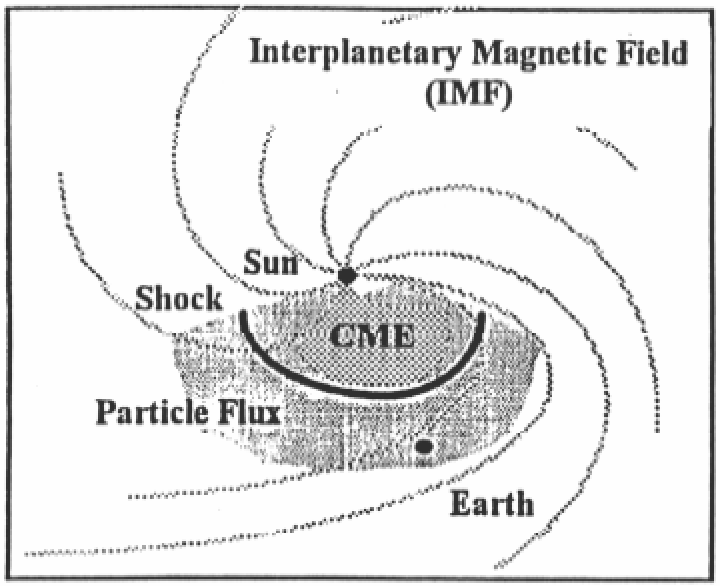

Proton-Rich
Long-Lived (Days)
60-180 Degrees Solar Longitude

Fe/O ≈ 0.1 - 0.2
$^3He/^4He$ ≈ .0004
Q(Fe) ≈ 14
Shocks accelerate solar wind

Impulsive Flare-Associated (Impulsive Event)

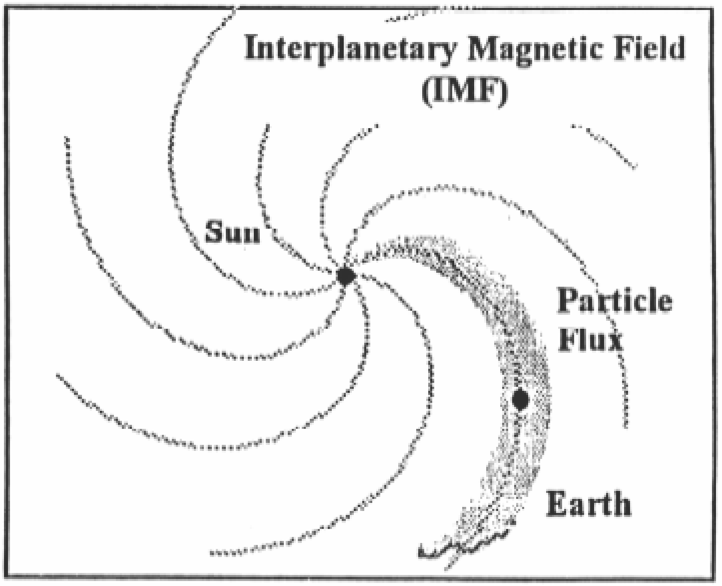

Electron-Rich
Short-Lived (Hours)
30-45 Degrees Solar Longitude

Fe/O ≈ 1
$^3He/^4He$ ≈ 0.1 - 10
Q(Fe) ≈ 20
Heated flare material accelerated

Criteria summarized by Reames (1995)

Basic diffusive shock acceleration theory

2nd-Order Fermi Acceleration: In original model of Enrico Fermi, "magnetic clouds" or "scattering centers," moving randomly, scattered particles. More "head-on" collisions than "overtaking" collisions ensures particle slowly gains energy – slow diffusive gain in energy.

1st-Order Fermi Acceleration: Suppose some agency organizes the scatterers so that, only "head-on" collisions. Energy gain faster - a f*irst-order* process. Shock separates high-speed and a low-speed flow, therefore scattering centers approach one another from each side of the shock. Thus, only head-on collisions. Called Diffusive Shock Acceleration.

Astrophysical shock waves

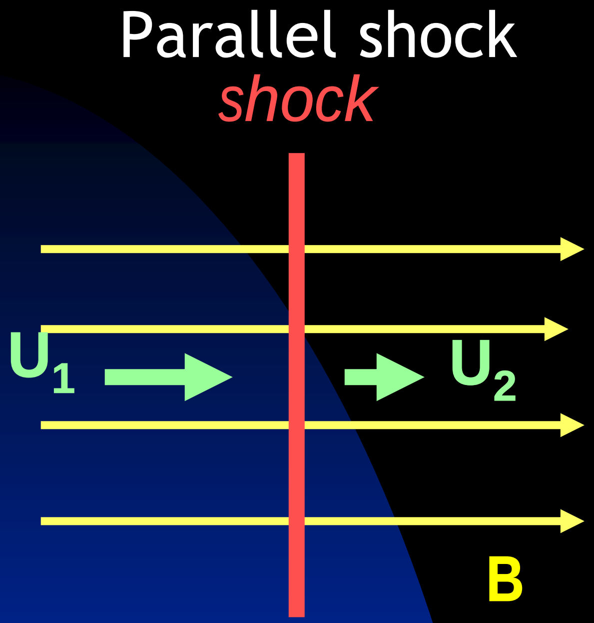

- Acceleration time can be very long.
- Can accelerate thermal-energy particles -- good "injectors"

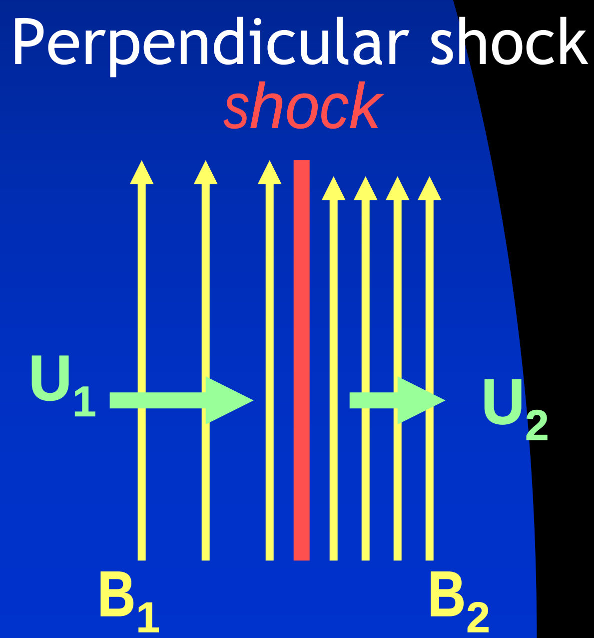

- Acceleration time is very short compared to a parallel shock
- Cannot easily accelerate low energy particles -- poor "injectors"

Diffusive shock acceleration theory: cont.

Start from the cosmic ray transport equation:

$$\frac{\partial f}{\partial t} = -V_{w,i}\frac{\partial f}{\partial x_i} + \frac{\partial}{\partial x_i}\kappa_{ij}\frac{\partial f}{\partial x_j} - V_{D,i}\frac{\partial f}{\partial x_i} + \frac{1}{3}\frac{\partial V_{w,i}}{\partial x_i}\frac{\partial f}{\partial \ln p} + Q$$

convection diffusion drift energy change

Solve the cosmic-ray transport equation for the following geometry

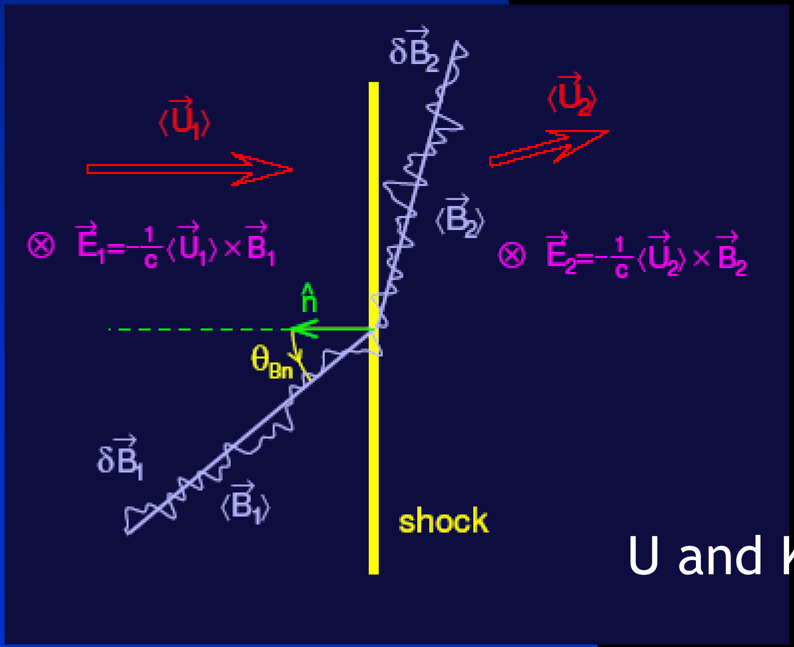

U and K_{xx} change discontinuously across the shock

The steady-state solution for *f(x, p)*, for an infinite system, is given by

$$f(x,p) = \begin{cases} f_0\left(\frac{p}{p_0}\right)^{-\gamma} \exp\left(-U_1|x|/\kappa_{xx,1}(p)\right) & x < 0 \\ f_0\left(\frac{p}{p_0}\right)^{-\gamma} & x \geq 0 \end{cases}$$

where $\gamma = 3U_1/(U_1 - U_2)$

The downstream distribution is a **power law** with a spectral index that depends only on the shock compression ratio!

Diffusive shock acceleration

- The accelerated particle intensities are constant downstream of the shock and exponentially decaying upstream of the shock.
- The scale length of the decay is determined by the momentum dependent diffusion coefficient (steady state solution).

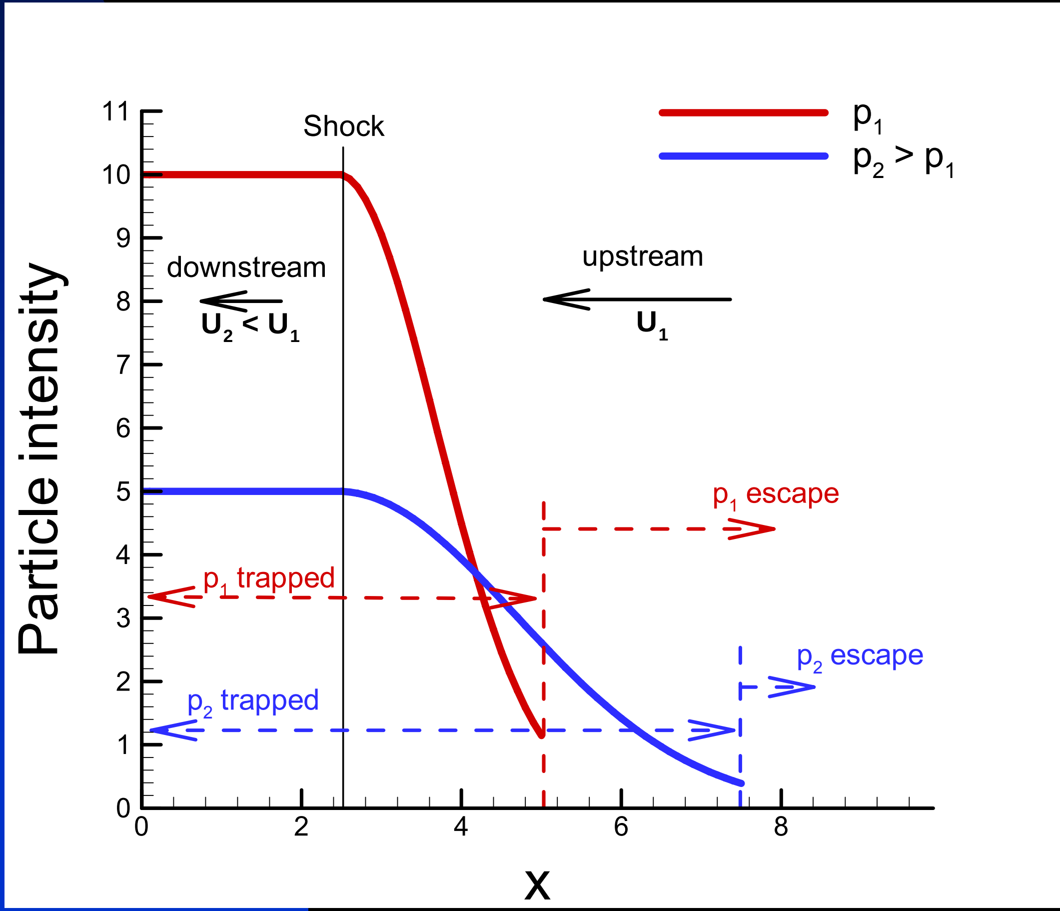

Trapped particles

- convect
- cool
- diffuse.

Escaped particles

- Transport to 1 AU (weak scattering).

The observed quite-time cosmic-ray spectrum

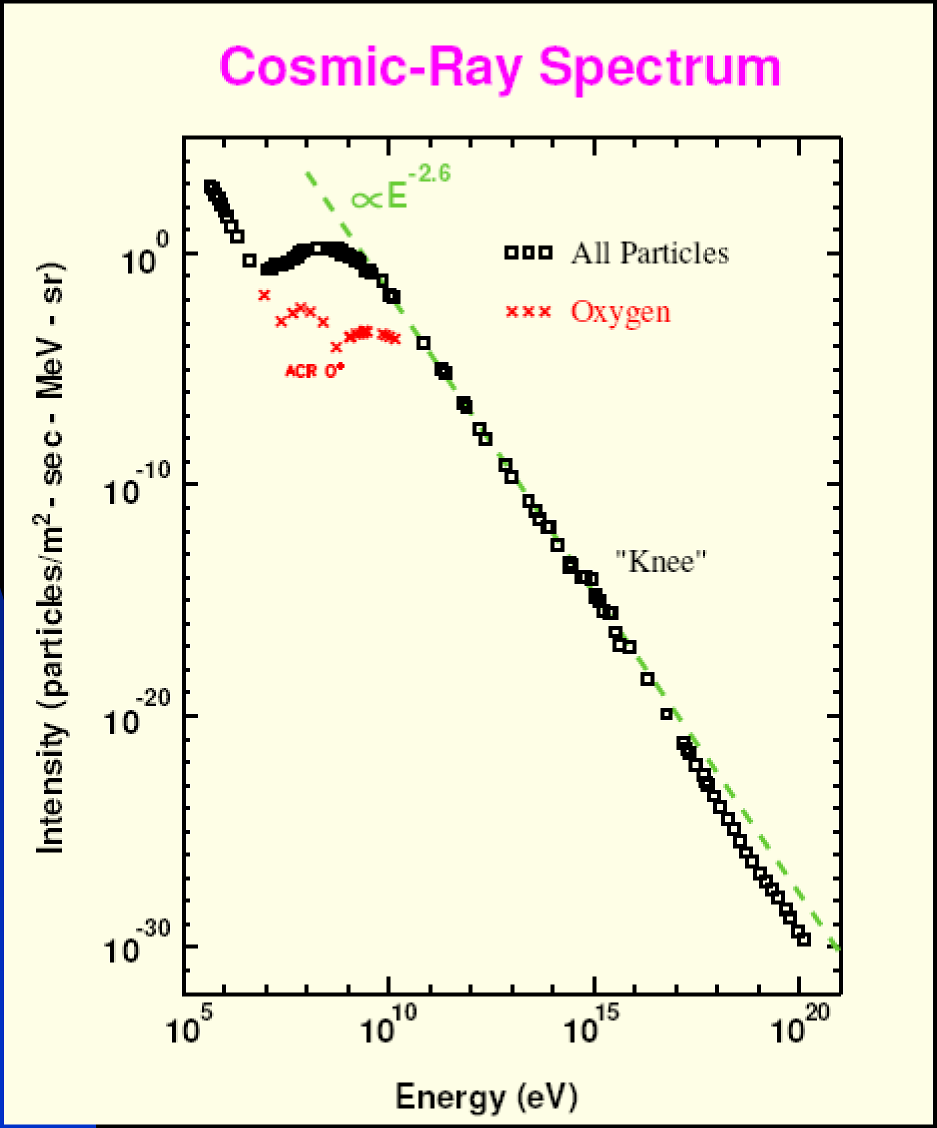

The great success of the simple theory but …
what is the source? Steady-state? ….

Final digression into theory – Alfven wave/turbulent scattering

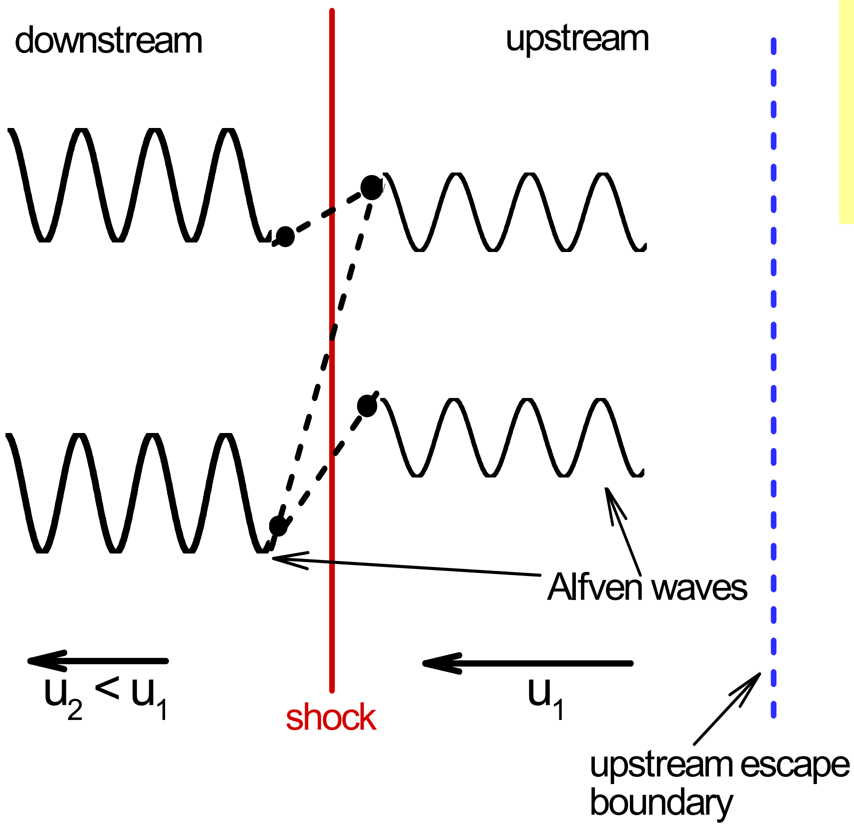

Near the shock front, Alfven waves are responsible for particle scattering. The particle distribution f, and wave energy density A are coupled together through:

$$\frac{\partial A}{\partial t} + u\frac{\partial A}{\partial r} = \Gamma A - \gamma A,$$

$$\frac{\partial f}{\partial t} + u\frac{\partial f}{\partial r} - \frac{p}{3}\frac{\partial u}{\partial r}\frac{\partial f}{\partial p} = \frac{\partial}{\partial r}\left(\kappa\frac{\partial f}{\partial r}\right),$$

$$\kappa(p) = \frac{\kappa_0}{A(k)}\frac{B_0}{B}\frac{(p/p_0)^2}{\sqrt{(m_p c/p_0)^2 + (p/p_0)^2}},$$

$$\kappa_0 = \frac{4}{3\pi} r_{g0} c = \frac{4}{3\pi}\frac{p_0 c}{e B_0},$$

Gordon et al., 1999 used to evaluate wave intensity. P_max, N_inj, p_inj, s, etc. Bohm limited applied when wave energy density per log bandwidth exceeds local solar wind magnetic energy density.

Particle acceleration: a microscopic point of view

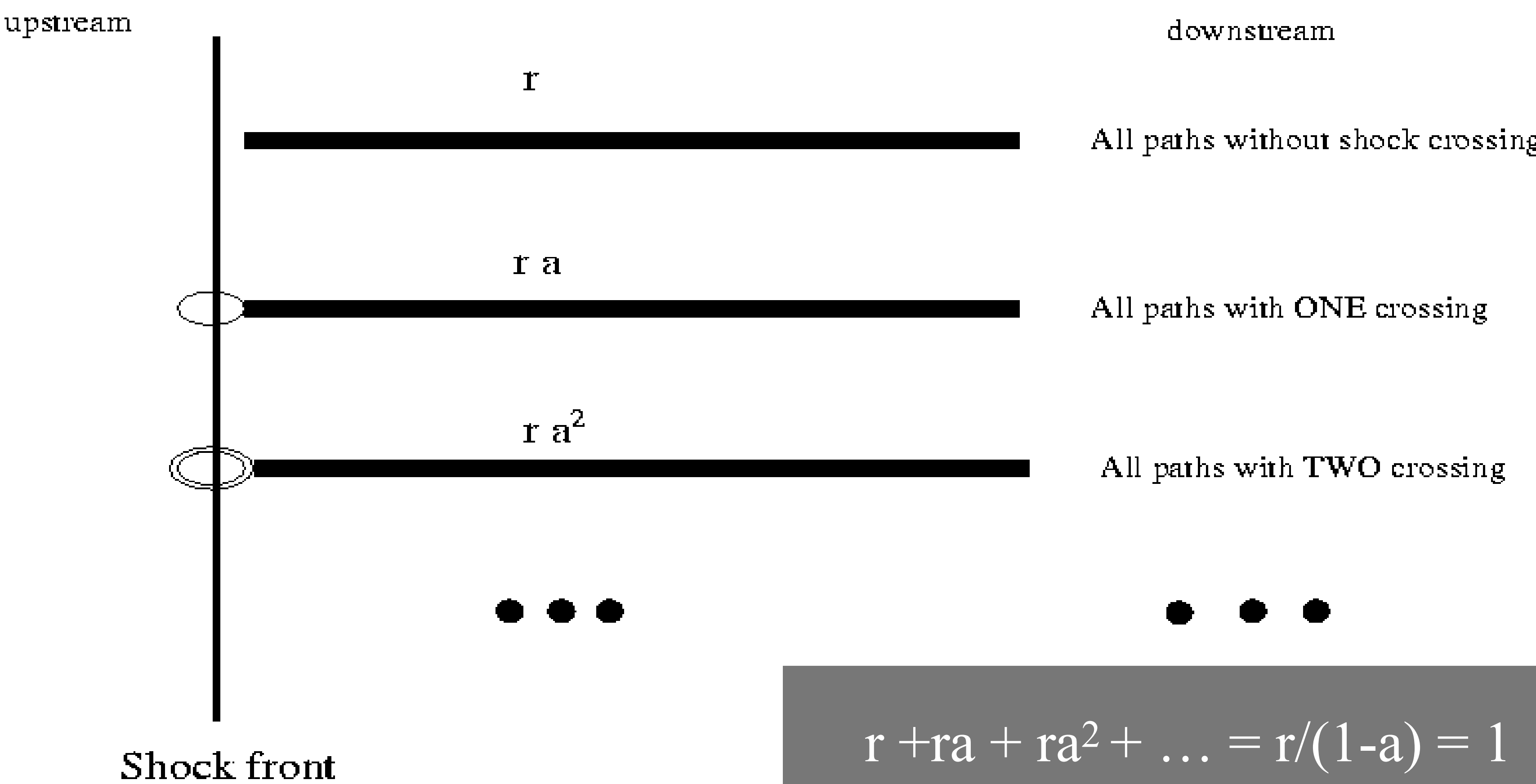

$$r + ra + ra^2 + \ldots = r/(1-a) = 1$$

Particle acceleration: a microscopic point of view (2)

Assume v>u1, u2 and only keep to order Δu/v,

momentum gain per cycle

$$< \delta p/p > = \frac{\Delta u \int_0^1 d\mu_1 \int_{-1}^0 d\mu_2 |\mu_1\mu_2|(\mu_1 - \mu_2)}{v \int_0^1 d\mu_1 \int_{-1}^0 d\mu_2 |\mu_1\mu_2|} = \frac{4}{3}\frac{\Delta u}{v}$$

possibility of reaching far downstream

$$r = \frac{\int_{-1}^{+1} d\mu (\mu v + u_2) f(p)}{\int_{-u_2/v}^{+1} d\mu |\mu v + u_2| f(p)} = \frac{4u_2}{v}$$

$$\frac{N(p+\delta p)}{N(p)} = \frac{f(p+\delta p) d^3(p+\delta p)}{f(p) d^3(p)} = \frac{f(p+\delta p)}{f(p)}(1 + 3 < \delta p/p >)$$

$$\frac{N(p+\delta p)}{N(p)} = \frac{ra}{r} = a = 1 - r$$

$$\frac{f(p+\delta p)}{f(p)} \sim 1 + \frac{\delta p}{p} \frac{df(p)/dp}{f(p)} p$$

$$f(p) \sim p^{-3s/s-1}$$

Origin of galactic cosmic rays

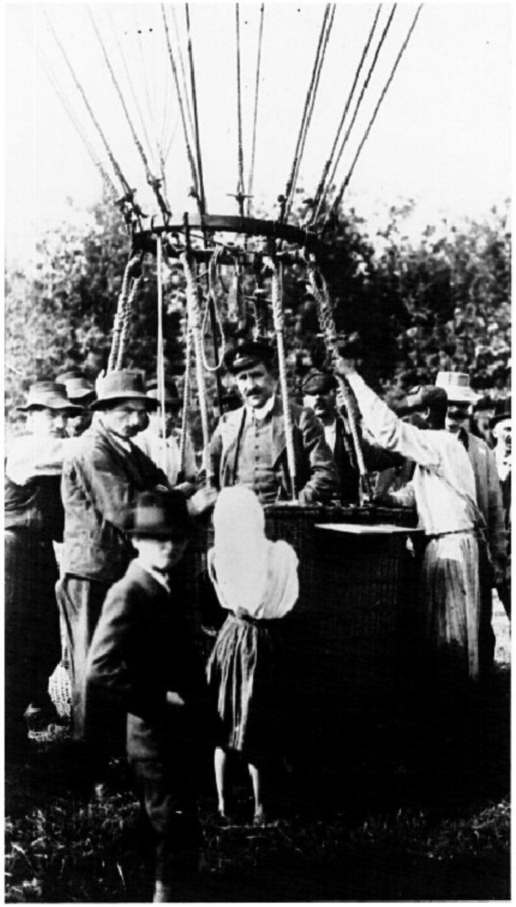

Discovered in 1912 by Victor Hess (atmospheric ionization).

"Here in the Erice maze

Cosmic rays are the craze

and this because a guy named Hess

ballooning up found more not less."

- Baade and Zwicky - 1934.
    - Originate in supernovae (extragalactic?).
    - Supernovae associated with the formation of neutron stars!

Origin of galactic cosmic rays

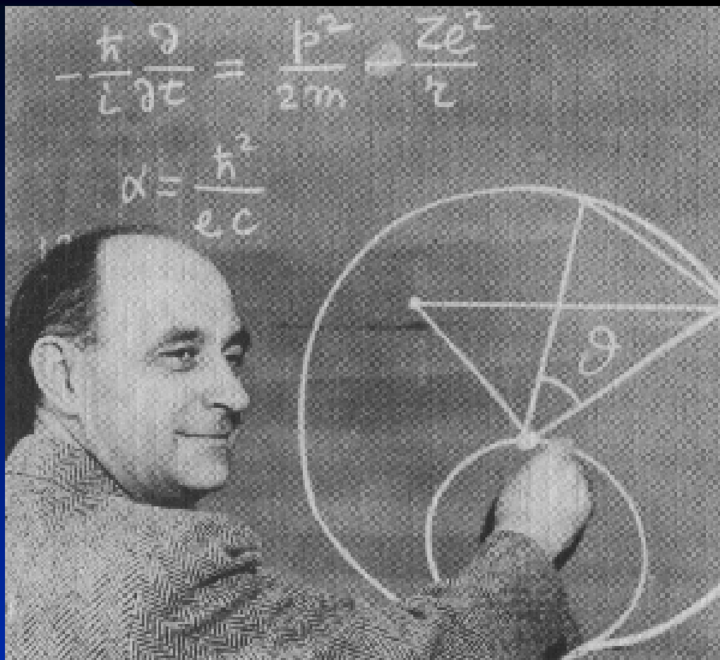

- Acceleration in interstellar space – Fermi I, Fermi II.
- The survival of heavy nuclei requires Fermi I (faster).

- Hoyle – 1960 – Shocks in interstellar space.
- Colgate/Johnson – 1960 - Supernova explosions – relativistic shocks.
- Acceleration by SNRs Requires 10 - 20% efficiency.

Origin of galactic cosmic rays

- SN followed by massive blast wave which goes through sweep-up phase before evolving into Sedov stage i.e., not steady-state.
- SNR shock expands and eventually merges with ambient ISM i.e., what is effect of cooling on CRs?
- ISM is admixture of different phases therefore SNR shock expands differently.
- $E^{-2.6}$ suggests CRs accelerated at middle to late stages of SNR shock evolution. Is the diffusive shock acceleration process still effective?
- Need to model cosmic ray acceleration at an evolving SNR shock wave.

Origin of galactic cosmic rays

	B (Gauss)	a_1 (cm s^{-1})	P_1 (dyne cm^{-2})	n_1 (cm^{-3})	T (K)	v (cm s^{-1})	V_p (cm s^{-1})
Hot model	$1.4\,10^{-6}$	$1.13\,10^{7}$	$2.9\,10^{-13}$	$3\,10^{-3}$	$7\,10^{5}$	$5.58\,10^{6}$	$7.6\,10^{6}$
Warm model	$5\,10^{-6}$	$1.384\,10^{6}$	$2.76\,10^{-13}$	0.2	$1\,10^{4}$	$2.44\,10^{6}$	$9.1\,10^{5}$

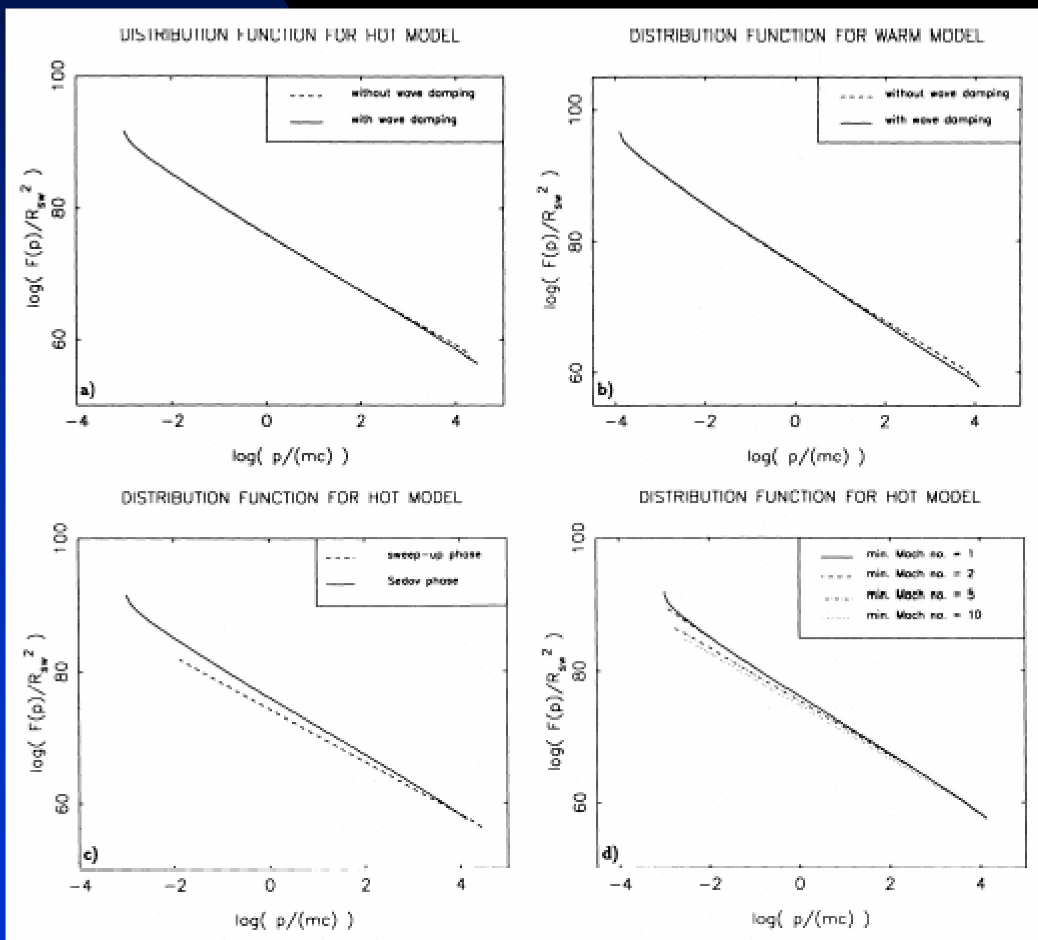

Spatially integrated energetic particle momentum spectrum *F(p).*

Spectral slope ranges from 4.2 – 4.35 (hot model, with/out wave damping) and 4.23 – 4.5 (warm model, …).

Voelk, Zank, & Zank, 1988

Origin of galactic cosmic rays

- Fermi I by supernova shock waves in interstellar space.
- Predicts power law spectrum.
- Becomes ineffective beyond 10^{15} eV (“knee”).

Supernova 1006

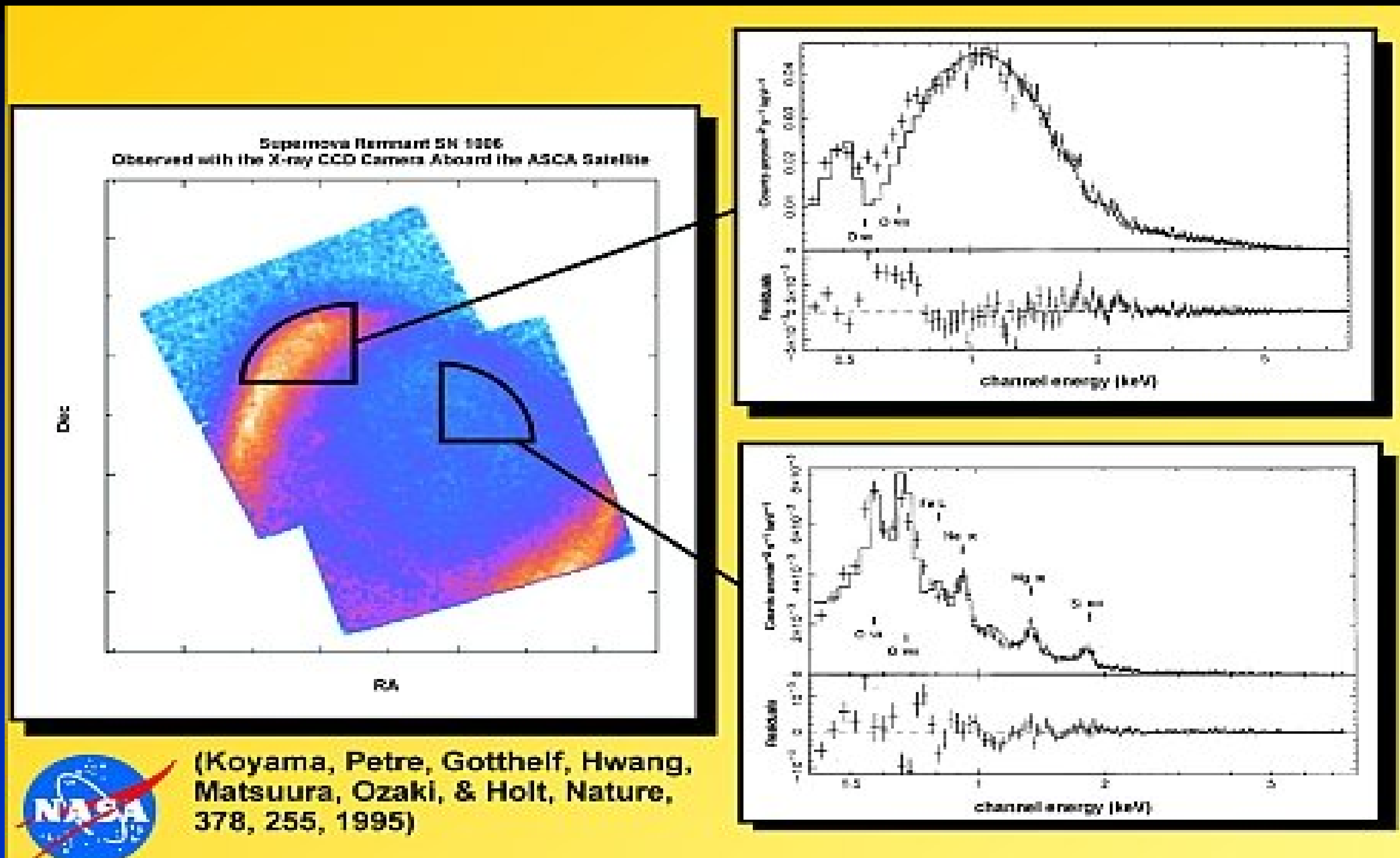

- 1000 years after explosion.
- 4000 km/sec expansion speed.
- Synchrotron, radio/x-ray ⇒ 1014 eV electrons.

Particle acceleration within 1AU at interplanetary shocks

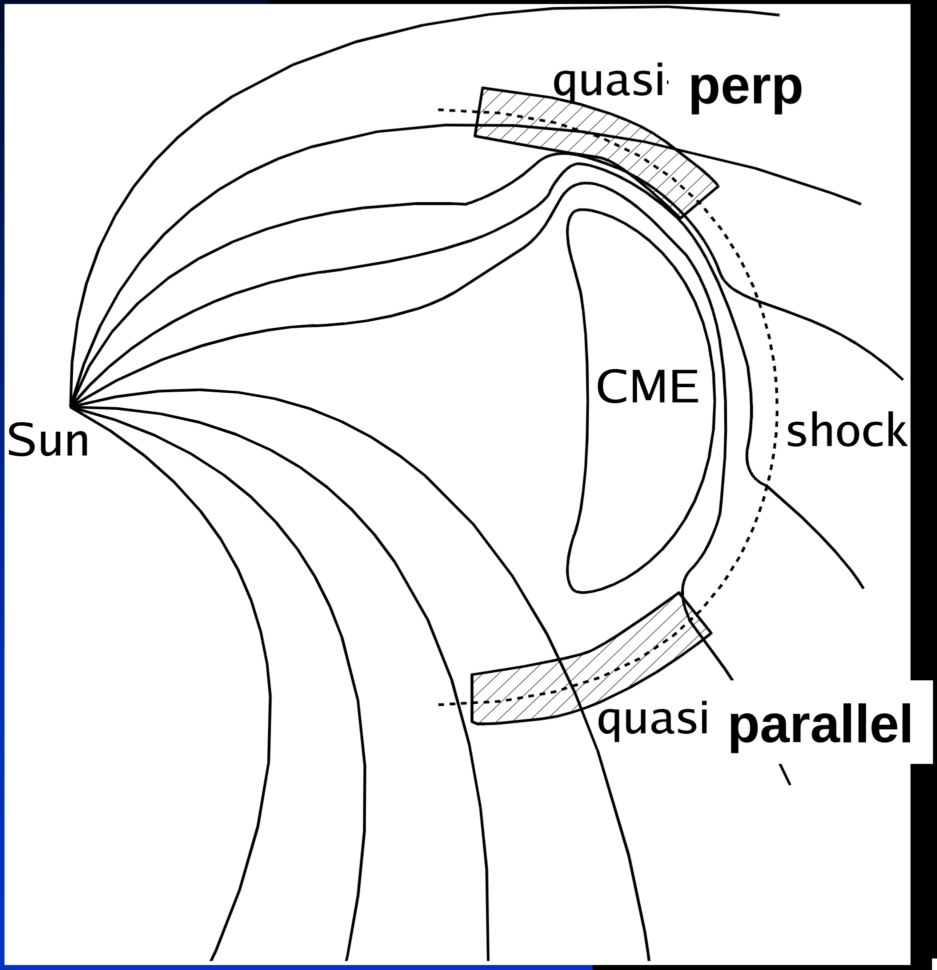

Blast wave or driven shock

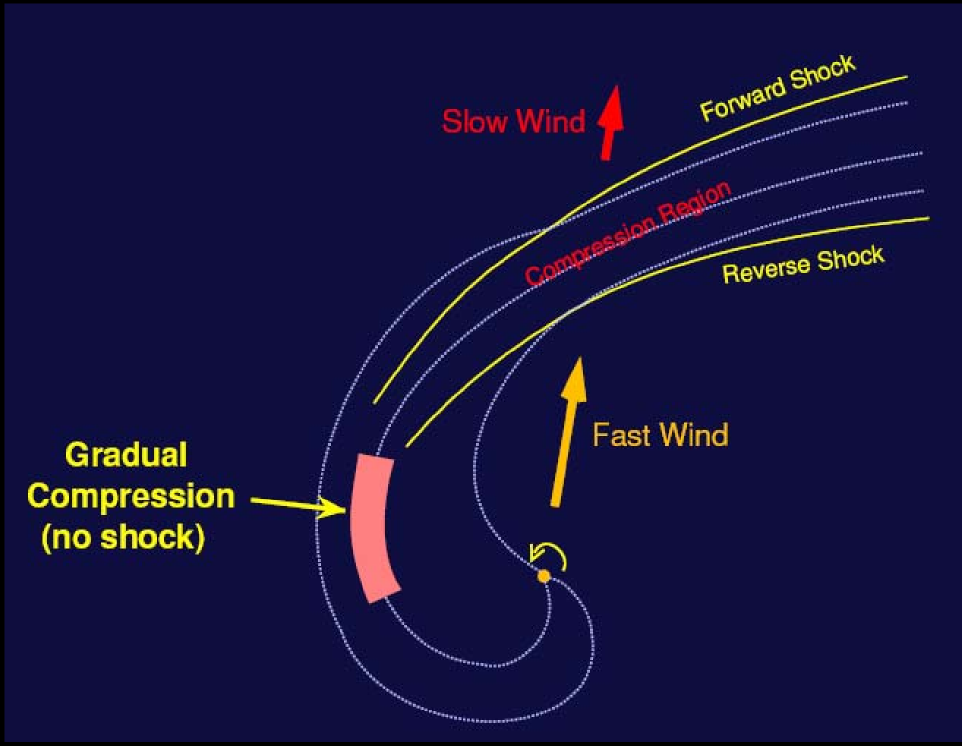

In situ shock formation in the solar wind

- Understanding the problem of particle acceleration at interplanetary shocks is assuming increasing importance, especially in the context of understanding the space environment.

- Basic physics thought to have been established in the late 1970’s and 1980’s, but detailed interplanetary observations are not easily interpreted in terms of the simple original models of particle acceleration at shock waves.

- Three fundamental aspects make the interplanetary problem more complicated than typical astrophysical problem: *the time dependence of the acceleration* and the *solar wind background*; the *geometry of the shock*; and the *long mean free path for particle transport away from the shock*.

- Multiple shocks can be present simultaneously in the solar wind.

- Consequently, the shock itself introduces a multiplicity of time scales, ranging from shock propagation time scales to particle acceleration time scales at parallel and perpendicular shocks, and many of these time scales feed into other time scales (such as determining maximum particle energy scalings, escape time scales, etc.).

Outline

- Overview of shock acceleration at quasi-parallel shocks
- Acceleration of heavy ions at interplanetary shocks
- Perpendicular shocks (if time) [$(Q/A)^{1/2}$ or $(Q/A)^{4/3}$ depending on ratio of gyro to turbulence correlation scales]

SHOCK EVOLUTION

Shock evolution is computed numerically by solving the fully 2D MHD equations and using realistic solar wind parameters as input into the model.

- Models "background" solar wind
- Traces an evolving spherically symmetric interplanetary shock wave throughout the solar wind.
  - Creates a succession of “shells” that convect with the solar wind and expand adiabatically.

Shell model of a CME-driven shock

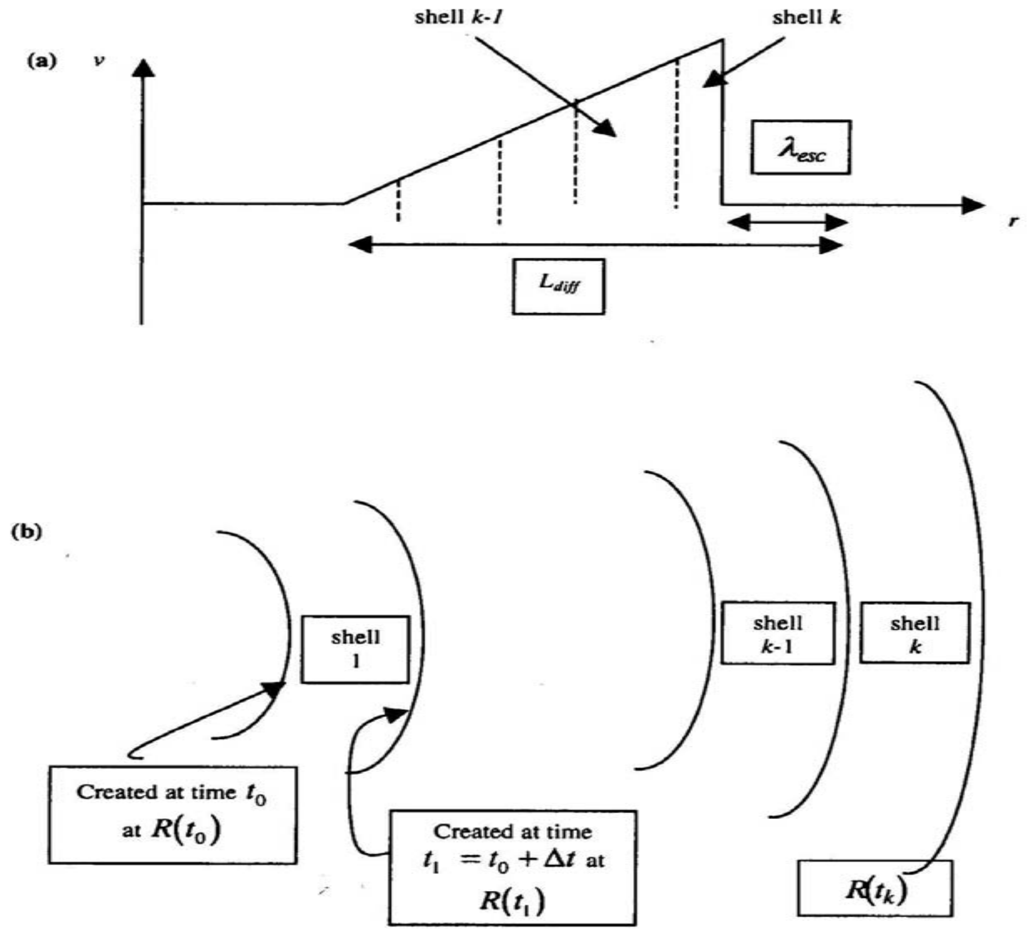

Figure 1. (a) Schematic of the density structure of an interplanetary blast wave. The total structure is subdivided into a series of concentric shells with the most recently formed shells labeled k-1 and k. Two length scales are identified: the escape length scale ahead of the shock front, λ_{esc}, beyond which energetic particles do not scatter diffusively back to the shock, and the scale size of the structure within which energetic ions are transported diffusively, L_{diff}. (b) A related schematic showing the concentric shells and their formation time as the shock propagates into the inhomogeneous solar wind. At time t_k the shock front is located at $R(t_k)$, which creates the edge of the outermost shell, identified as shell k. After formation the shells continue to evolve, being convected with the solar wind and expanding adiabatically.

JGR, Zank et. al. Vol. 105 P 25,079 – 25,095

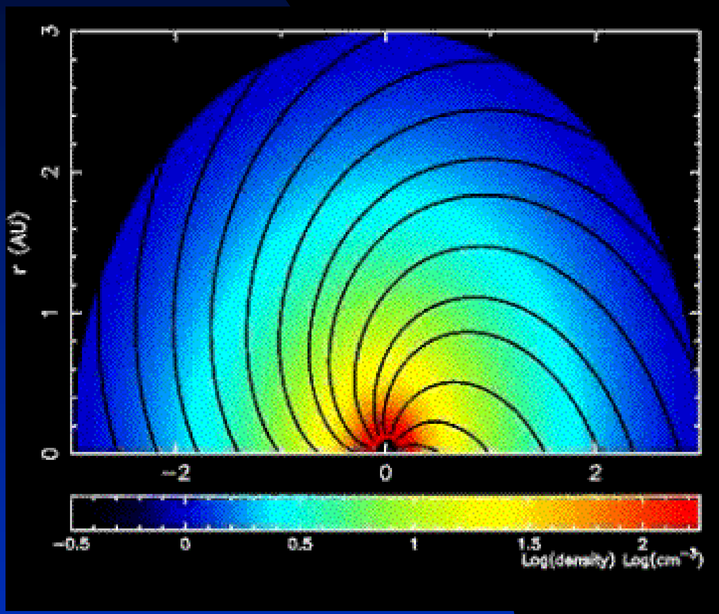

r (AU)
Log(density) Log(cm^{-3})

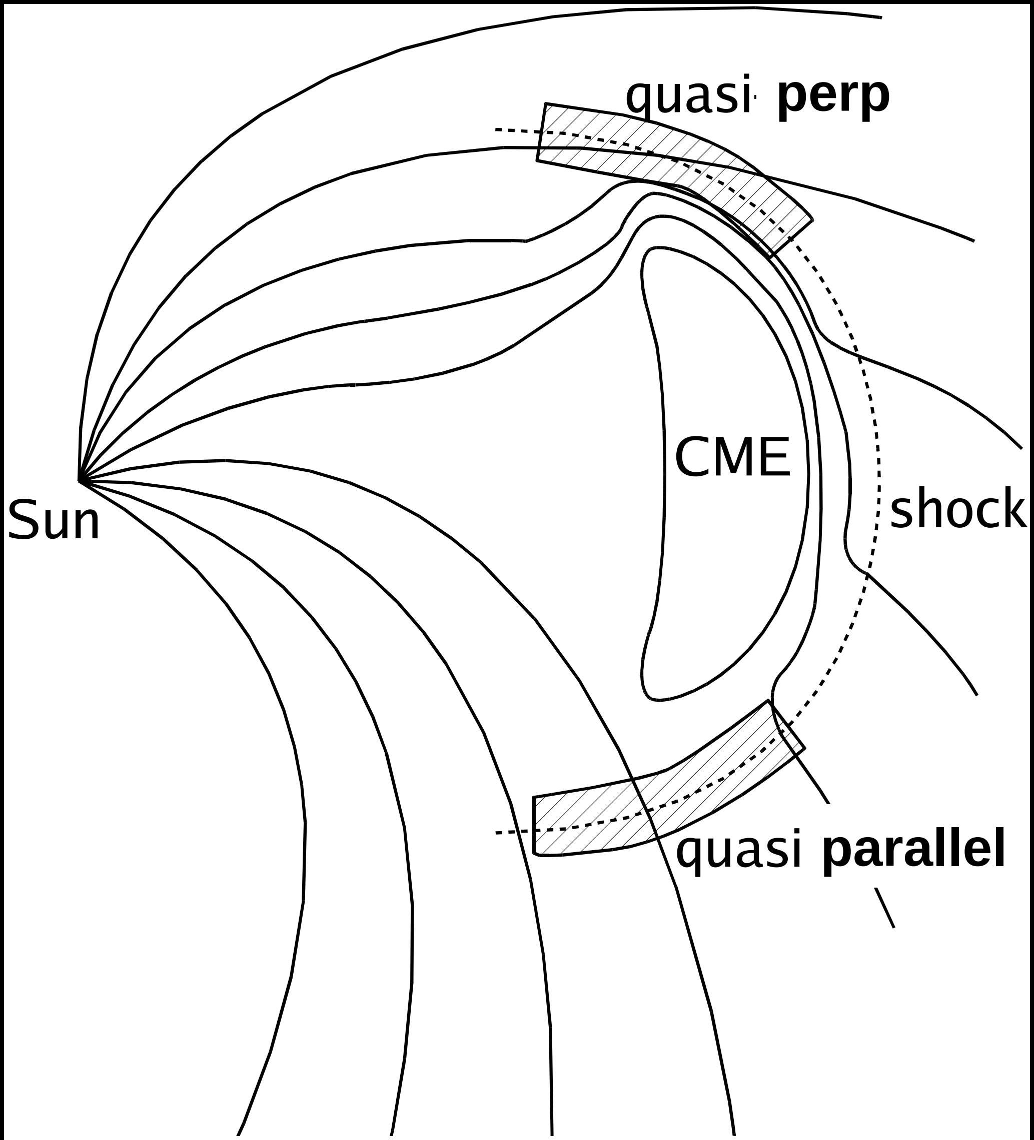

quasi perp
CME
Sun
shock
quasi parallel

Intensity profiles

after Cane et al. (1988); Reames et al. (1996).

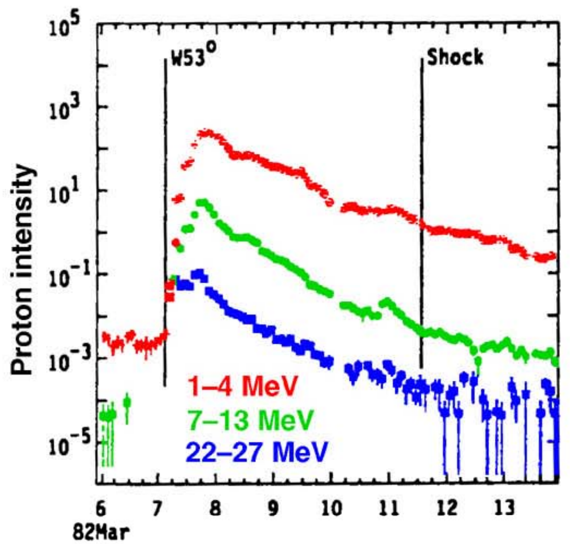

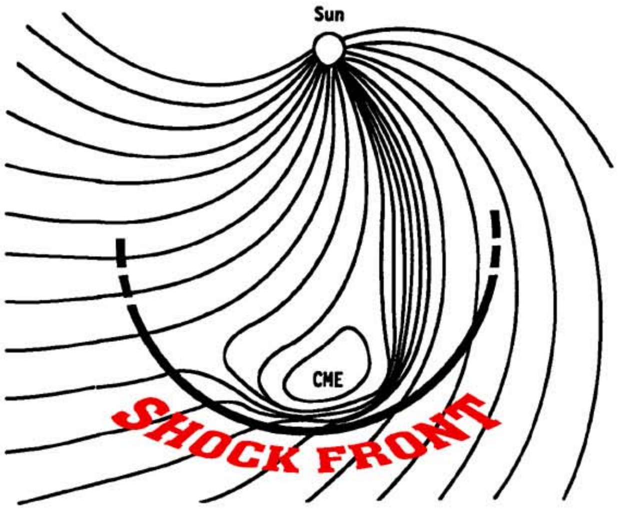

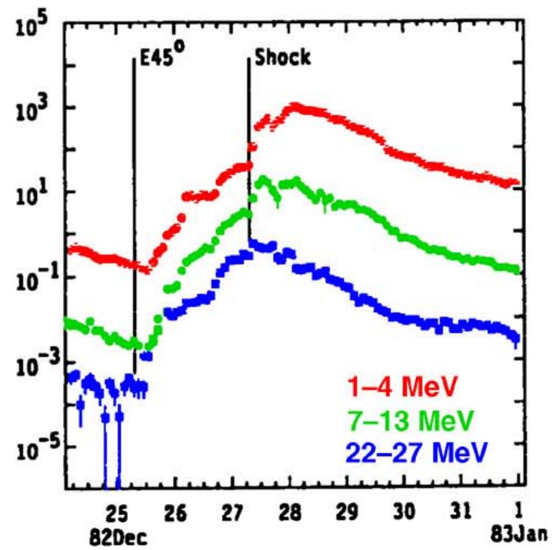

Only the fastest CMEs (~1-2 %) drive shocks which make high-energy particles.

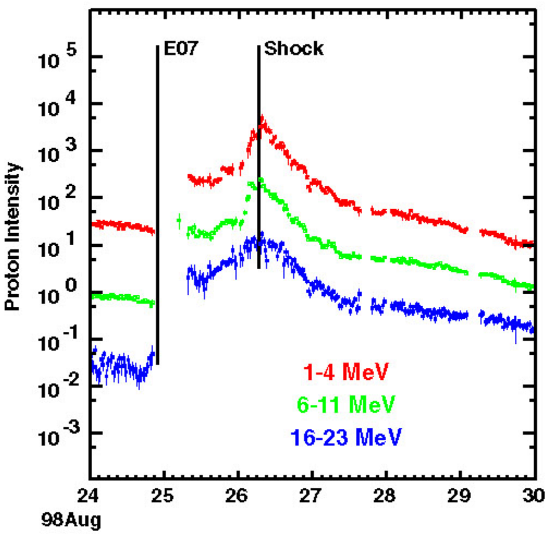

Particle Acc^n at the Shock

- Particles are injected into the shock, are energized by diffusive shock acceleration (DSA), and escape from the shock.

- The important component of the DSA mechanism is the presence of turbulence near the shock to enable particle scattering between upstream and downstream. Momentum gain of a particle after each crossing is proportional to the velocity difference between downstream and upstream flows.

- Particle transport of energetic particles at shock modelled by standard convection diffusion equation.

- Accelerated particles convect with the current shell and diffuse to other shells. Sufficiently far upstream of the shock, particles can escape into the solar wind.

Need to solve at the shock:

$$\frac{\partial f}{\partial t}+u\frac{\partial f}{\partial r}-\nabla\cdot u\frac{p}{3}\frac{\partial f}{\partial p}=\frac{1}{r^2}\frac{\partial}{\partial r}\left(r^2\kappa_{rr}\frac{\partial f}{\partial r}\right)+Q$$

Local shock accelerated distribution:

$$f(t_k;t_k,p)=\frac{Q(t_k)\eta R^2(t_k)}{p_0^3}\frac{3-q(t_k)}{\left[p_{\max}(t_k)\big/p_{inj}(t_k)\right]^{3-q(t_k)}-1}\left(\frac{p_0}{p_{inj}(t_k)}\right)^{3-q(t_k)}\left(\frac{p}{p_0}\right)^{-q(t_k)}$$
$$\times\left\{H\left(p-p_{inj}(t_k)\right)-H\left(p-p_{\max}(t_k)\right)\right\}$$

Injection rate per unit area Area of shock wave Injection momentum Local maximum energy

$$q(t_i)=3r_i/(r_i-1)$$

Spatial injection flux (particles per unit time):

$$4\pi R^2(t)\int\overline{Q}(p,t)d^3p=4\pi R^2(t)\dot{R}n_{inj}=\begin{cases}\sim t^2\,(\text{Sweep-up phase})\\ \sim t^{1/5}\,(\text{Sedov phase})\end{cases}$$

$$n_{inj}=\delta\cdot n_1\propto(r)^{-2}$$

Young interplanetary shocks which have not yet experienced any significant deceleration inject and accelerate particles far more efficiently than do older shocks which are in a decaying phase.

Timescales and particle energies

- The use of the steady state solution in this time dependent model is based on the assumption that the shock wave, at a given time in the simulation, has had sufficient time to accelerate all the particles involved in the simulation.

  - The acceleration time is

$$t_{acc} = p\frac{\Delta t}{\Delta p} = \frac{3u_1}{u_1 - u_2}\frac{\kappa(p)}{u_1^2}$$

giving

$$\Delta t = \frac{q}{u_1^2}\kappa(p)\frac{\Delta p}{p}$$

where

$$q = \frac{3s}{s-1}$$

$$s = \frac{u_1}{u_2} = \frac{\rho_2}{\rho_1}$$

- The maximum particle energy can be determined by equating the dynamic timescale of the shock with the acceleration timescale (Drury [1983], Zank et al. 2000).

$$\frac{\dot{R}(t)}{R(t)} \approx \frac{q(t)}{u_1^2}\int_{p_{\text{inj}}}^{p_{\max}} \kappa(p')\,d(\ln(p'))$$

$$\kappa(p) \propto \frac{1}{B(r)}$$

The maximum particle momentum obtained for a strong shock at early times can be as high as a few GeV – consistent with results obtained by Kahler [1994].

ACCELERATION TIME SCALE

$$\tau_{acc} = \left(\frac{1}{p} \frac{dp}{dt} \right)^{-1} \approx \frac{3r\mathrm{K}_{xx}}{u^2 (r-1)}$$

Particle scattering strength

Hard sphere scattering: $\mathrm{K}_{\perp} = \frac{\mathrm{K}_{\parallel}}{1+\eta_c^2}$ $\eta_c = \lambda_{\parallel} / r_g$ $\lambda_{\parallel} = 3\kappa_{\parallel} / v$

Weak scattering: $\lambda_{\parallel} / r_g \gg 1$ → $\kappa_{\perp} / \kappa_{\parallel} = \left(\lambda_{\parallel} / r_g \right)^2 \ll 1$

Strong scattering: $\langle \delta B^2 \rangle \sim B^2$ $\lambda_{\parallel} / r_g \approx 1$ → $\kappa_{\perp} \approx \kappa_{\parallel}$

→ $\mathrm{K}_{\parallel} = \mathrm{K}_{Bohm} = {vr_g}/{3}$

Acceleration time at quasi-par shock much greater than at quasi-perp shock assuming equivalent turbulent levels.

Maximum particle energy at quasi-parallel shock:

$$\frac{R(t)}{\dot{R}(t)} \approx \frac{q(t)}{u_1^2}\int_{p_{inj}}^{p_{\max}} \kappa(p')\, d(\ln(p')) = \frac{q(t)}{\dot{R}^2(t)}\left(\frac{5M^2(t)+3}{M^2(t)+3}\right)\int_{p_{inj}}^{p_{\max}} \kappa(p')\, d(\ln(p'))$$

Age Strength Magnetic field heliocentric dependence

$$p_{\max} = \left\{\left[\frac{M^2(t)+3}{5M^2(t)+3}\,\frac{R(t)\dot{R}(t)}{q(t)\kappa_0}\,\frac{B}{B_0} + \sqrt{\left(\frac{m_p c}{p_0}\right)^2 + \left(\frac{p_{inj}}{p_0}\right)^2}\,\right]^2 - \left(\frac{m_p c}{p_0}\right)^2\right\}^{1/2}$$

$$\frac{B}{B_0} = \left(\frac{R_0}{r}\right)^2\left[1 + \left(\frac{\Omega_0 R_0}{u}\right)^2\left(\frac{r}{R_0} - 1\right)^2 \sin^2\theta\right]^{1/2}$$

Particle Transport

Particle transport obeys Boltzmann (Vlasov) equation:

$$\frac{df(x,p,t)}{dt} + q[E + \mathrm{v} \times B] \bullet \frac{\partial f(x,p,t)}{\partial p} = \left.\frac{df(x,p,t)}{dt}\right|_{coll}$$

The LHS contains the material derivative and the RHS describes various “collision” processes.

•Collision in this context is pitch angle scattering caused by the irregularities of IMF and in quasi-linear theory,

•The result of the parallel mean free path $\lambda//$, from a simple QLT is off by an order of magnitude from that inferred from observations, leading to a 2-D slab model.

$$\frac{\lambda}{10^6\,\mathrm{km}} = 8.30\,\frac{(B/B_0)^2}{\delta B_x^2/\delta B_{x0}^2}\left(\frac{l}{l_0}\right)^{2/3}\left(\frac{p/M_n}{B/B_0}\right)^{1/3}$$

Allows use of a Monte-Carlo technique.

Wave spectra and diffusion coefficient at shock

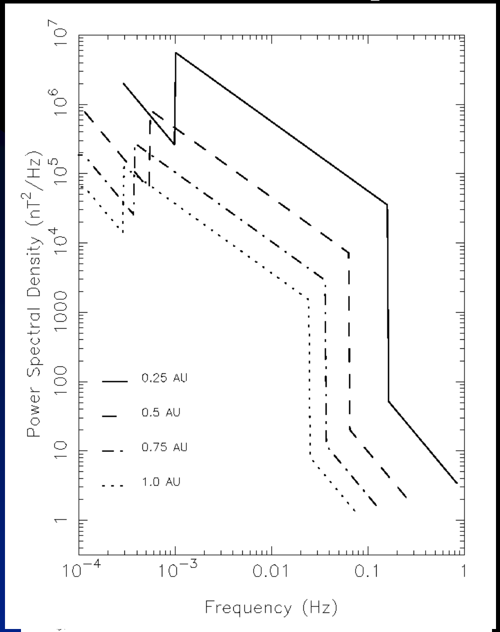

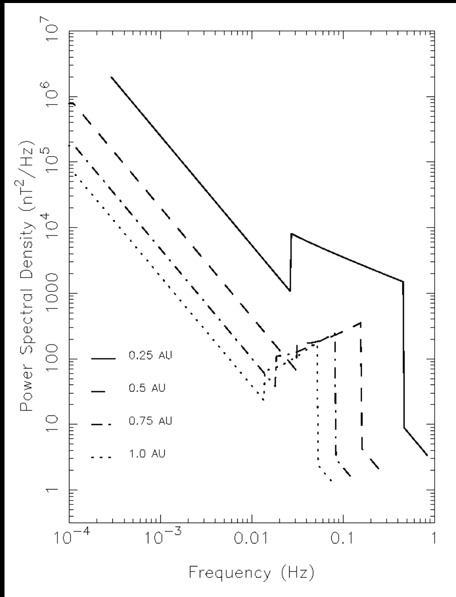

Wave intensity

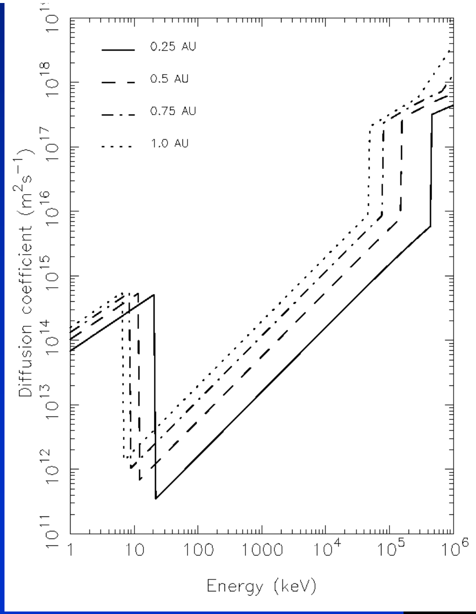

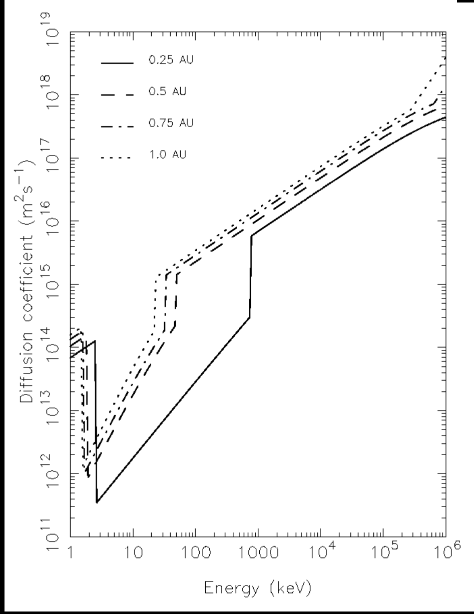

Diffusion coefficient

Strong shock

Weak shock

Upstream particle spectrum(strong shock)

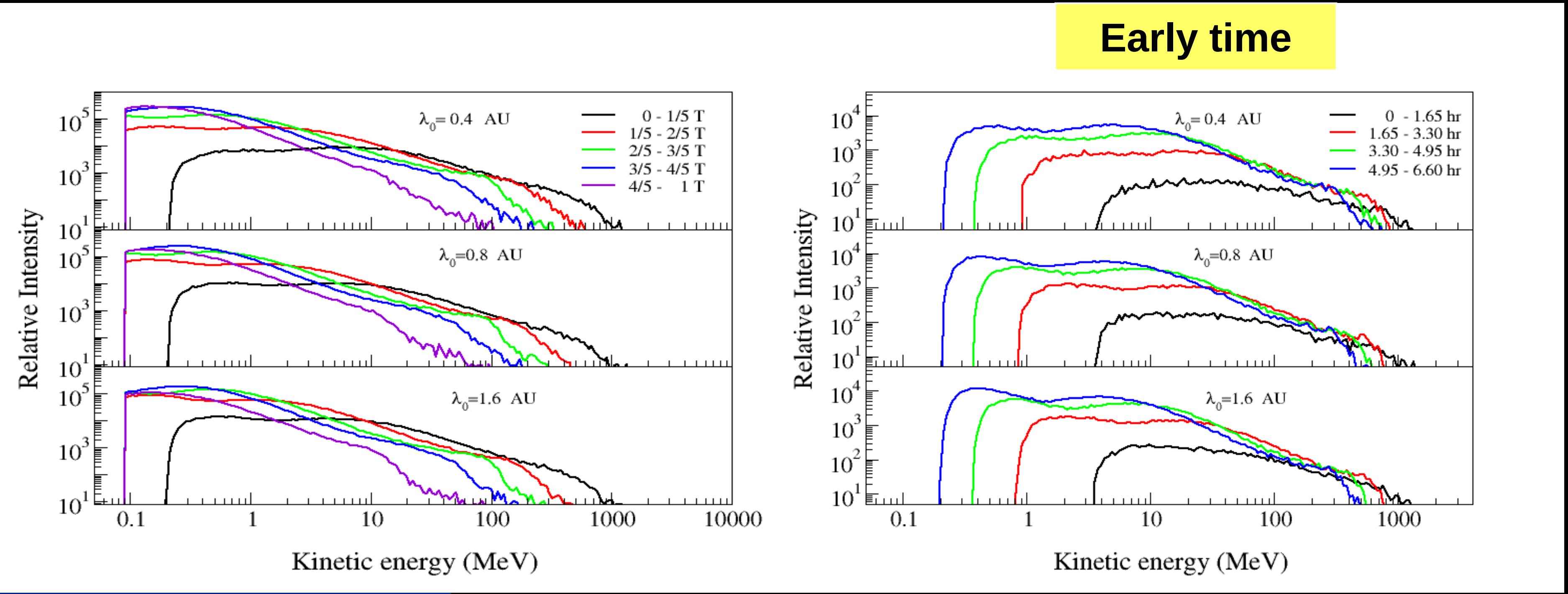

- Cumulative spectra at 1 AU for five time intervals are shown, T=1.3 days.
- Spectra exhibit a power law feature.
- Broken power law at later times, especially for larger mfp (λ_0 = 1.6AU). E.g., K=20 MeV for the time interval t = 4/5-1 T – particle acceleration no longer to these energies.

Event Integrated spectra

Total or cumulative spectrum at 1AU, integrated over the time from shock initiation to the arrival of the shock at 1AU.

Strong shock case

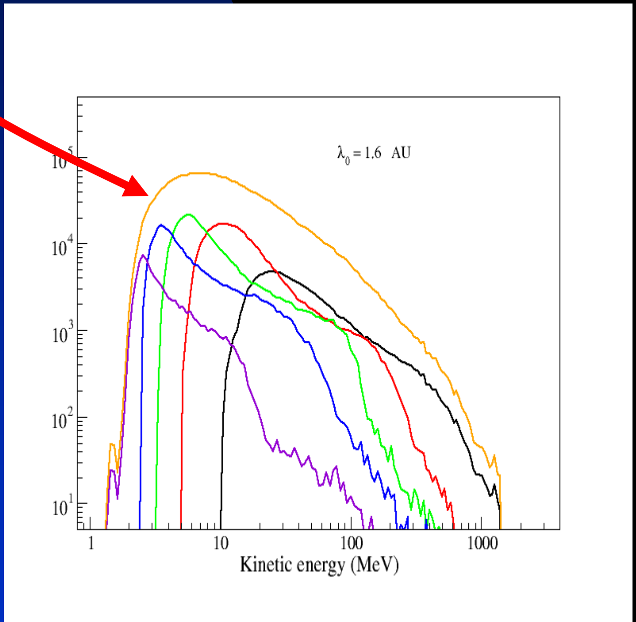

Weak shock case

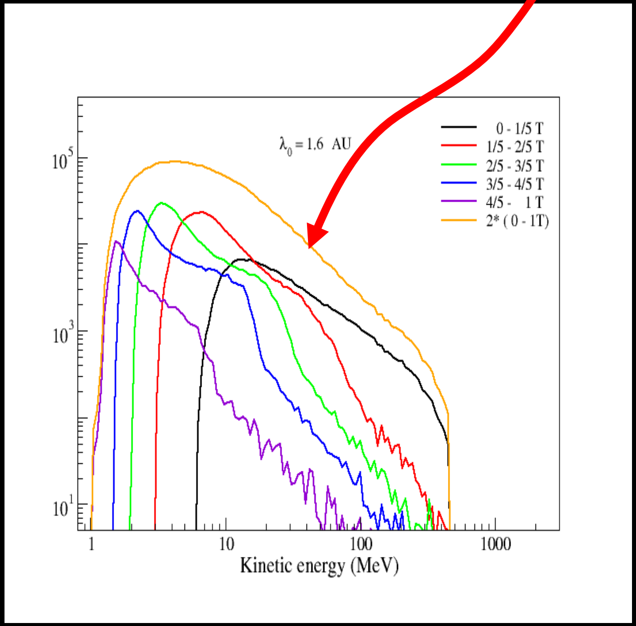

Note the relatively pronounced roll-over in the cumulative strong shock spectrum and the rather flat power-law spectrum in the weak shock case.

Intensity profile (strong shock)

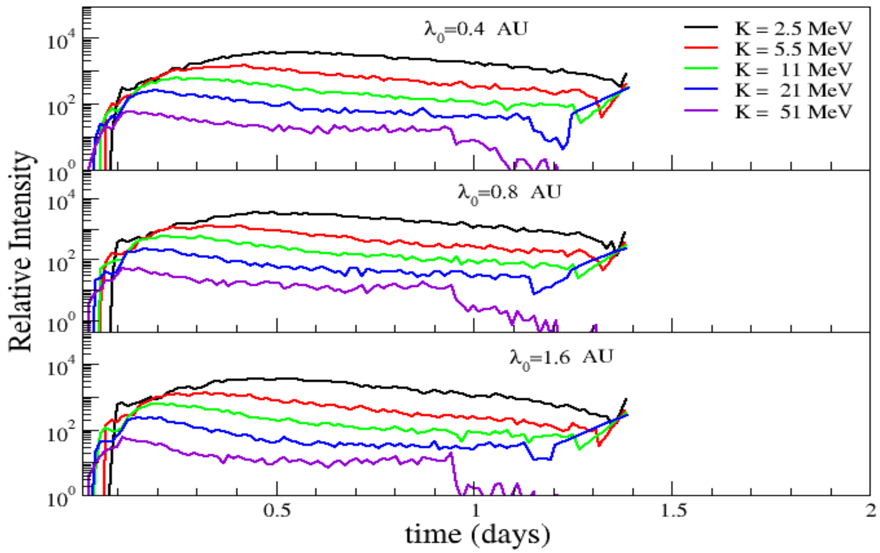

Early time

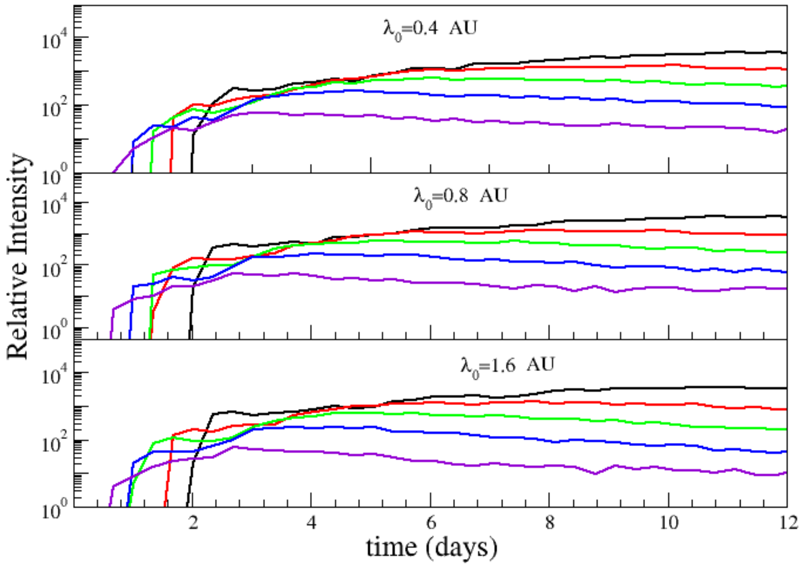

- Shock arrives 1.3 days after initiation
- No K ~ 50 MeV particles at shock by 1 AU since shock weakens and unable to accelerate particles to this energy and trapped particles have now escaped.
- A slowly decreasing plateau feature present –result of both pitch angle scattering and shock propagation.
- Early time profile shows the brief free streaming phase.

Multiple particle crossings at 1AU

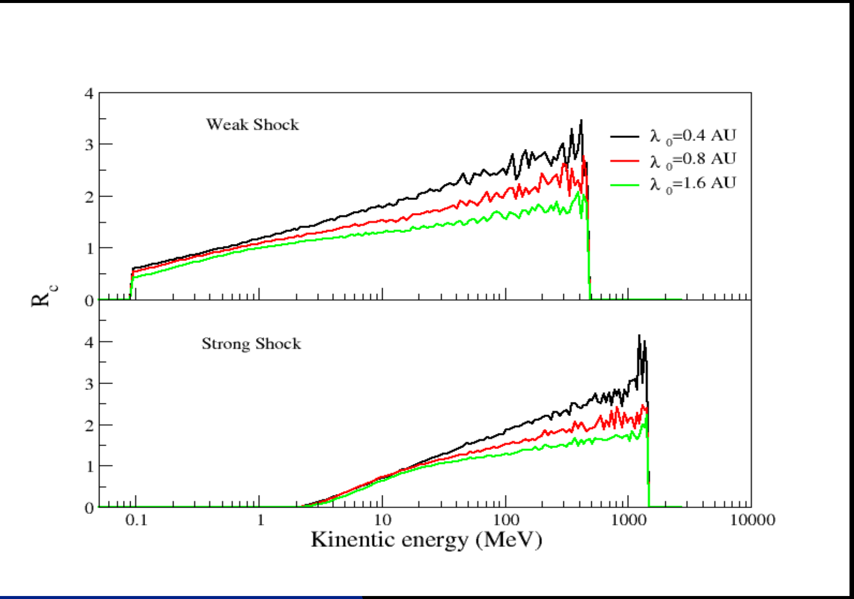

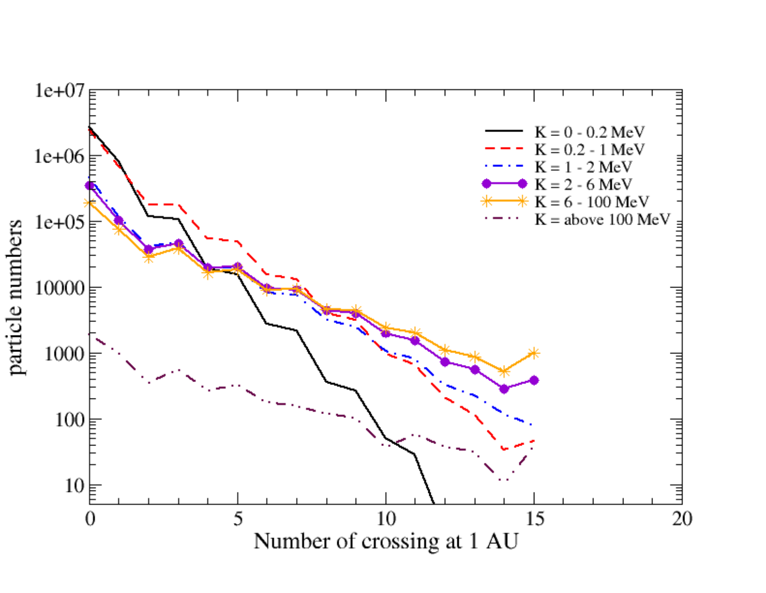

$$R_c(K) \equiv \frac{\text{number of particles of energy K that cross 1 AU}}{\text{number of particles of energy K that leave the shock}}$$

Due to pitch angle scattering, particles, especially of high energies, may cross 1 AU more than once, and thus from both sides. In an average sense, a 100 MeV particle has Rc ~ 2, or on average, two crossings. Histogram shows that some particles may cross as many as 15 times. A smaller mfp leads to a larger Rc since particles with smaller mfp will experience more pitch angle scatterings.

Anisotropy at 1 AU (weak shock)

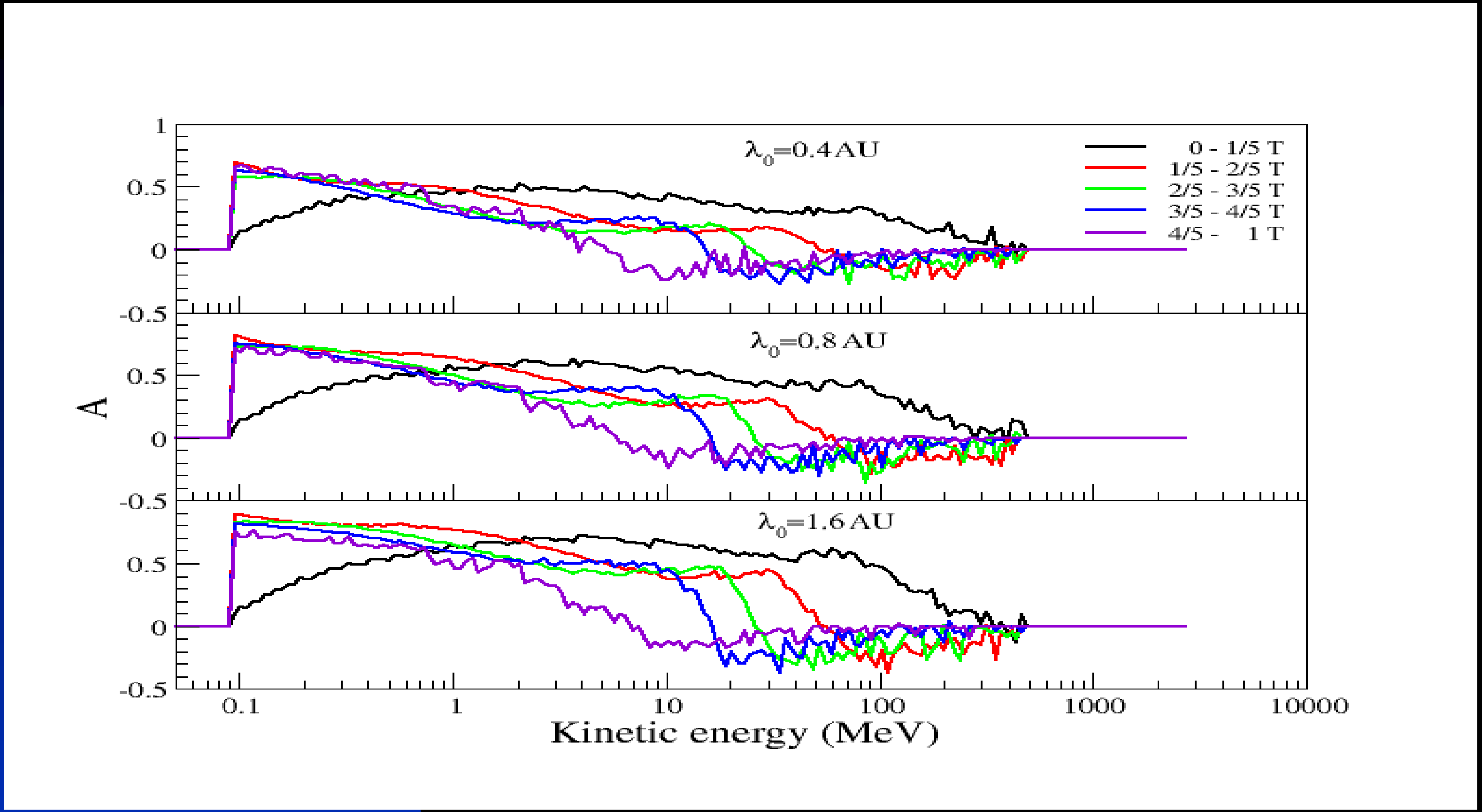

- Similar to the strong shock case.

- The value of asymmetry for larger λ_0 is consistently larger than that of a smaller λ_0 become fewer particles will propagate backward for a larger λ _0.

Time evolution of number density in phase space

- Snap shots of the number density observed at 1 AU prior to the shock arrival at t = 1/20, 2/20, …. T, with a time interval of 1/20 T in (v_par, v_perp)-space.
- Coordinates:

$$Z_x = cos(\theta_{\hat{\mathbf{B}},\hat{\mathbf{p}}})(log(p/\mathrm{MeV}) - 4.25);$$
$$Z_y = sin(\theta_{\hat{\mathbf{B}},\hat{\mathbf{p}}})(log(p/\mathrm{MeV}) - 4.25).$$

- B field along positive Zx direction
- Particle energies from innermost to outermost circle are K = 4.88, 8.12, 10.47, 15.35, 21.06, 30.75, 50.80, 100.13 MeV respectively.

The next figures exhibit the following characteristics:

- At early times, more high energy particles cross 1 AU along +B direction, followed by lower energies later.

- Number density of higher energy particles at later times exhibits a “reverse propagation” feature corresponding to A < 0.

- The gap at Θ = 90 degree reflects that particles must have a component along B to be observed.

Phase space evolution

Strong shock

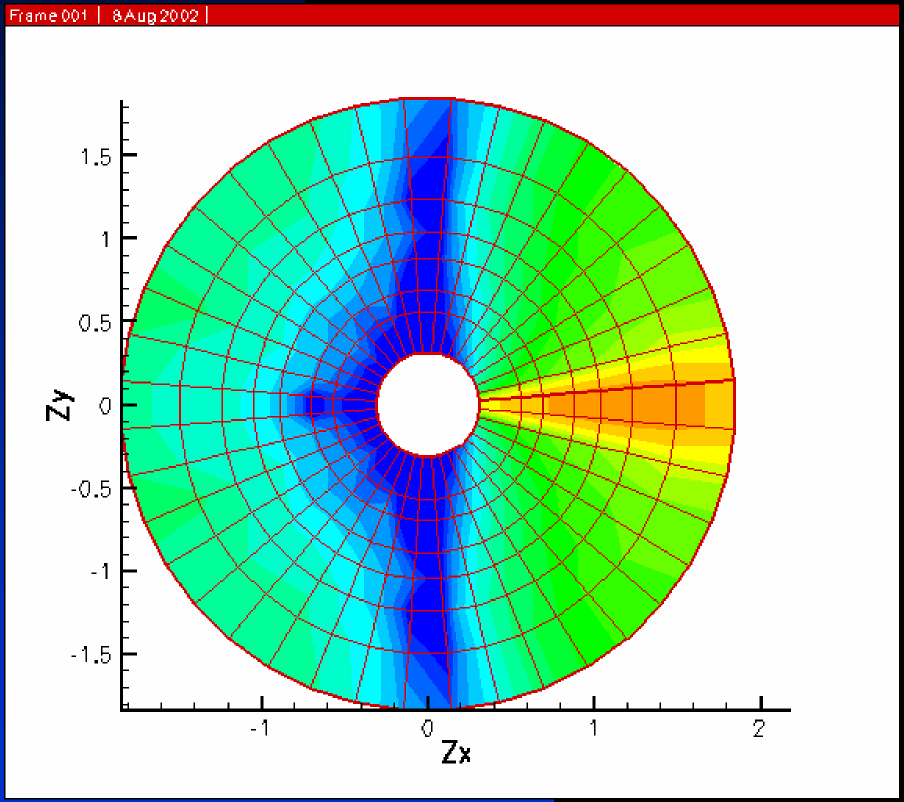

Weak shock

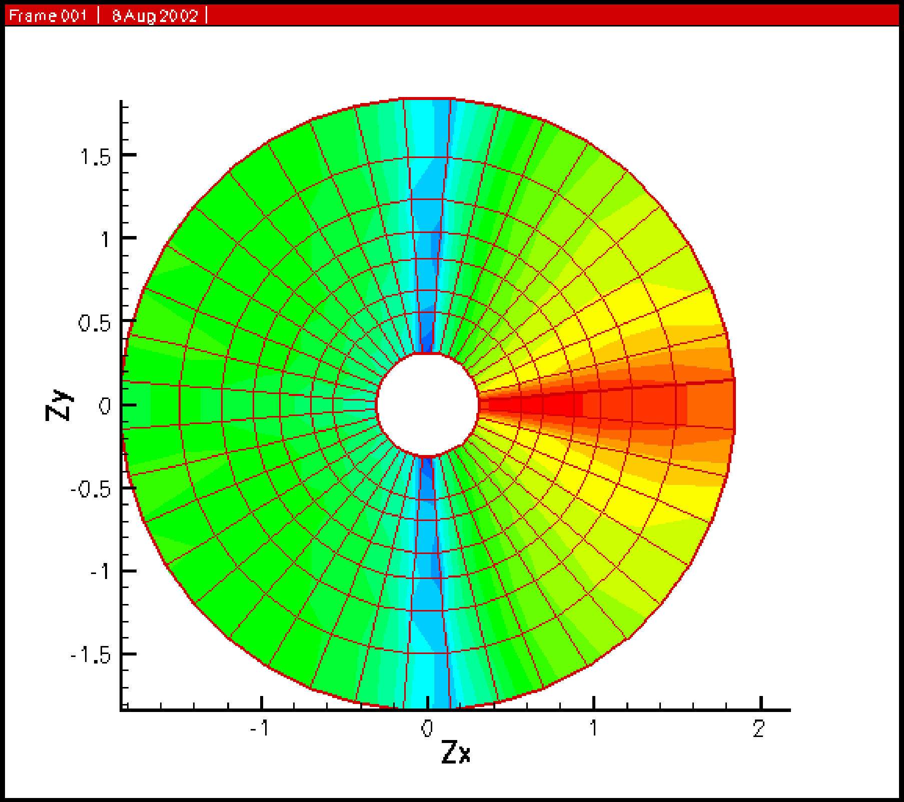

Phase space evolution – time sequence

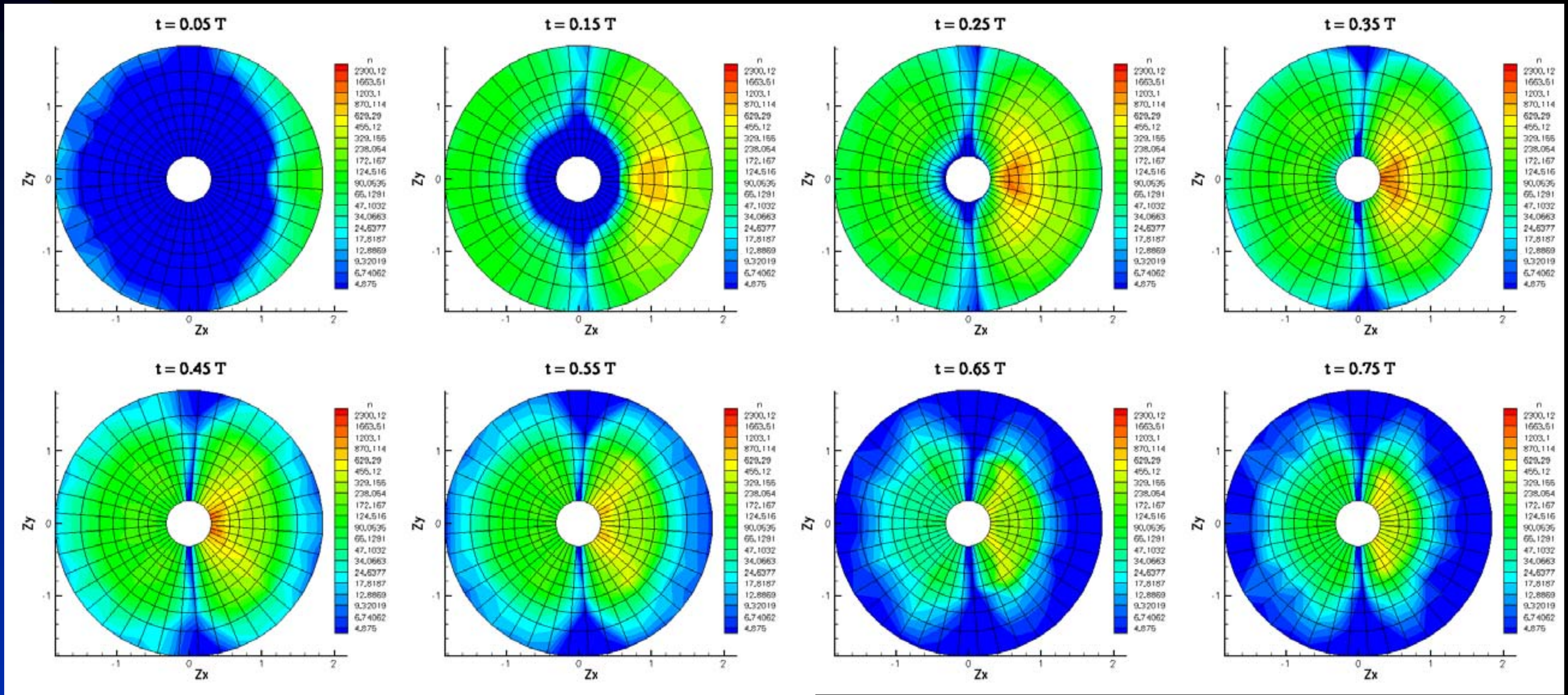

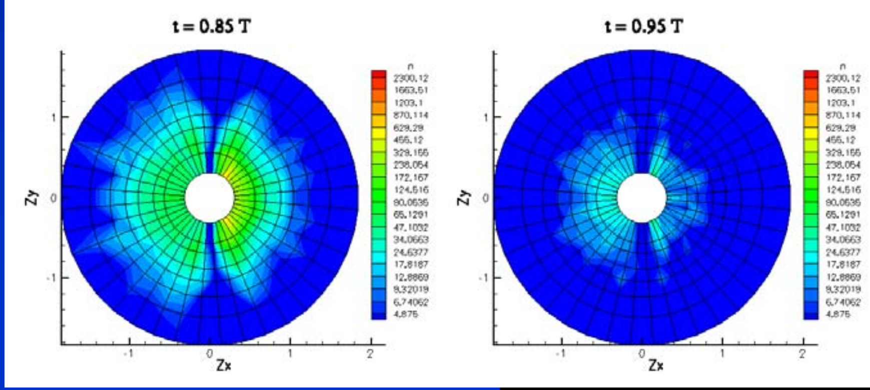

At t=0.85 T, we can see clearly that there are more backward propagating particles than forward ones between 20<K<30 MeV.

At t=0.95 T, it is more pronounced for K~10 MeV.

HEAVY IONS (CNO and Fe)

CNO: Q = 6, A = 14
Fe: Q = 16, A = 54

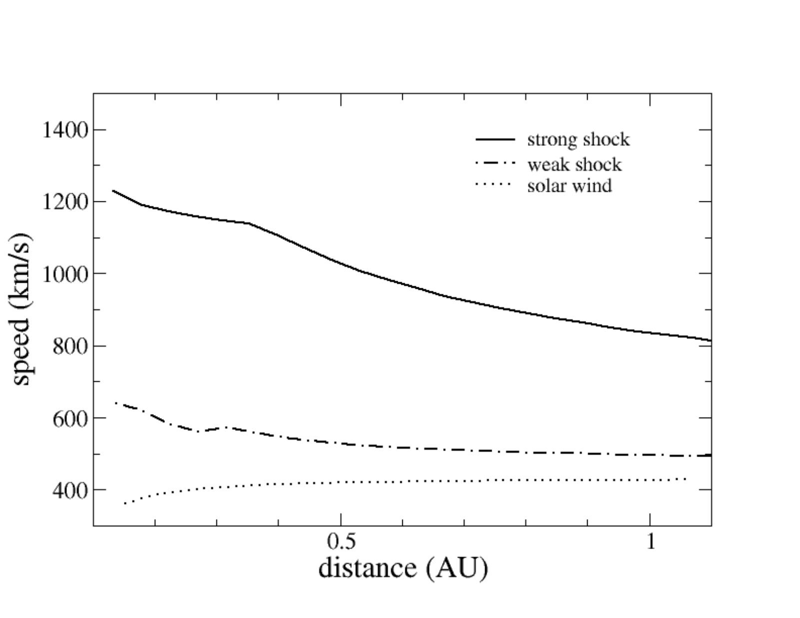

Shock speeds for strong and a weak shock.

Effect of heavy ions is manifested through the resonance condition, which then determines maximum energies for different mass ions and it determines particle transport – both factors that distinguish heavy ion acceleration and transport from the proton counterpart.

$$k = \frac{\gamma m_p \Omega}{\mu p}$$

$$\Omega = \frac{(Q/A)eB}{\gamma m_p c}$$

$$\lambda_{\parallel} = \lambda_0 \left(\frac{\tilde{p}c}{1GeV}\right)^{1/3} \left(\frac{A}{Q}\right)^{1/3} \left(\frac{r}{1AU}\right)^{2/3}$$

Wave power and particle diffusion coefficient

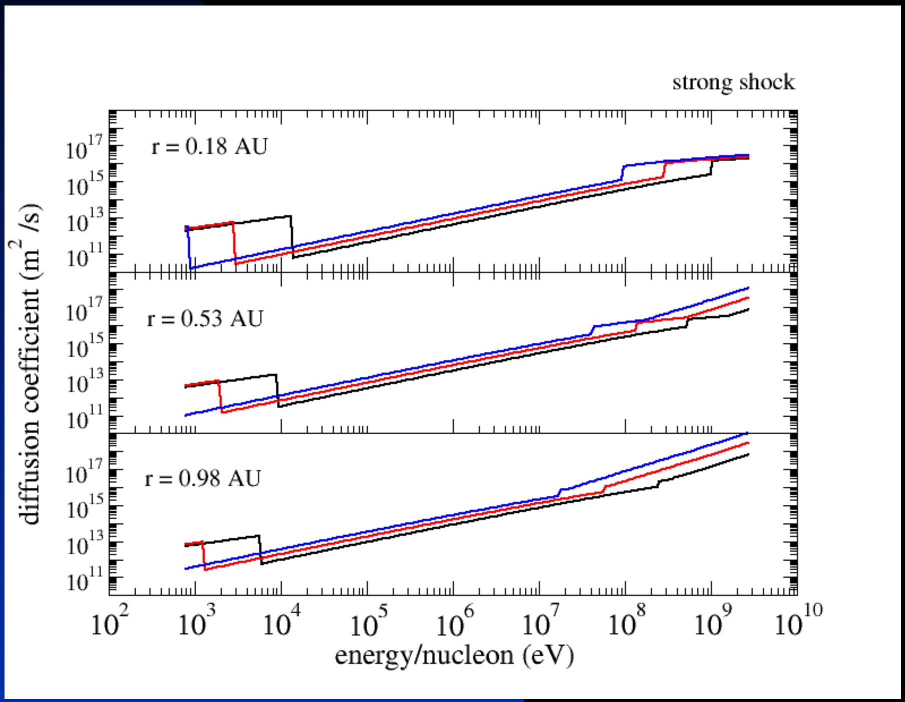

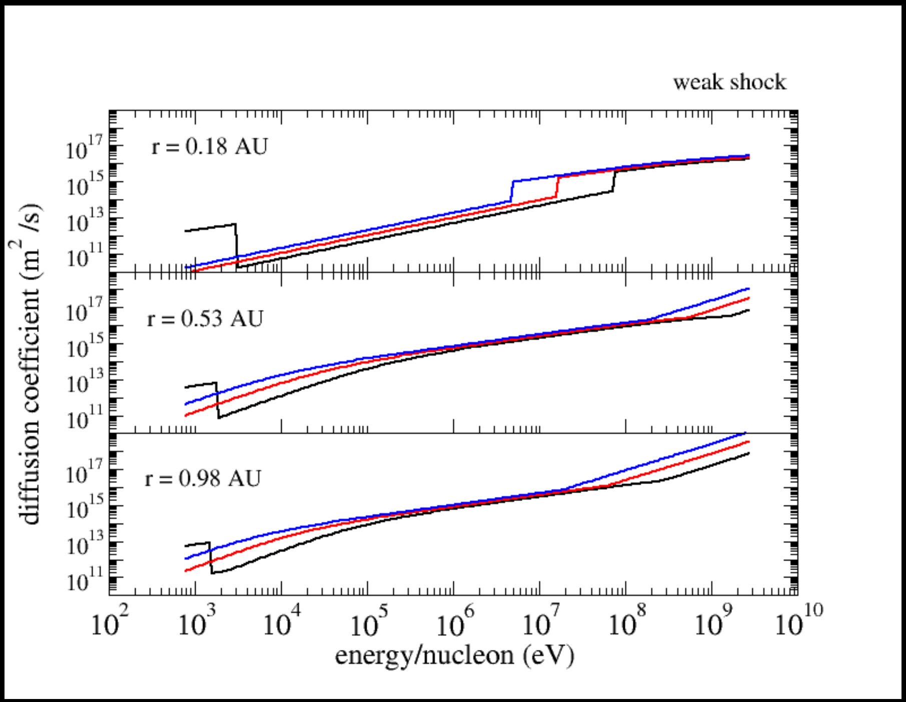

Strong shock example reduces to Bohm approximation.

Weak shock example.

The black curve is for protons, the red for CNO and the blue for Fe. The maximum energy of heavy ion shifts to lower energy end by Q/A --- a consequence of cyclotron resonance.

Deciding the maximum energy

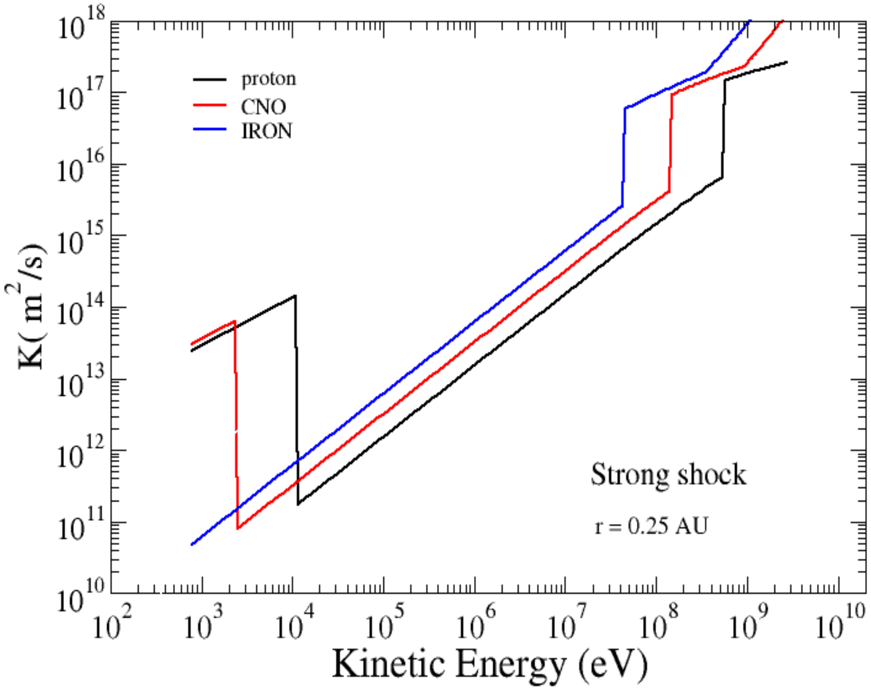

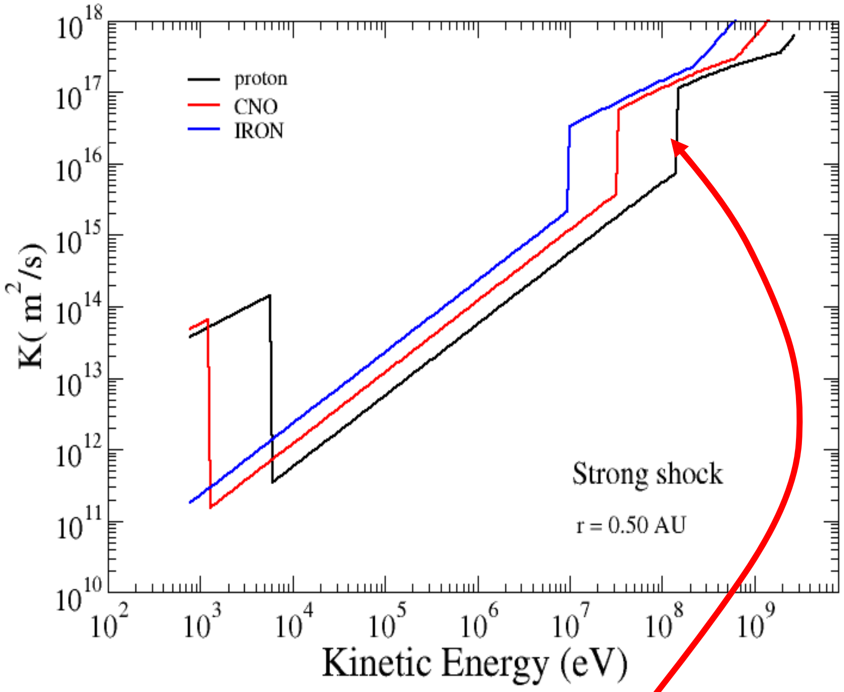

Evaluate the injection energy by assuming it is a half of the down stream thermal energy per particle.

$$\frac{R(t)}{\dot{R}(t)} \approx \frac{q(t)}{u_1^{\,2}} \int_{p_{\mathrm{inj}}}^{p_{\max}} \kappa(p')\,d(\ln(p'))$$

Maximum accelerated particle energy

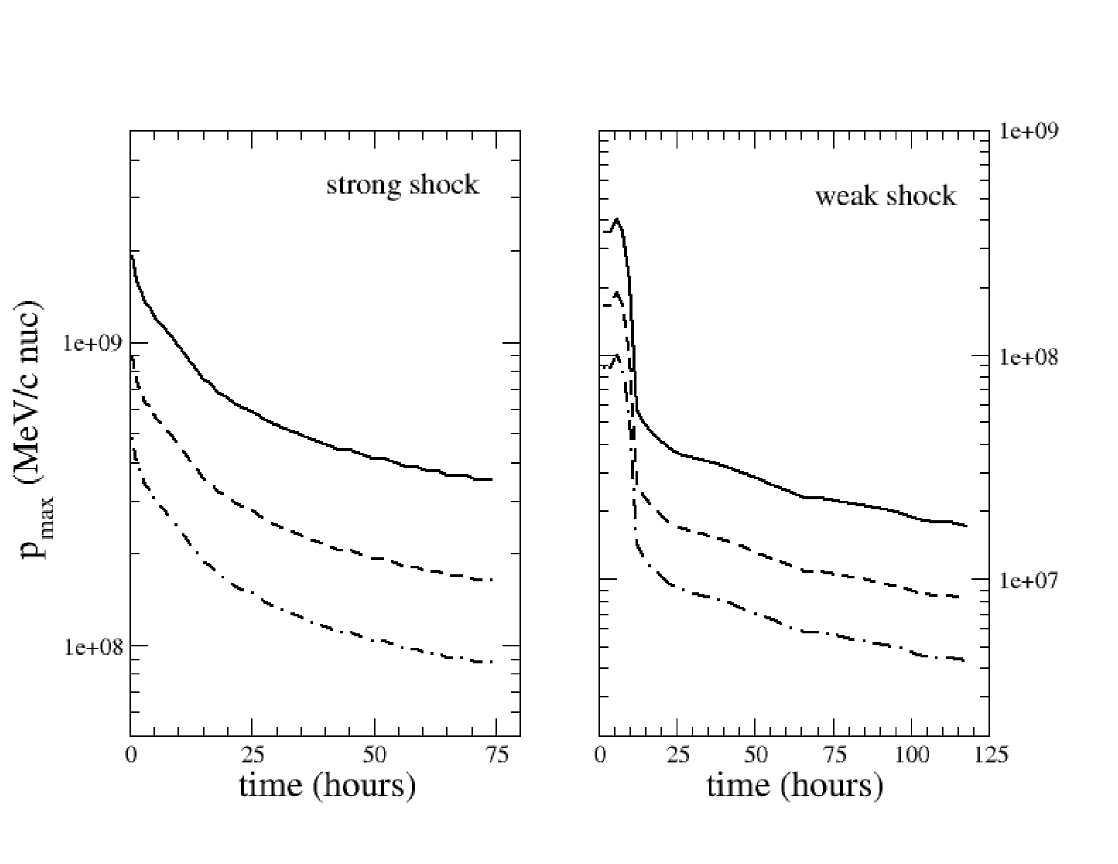

The maximum energy accelerated at the shock front. Particles having higher energies, which are accelerated at earlier times but previously trapped in the shock complex, will "see" a sudden change of κ. The maximum energy/nucleon for CNO is higher than iron since the former has a larger Q/A, thus a smaller κ.

Bohm approximation used throughout strong shock simulation but only initially in weak shock case.

Spectral evolution

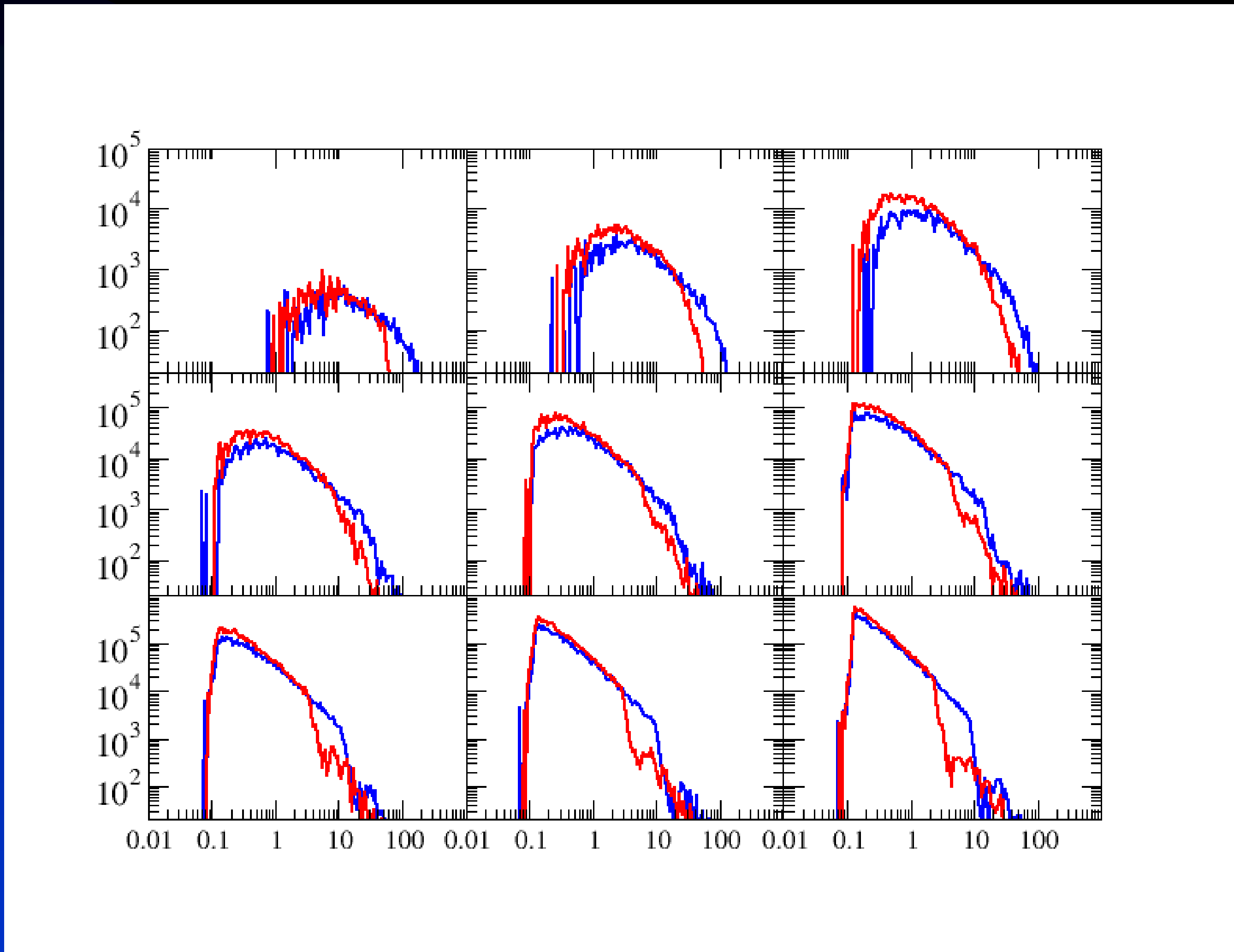

t = 0- 1/9 T,

t = 1/9-2/9 T,

…………

t = 9/10 – 1 T

Early time: more iron particles than CNO at low and mid energies, no clear power law. Both due to transport effect.

Late time: getting close to the shock, clear power low at low energies with break at high energy, signaling the current maximum attainable energy.

T = 50 hr

Event integrated spectra

Count only those particles before the shock arrival.

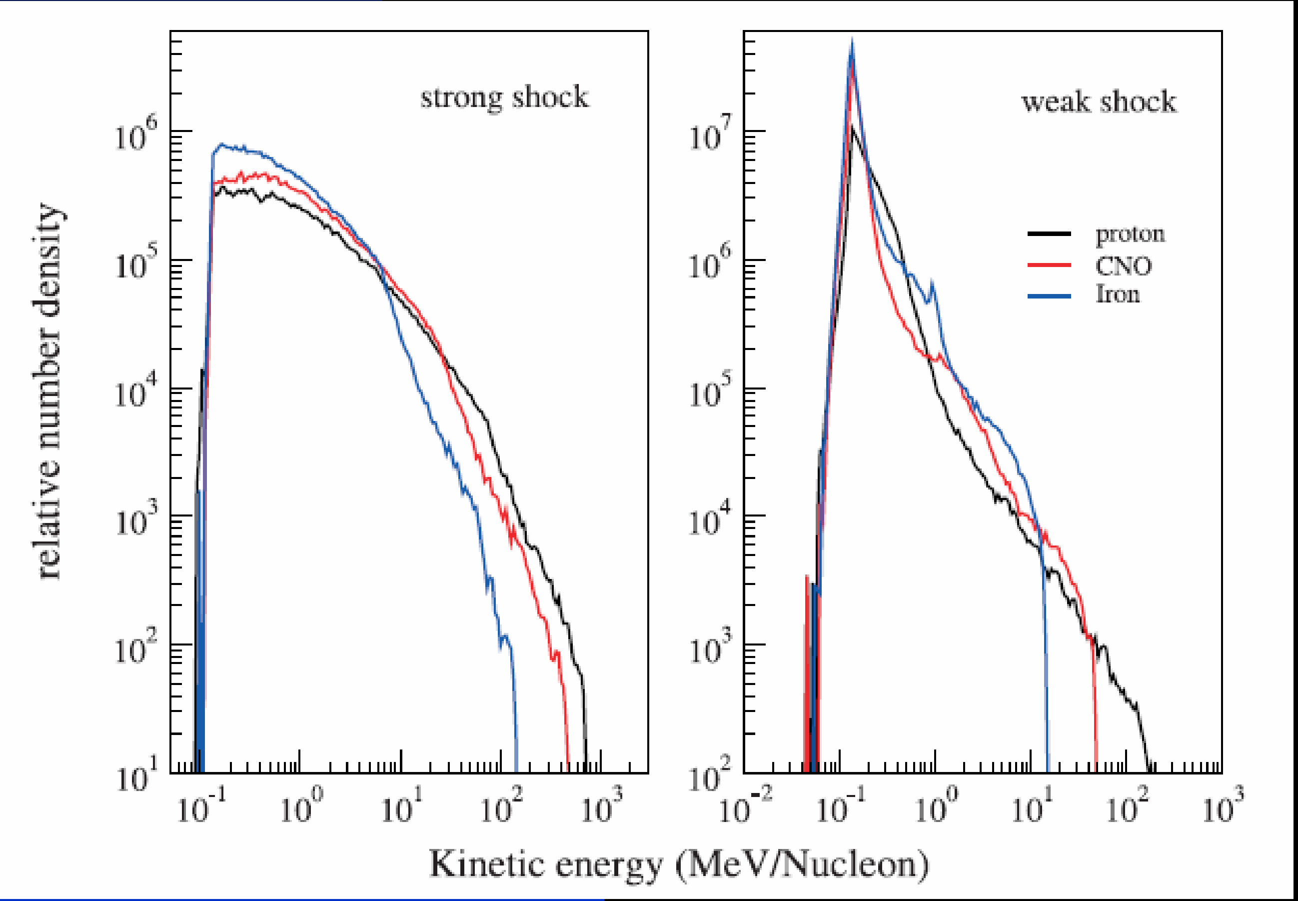

Iron Q = 14, A =56

CNO Q = 6. A = 14

Similar spectral indices at low energies, with Iron slightly softer.

Roll-over feature at high energy end with approximately $(Q/A)^2$ dependence.

Fe/O Ratio:

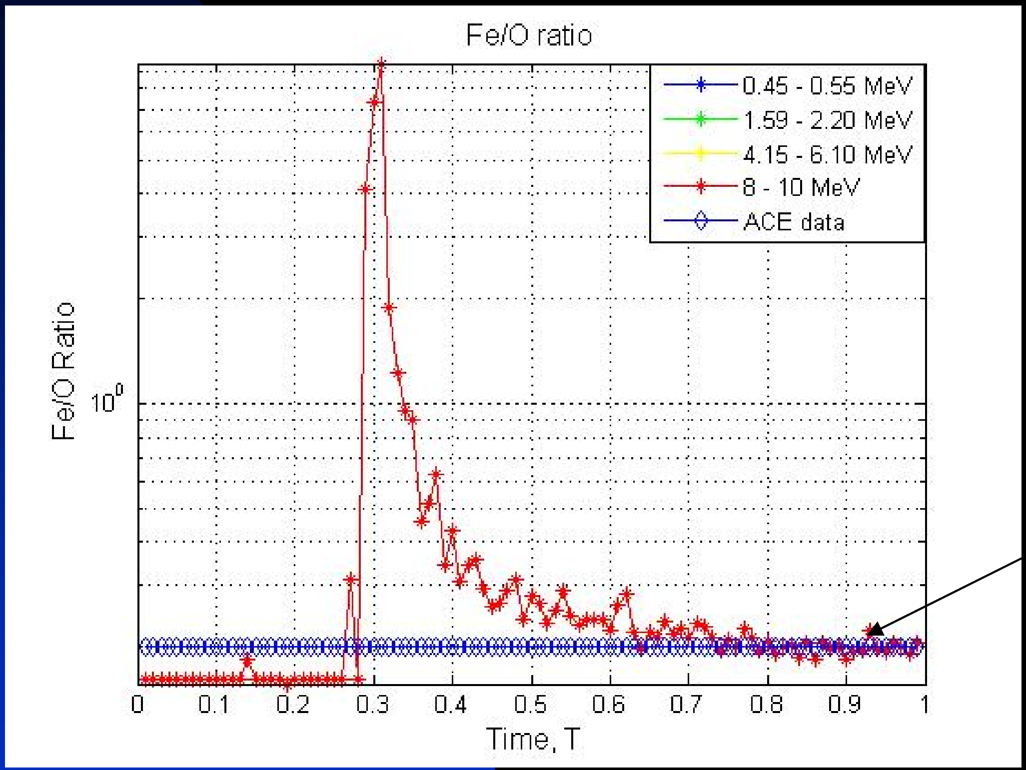

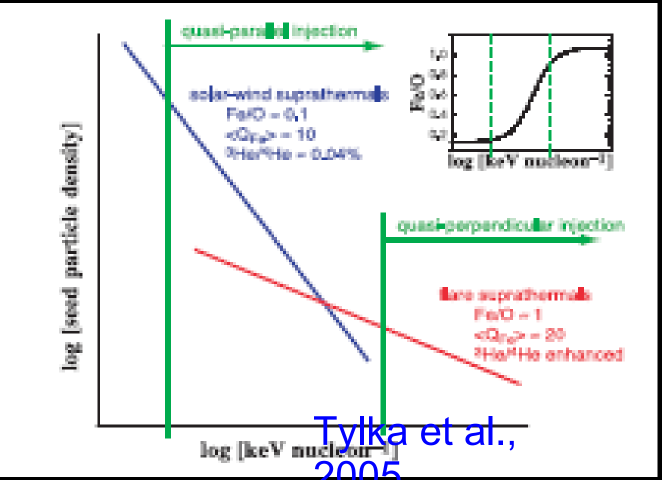

Tylka et al., 2005

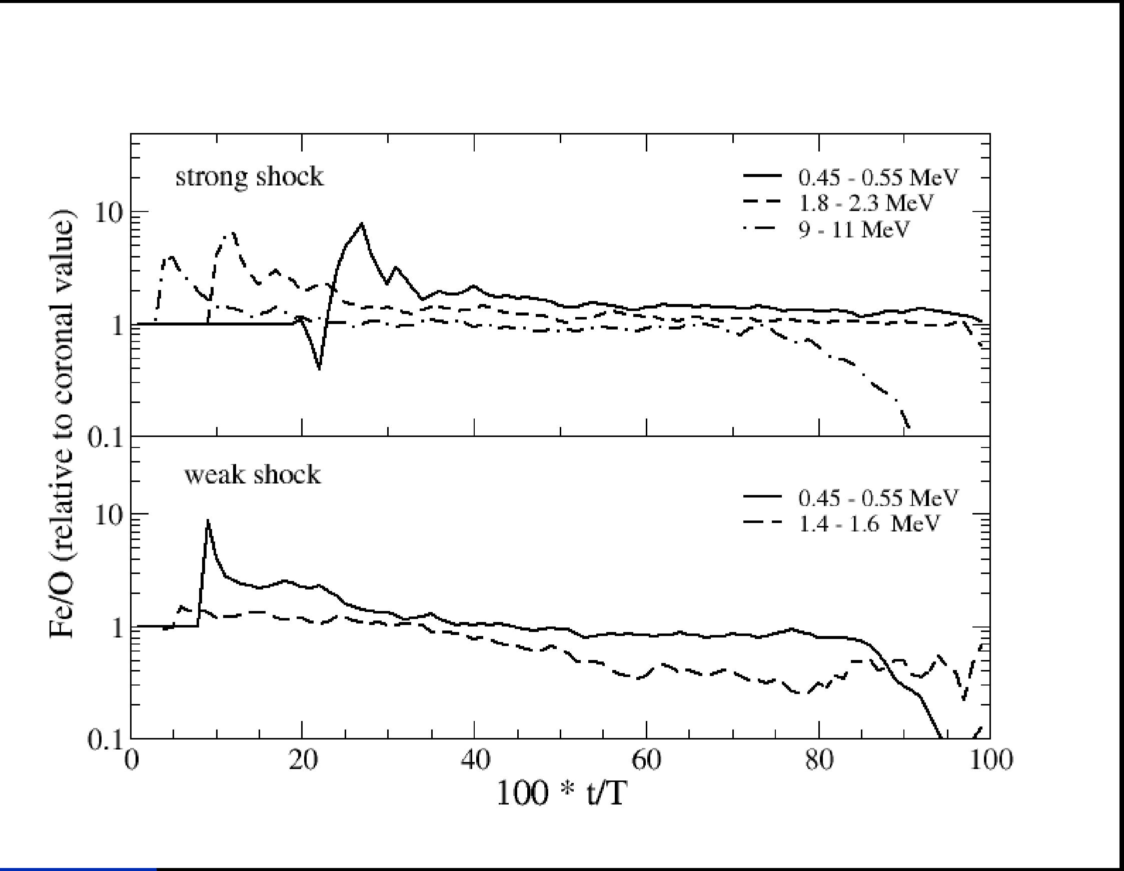

Fe to O ratio for two cases. Differences can be ascribed to propagation and trapping

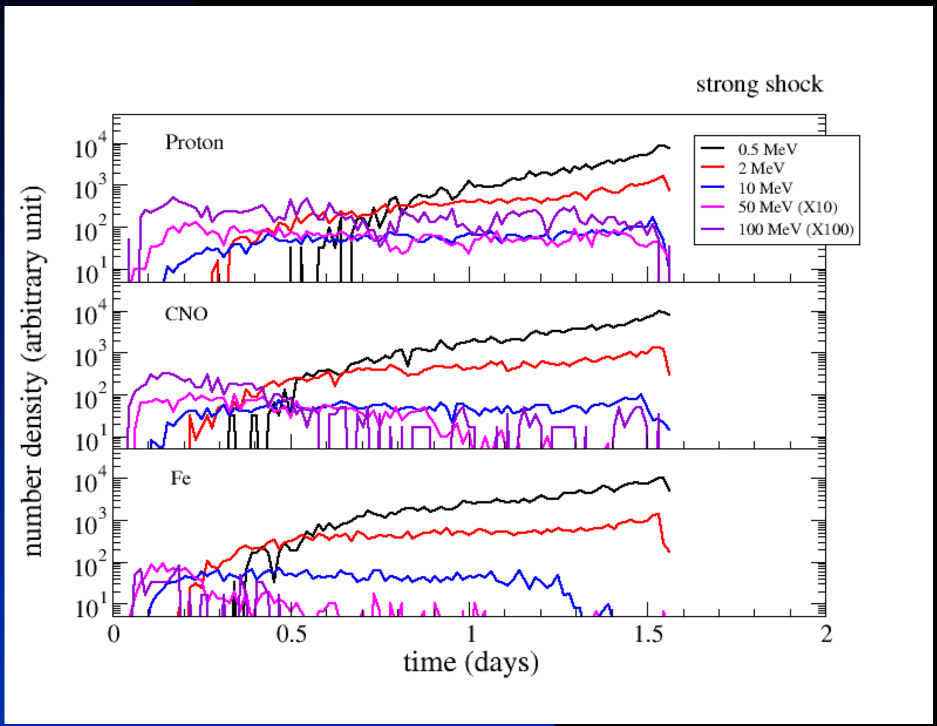

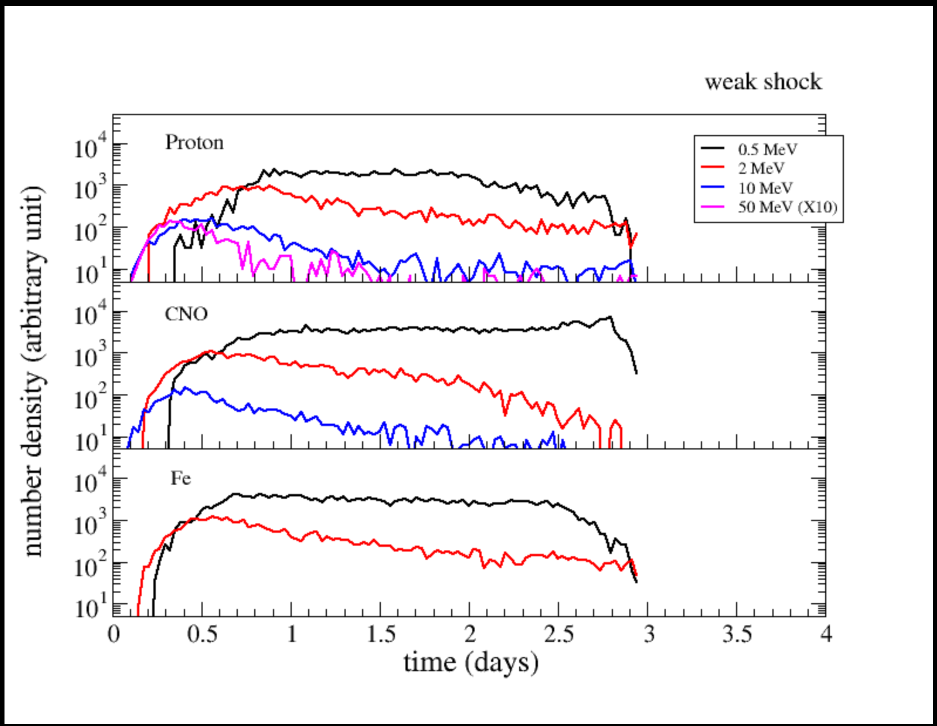

Intensity profiles for protons, CNO, and Fe for energy/nucleon.

Pre-existing or no pre-existing “injection” population – Cane et al., 2003

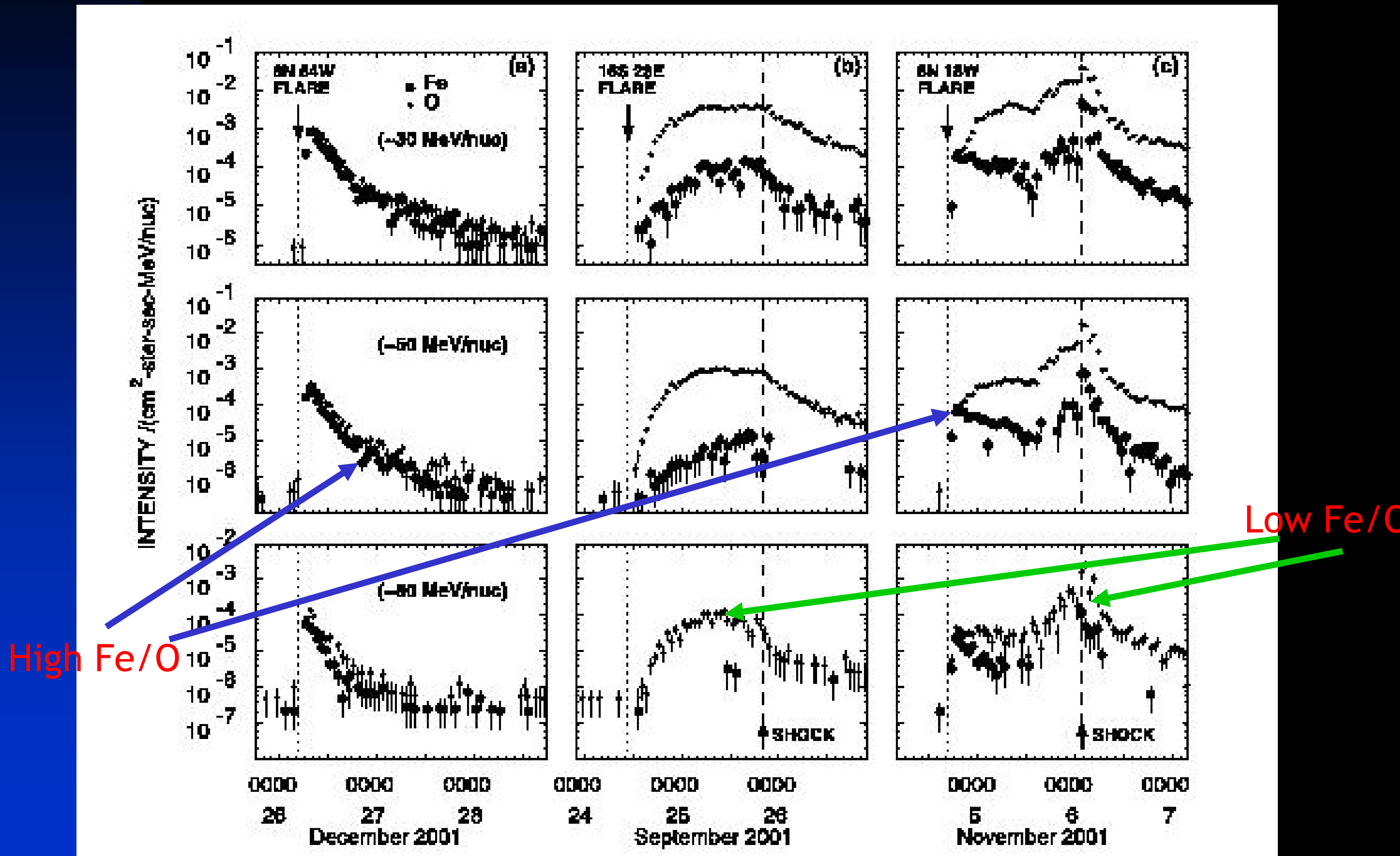

Modeling the 3 Cane possibilities

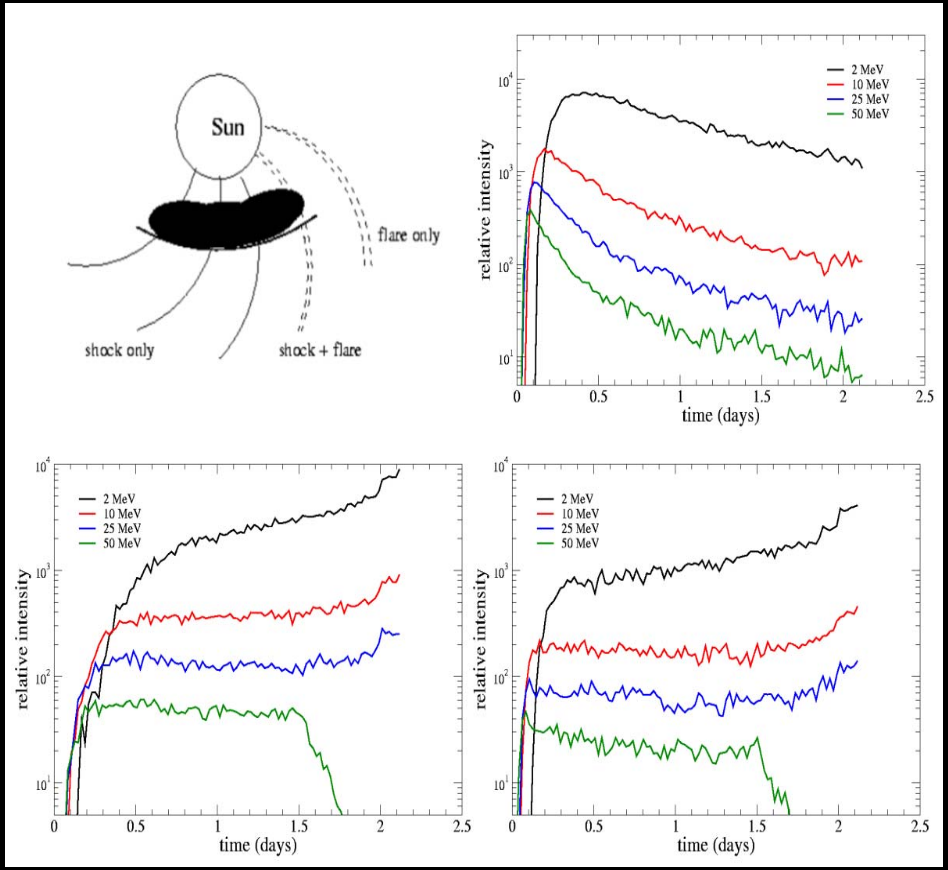

Verkhoglyadova et al. 2007 results

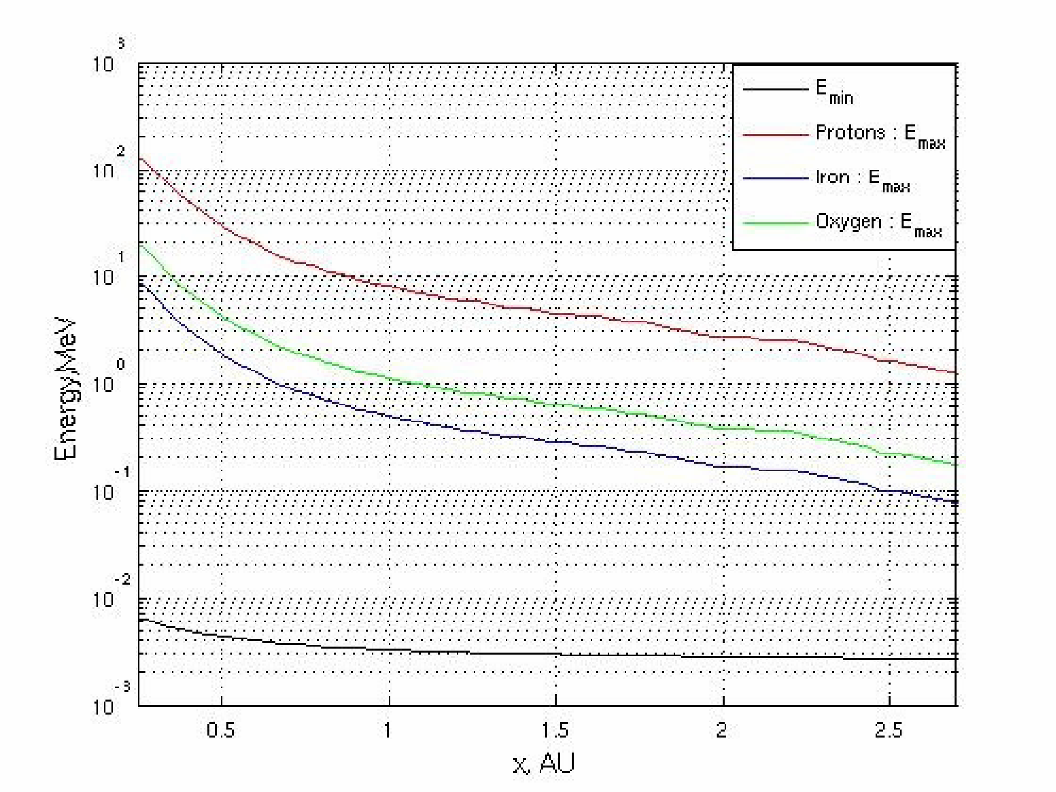

Dynamical evolution of the maximum energies for protons (red), oxygen (green) and iron (blue) ions as the quasi-parallel shock propagates from ~0.1 AU. The minimum energy (shown in black) is the same for all species.

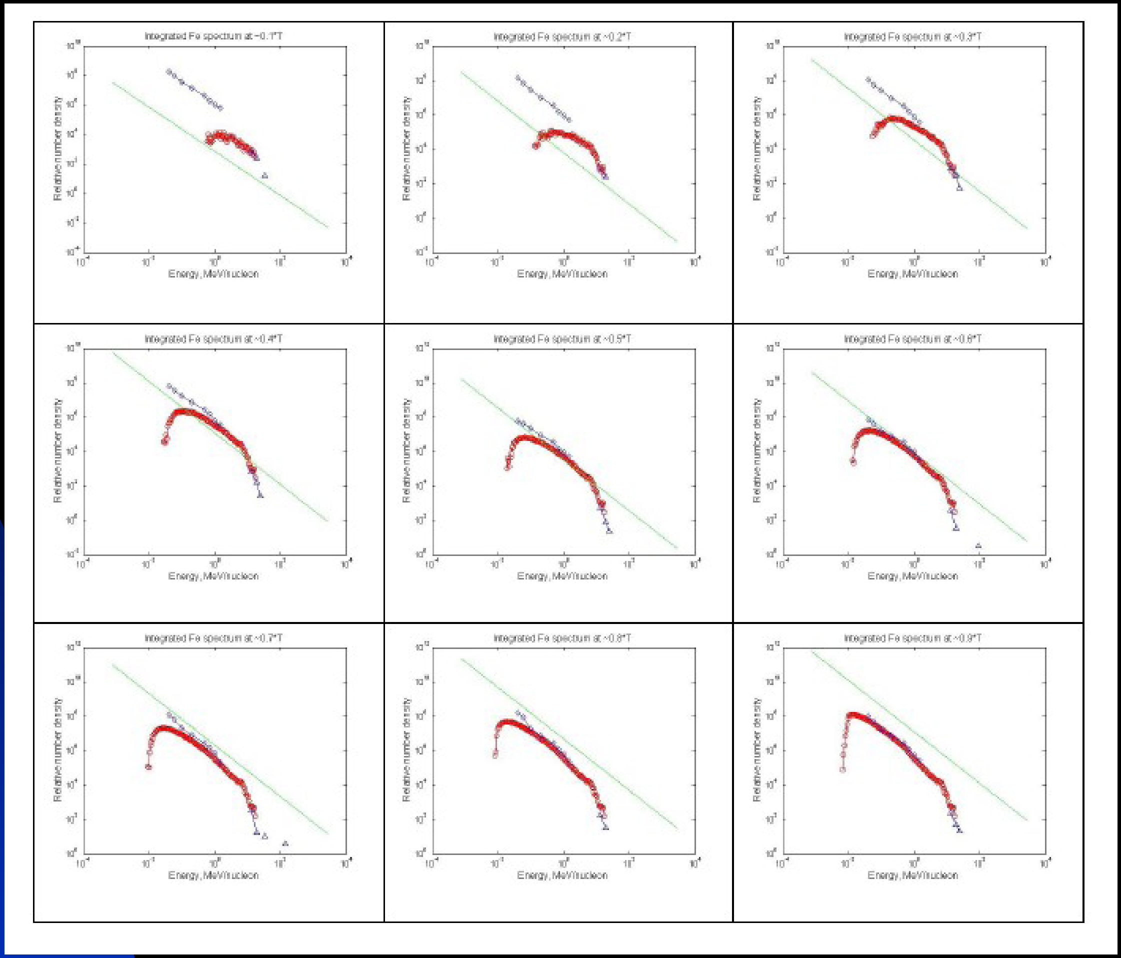

Dynamical spectra of iron ions averaged over consecutive ~5hrs time intervals until shock arrival at 1AU. ULEIS and SIS measurements are shown by blue diamonds and triangles, respectively. The straight line shows the theoretical limit for a power-law spectrum corresponding to shock parameters at 1 AU. Note the enhanced background at early times prior to the shock arrival at ~ 1AU.

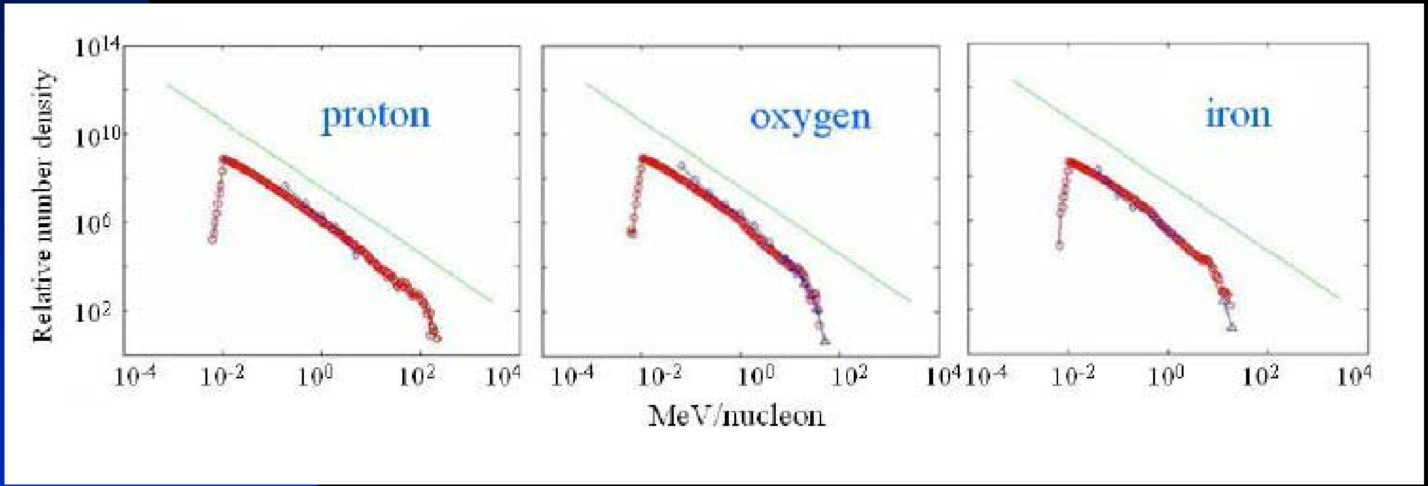

Event-integrated spectra for (a) protons, (b) oxygen and (c) iron ions.

Summary of modeling – quasi-parallel shocks

- A time-dependent model of shock wave propagation (1- and 2-D), local particle injection, Fermi acceleration at the shock, and non-diffusive transport in the IP medium has been developed to describe observed SEP events: This includes spectra, intensity profiles, anisotropies.
- We can similarly model heavy ion acceleration and transport in gradual events, even understanding differences in Fe / O ratios, for example.
- We have begun to model mixed events to explore the consequences of a pre-accelerated particle population (from flares, for example) and have also related this to the timing of flare – CME events.

Perpendicular shocks

Particle acceleration at perpendicular shocks

The problems: 1) High injection threshold necessary
2) No self-excited waves

$$\frac{\partial f}{\partial t}+u\frac{\partial f}{\partial r}-\frac{p}{3}\frac{\partial u}{\partial r}\frac{\partial f}{\partial r}=\frac{\partial}{\partial r}\left(\kappa\frac{\partial f}{\partial r}\right);\qquad \frac{\partial A}{\partial t}+u\frac{\partial A}{\partial r}=\Gamma A-\gamma A;$$

$$\kappa(p)=\frac{\kappa_0}{A(k)}\frac{B_0}{B}\frac{(p/p_0)^2}{\sqrt{(m_p c/p_0)^2+(p/p_0)^2}};\quad \kappa_0=\frac{4}{3\pi}r_{g0}c=\frac{4}{3\pi}\frac{p_0 c}{eB_0},$$

TRANSVERSE COMPLEXITY

Qin et al. [2002a,b] - perpendicular diffusion can occur only in the presence of a transverse complex magnetic field. Flux surfaces with high transverse complexity are characterized by the rapid separation of nearby magnetic field lines.

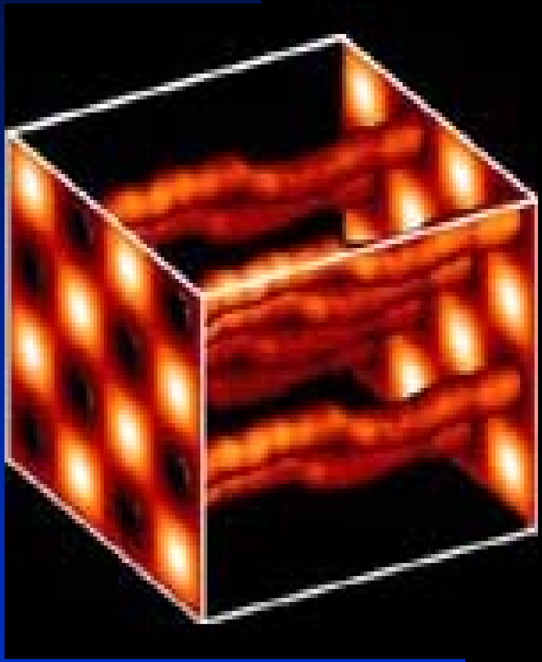

Slab turbulence only – no development of transversely complex magnetic field.

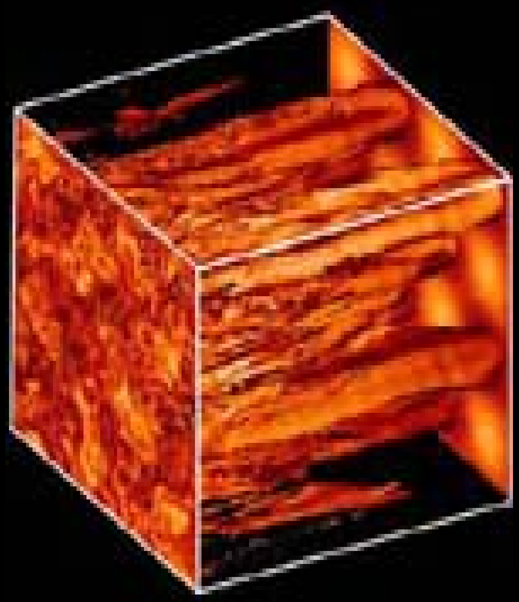

Superposition of 80% 2D and 20% slab turbulence, with the consequent development of a transversely complex magnetic field.

INTEGRAL FORM OF THE NONLINEAR GUIDING CENTER THEORY

Matthaeus, Qin, Bieber, Zank [2003] derived a nonlinear theory for the perpendicular diffusion coefficient, which corresponds to a solution of the integral equation

$$\kappa_{xx} = \frac{a^2 v^2}{3B_0^2} \int_0^{\infty} \frac{S_{xx}(\mathbf{k})\, d^3\mathbf{k}}{v/\lambda_{\parallel} + k_{\perp}^2 \kappa_{xx} + k_z^2 \kappa_{zz}}$$

Superposition model: 2D plus slab

$$S_{xx}(\mathbf{k}) = S_{xx}^{2D}\delta(k_{\perp})\delta(k_z) + S_{xx}^{slab}\delta(k_{\perp})$$

Solve the integral equation approximately (Zank, Li, Florinski, et al, 2004):

$$\lambda_{xx} \simeq \left(\sqrt{3}\pi a^2 C\right)^{2/3} \left(\frac{\left\langle b_{2D}^2 \right\rangle}{B_0^2}\right)^{2/3} \lambda_{2D}^{2/3} \lambda_{\parallel}^{1/3} \left[1 + \frac{\left(a^2 C\right)^{1/3}}{\left(\sqrt{3}\pi\right)^{2/3}} \frac{\left\langle b_{slab}^2 \right\rangle}{\left\langle b_{2D}^2 \right\rangle^{2/3} \left(B_0^2\right)^{1/3}} \frac{\min\left(\lambda_{slab}, \lambda_{\parallel}/\sqrt{3}\right)}{\lambda^{2/3}{}_{slab} \lambda_{\parallel}^{1/3}} \left(4.33 H\left(\lambda_{slab} - \lambda_{\parallel}/\sqrt{3}\right)\right) + 3.091 H\left(\lambda_{\parallel}/\sqrt{3} - \lambda_{slab}\right)\right]^{2/3}$$

$\lambda_{\parallel}$ modeled according to QLT.

WHAT ABOUT WAVE EXCITATION UPSTREAM?

Quasi-linear theory (Lee, 1983; Gordon et al, 1999): wave excitation proportional to cos ψ i.e.,

at a highly perpendicular shock.

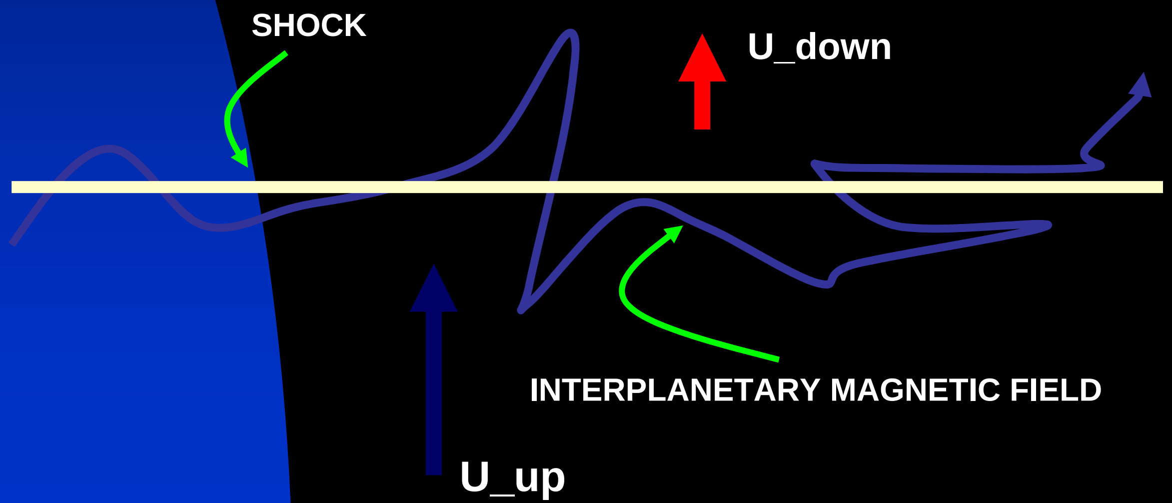

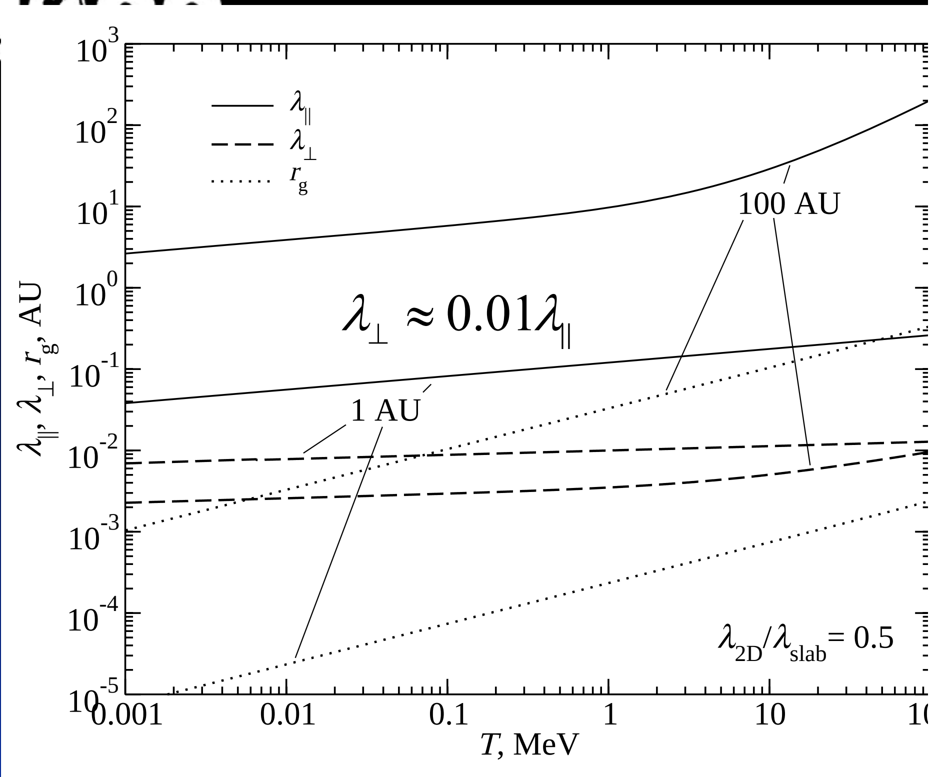

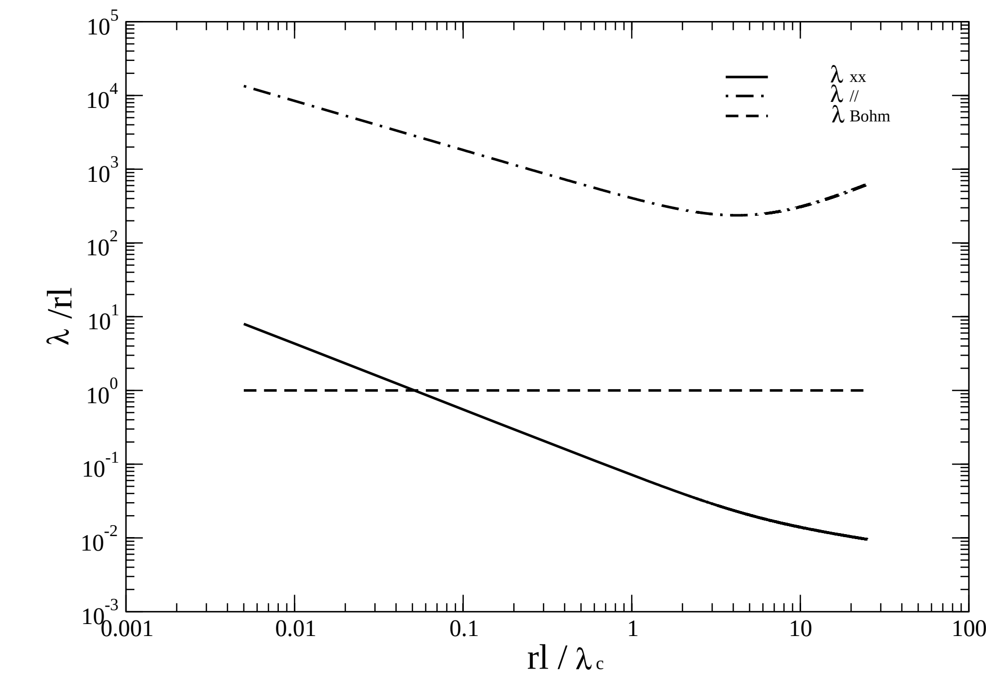

Left: Plot of the parallel (solid curve) and perpendicular mfp (dashed curve) and the particle gyroradius (dotted) as a function of energy for 100 AU (the termination shock) and 1 AU (an interplanetary shock).

Right: Different format - plots of the mean free paths at 1 AU as a function of particle gyroradius and now normalized to the correlation length. *The graphs are equivalent to the ratio of the diffusive acceleration time to the Bohm acceleration time, and each is normalized to gyroradius*. Solid line corresponds to normalized (to the Bohm acceleration time scale) perpendicular diffusive acceleration time scale, the dashed-dotted to parallel acceleration time scale, and the dashed to Bohm acceleration time scale (obviously 1).

ANISOTROPY AND THE INJECTION THRESHOLD

Diffusion tensor: $\kappa_{xx} = \kappa_{\perp} \sin^2 \theta_{bn} + \kappa_{\parallel} \cos^2 \theta_{bn}$

Since $\kappa_{\parallel} \gg \kappa_{\perp}$ the anisotropy is defined by

$$\xi = \frac{3u}{v}\left[\left(\frac{q}{3}-1\right)^2 + \frac{(\kappa_d^2 + \kappa_{\parallel}^2 \cos^2 \theta_{bn}) \sin^2 \theta_{bn}}{(\kappa_{\perp} \sin^2 \theta_{bn} + \kappa_{\parallel} \cos^2 \theta_{bn})^2}\right]^{1/2}$$

For a nearly perpendicular shock

$$\xi = \frac{3u}{v}\left[\frac{1}{(r-1)^2} + \frac{r_g^2 + \lambda_{\parallel}^2 \cos^2 \theta_{bn}}{(\lambda_{\perp} + \lambda_{\parallel} \cos^2 \theta_{bn})^2}\right]^{1/2}$$

DIFFUSION APPROXIMATION VALID IF

ANISOTROPY AND THE INJECTION THRESHOLD

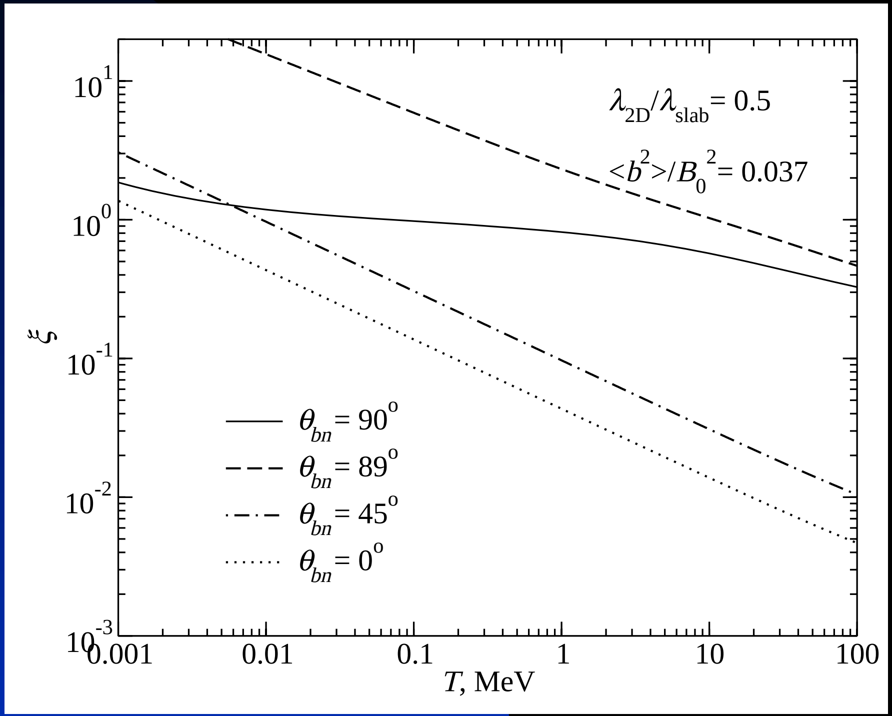

Anisotropy as a function of energy
(r = 3)

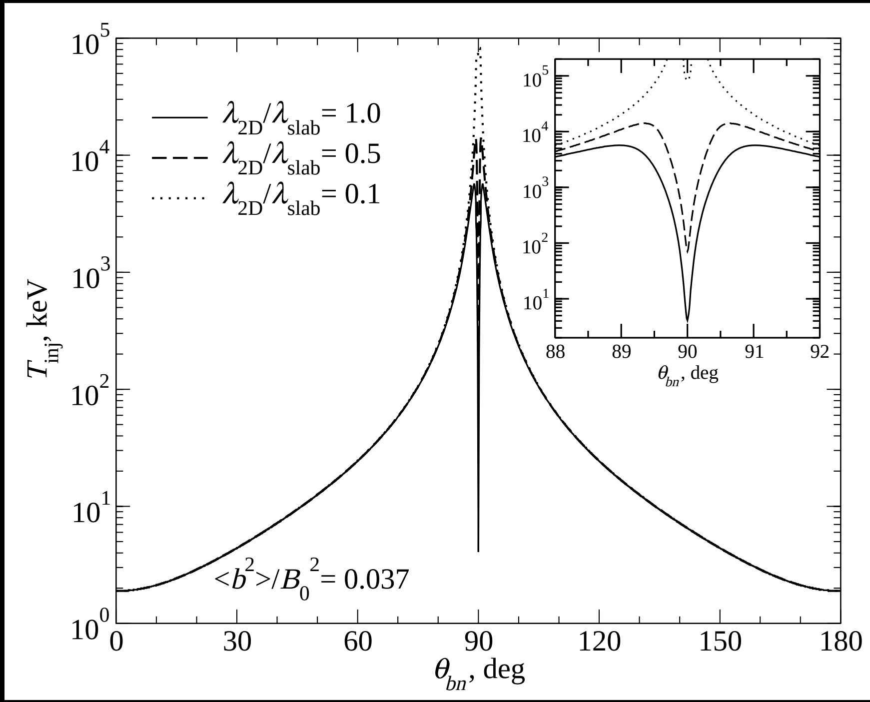

Injection threshold as a function of angle for

Remarks: 1)Anisotropy very sensitive to $\theta_{bn} \to 90^\circ$
2) Injection more efficient for quasi-parallel and strictly perpendicular shocks

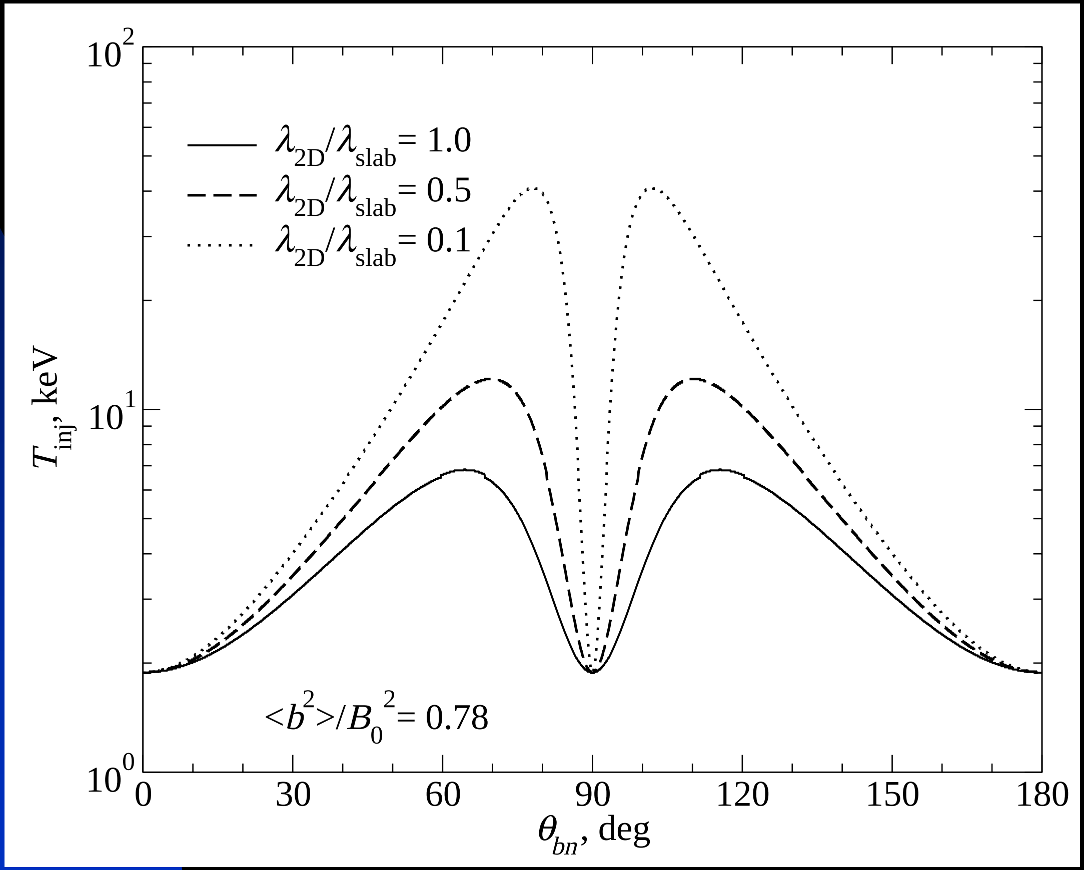
10^2
10^1
10^0
T_{inj}, keV
$\lambda_{2D}/\lambda_{slab} = 1.0$
$\lambda_{2D}/\lambda_{slab} = 0.5$
$\lambda_{2D}/\lambda_{slab} = 0.1$
$\langle b^2 \rangle / B_0^2 = 0.78$
0
30
60
90
120
150
180
θ_{bn}, deg

PARTICLE ACCELERATION AT PERPENDICULAR SHOCKS

- STEP 1: Evaluate K_perp at shock using NLGC theory instead of wave growth expression.

$$\kappa_{xx} \simeq \frac{v}{3}\left(\sqrt{3}\pi a^2 C\right)^{2/3}\left(\frac{\left\langle b_{2D}^2\right\rangle}{B_0^2}\right)^{2/3} \lambda_{2D}^{2/3}\lambda_{\parallel}^{1/3}$$

$$\times\left[1+\frac{\left(a^2C\right)^{1/3}}{\left(\sqrt{3}\pi\right)^{2/3}}\frac{\left\langle b_{slab}^2\right\rangle}{\left\langle b_{2D}^2\right\rangle^{2/3}\left(B_0^2\right)^{1/3}}\frac{\min\left(\lambda_{slab},\lambda_{\parallel}/\sqrt{3}\right)}{\lambda^{2/3}{}_{slab}\lambda_{\parallel}^{1/3}}\left(4.33H\left(\lambda_{slab}-\lambda_{\parallel}/\sqrt{3}\right)\right)+3.091H\left(\lambda_{\parallel}/\sqrt{3}-\lambda_{slab}\right)\right]^{2/3}$$

$$\left\langle b^2\right\rangle = \left\langle b_{slab}^2\right\rangle + \left\langle b_{2D}^2\right\rangle \quad 20\% : 80\%$$

$$\left\langle b^2\right\rangle \propto R^{-3}$$

Parallel mfp evaluated on basis of QLT (Zank et al. 1998.

PARTICLE ACCELERATION AT PERPENDICULAR SHOCKS

- STEP 2: Evaluate injection momentum p_min by requiring the particle anisotropy to be small.

$$v_{inj} \approx 3u\left[\frac{1}{(r-1)^2}+\frac{r_g^2+\lambda_\parallel^2\cos^2\theta_{bn}}{(\lambda_\perp+\lambda_\parallel\cos^2\theta_{bn})^2}\right]^{1/2}$$

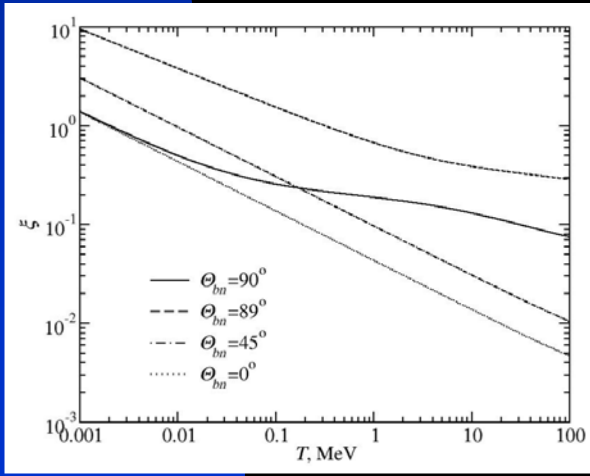

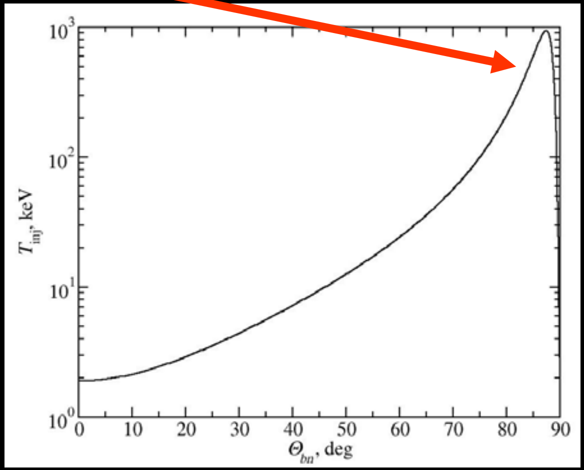

PARTICLE ACCELERATION AT PERPENDICULAR SHOCKS

- STEP 3: Determine maximum energy by equating dynamical timescale and acceleration timescale – complicated in NLGC framework. In inner heliosphere, particles resonate with inertial range (unlike outer heliosphere).

$$\frac{\dot{R}(t)}{R(t)} \approx \frac{q(t)}{u_1^{\,2}} \int_{p_{\text{inj}}}^{p_{\max}} \kappa(p')\, d(\ln(p'))$$

$$\frac{p_{\max}}{m_p} \approx \left(\frac{Q}{A}\right)^{1/4} \left(\frac{e}{m_p}\right)^{1/4} \left(\lambda_c^{slab}\right)^{-1/2} \left[0.148\, \frac{V_{sh}^2 (r-1)}{\alpha r} \frac{R}{\dot{R}}\right]^{1/4} \frac{\left\langle b_{slab}^2 \right\rangle^{3/4}}{B^{5/4}}$$

Remarks:

$$\frac{\left\langle b_{slab}^2 \right\rangle}{B^2} \sim R^{-1}$$

$$\frac{V_{sh}^2 R}{\dot{R}} \sim t^{2\beta-3}$$

$$\kappa_\perp \sim \alpha \kappa_\parallel^{1/3} \qquad \alpha = 0.1 - 0.001$$

Like quasi-parallel case, p_max decreases with increasing heliocentric distance.

Remarks re maximum energies

- Fundamental difference between the perpendicular and quasi-parallel expressions is that the former is derived from a quasi-linear theory based on pre-existing turbulence in the solar wind, whereas the latter results from solving the coupled wave energy and cosmic ray streaming equation explicitly, i.e., in the perpendicular case, the energy density in slab turbulence corresponds to that in the ambient solar wind whereas in the case of quasi-parallel shocks, it is determined instead by the self-consistent excitation of waves by the accelerated particles themselves.

- From another perspective, unlike the quasi-parallel case, the resonance condition does not enter into the evaluation of p_max. The diffusion coefficient is fundamentally different in each case, and hence the maximum attainable energy is different for a parallel or perpendicular shock.

- In the inner heliosphere where the mean magnetic field is strong, the maximum momentum decreases with increasing field strength, this reflecting the increased "tension" in the mean field.

Remarks re maximum energies – different shock configurations and ionic species

Three approaches have been identified for determining p_max [Zank et al 2000; Li et al 2003].

- 1. For protons accelerated at quasi-parallel shock, p_max determined solely on basis of balancing the particle acceleration time resulting from resonant scattering with the dynamical timescale of the shock. The wave/turbulence spectrum excited by the streaming energized protons extends in wave number as far as the available dynamical time allows.
- 2. For heavy ions at a quasi-parallel shock, the maximum energy is also computed on the basis of a resonance condition but only up to the minimum k excited by the energetic streaming ions, which control the development of the wave spectrum. Thus, maximum energies for heavy ions are controlled by the accelerated protons and their self-excited wave spectrum. This implies a $(Q/A)^2$ dependence of the maximum attainable particle energy for heavy ions.
- 3. For protons at a highly perpendicular shock, the maximum energy is independent of the resonance condition, depending only on the shock parameters and upstream turbulence levels. For heavy ions, this implies either a $(Q/A)^{1/2}$ or a $(Q/A)^{4/3}$ dependence of the maximum attainable particle energy, depending on the relationship of the maximum energy particle gyroradius compared to turbulence correlation length scale.
- It may be possible to extract observational signatures related to the mass – charge ratio that distinguish particle acceleration at quasi-parallel and highly perpendicular shocks.

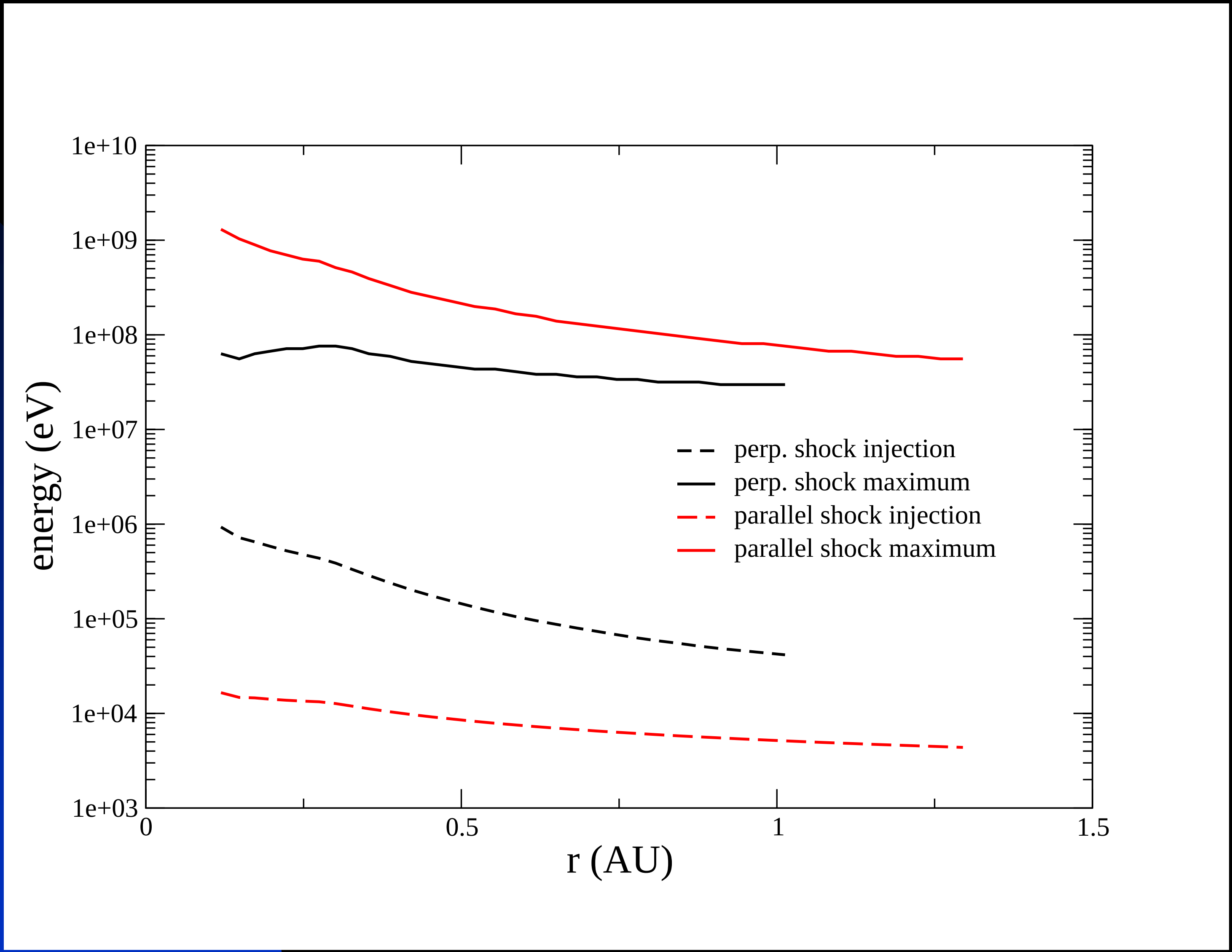

Remarks: 1) Parallel shock calculation assumes wave excitation implies maximum energies comparable

3) Injection energy at Q-perp shock much higher than at Q-par therefore expect signature difference in composition

Parallel and perpendicular diffusion
ts

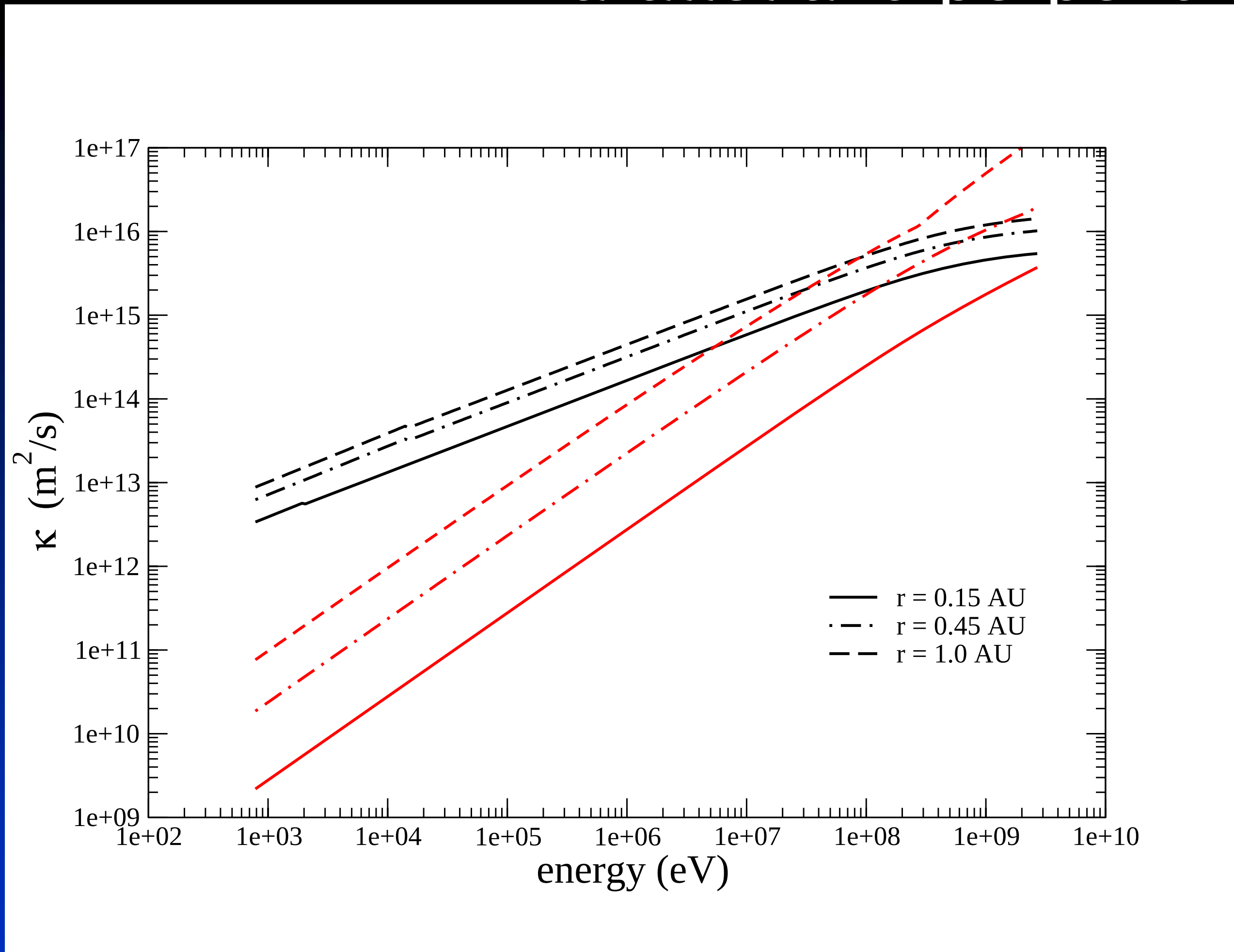

narks: 1) K_par includes
ves 2) The diffusion
fficients as a function of
etic energy at various
iocentric distances. The
lusion of wave self-excitation
kes K_parallel significantly
aller than K_perp at low
rgies, and comparable at
n energies.

Can utilize interplanetary shock acceleration models of Zank et al., 2000 and Li et al., 2003, 2005 for perpendicular shock acceleration to derive spectra, intensity profiles, etc.

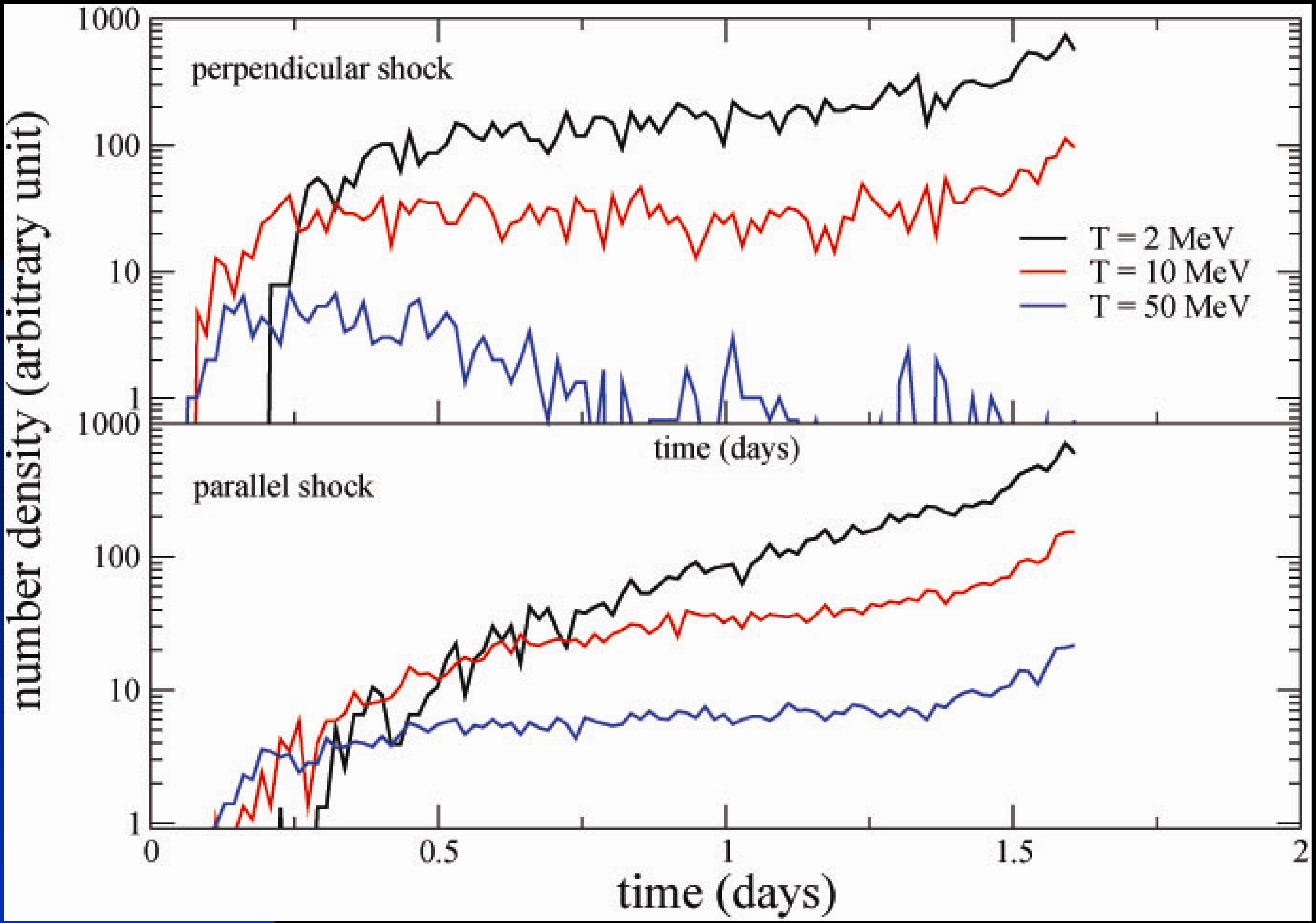

Intensity profiles emphasize important role of time dependent maximum energy to which protons are accelerated at a shock and the subsequent efficiency of trapping these particles in the vicinity of the shock. Compared to parallel shock case, particle intensity reaches plateau phase faster for a quasi-perpendicular shock – because K_perp at a highly perpendicular shock is larger than the stimulated K_par at a parallel shock, so particles (especially at low energies) find it easier to escape from the quasi-perpendicular shock than the parallel shock.

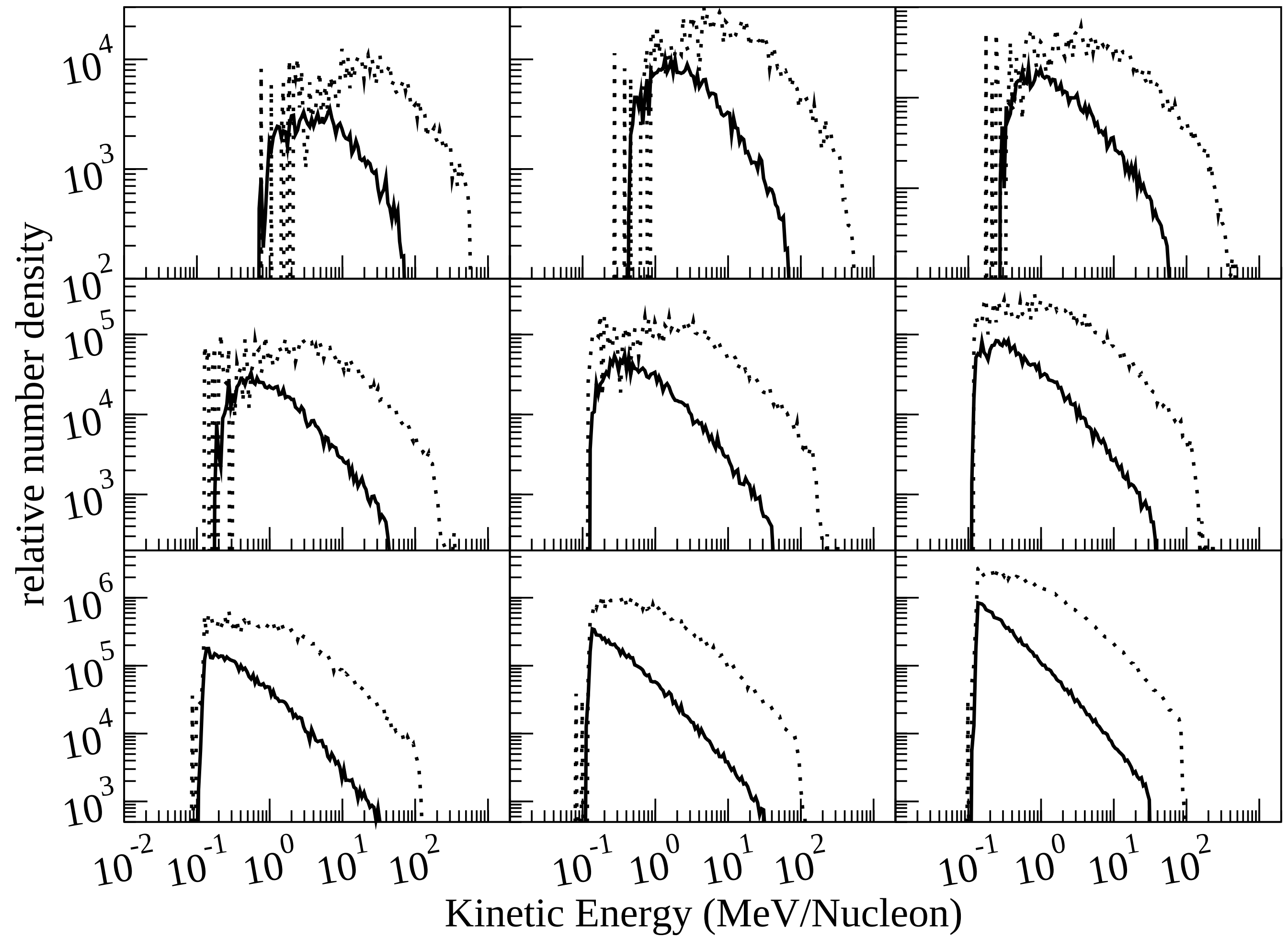

The time interval spectra for a **perpendicular (solid line) and a parallel shock (dotted line).** From left to right and top to bottom, the panels correspond to the time intervals t = (1 - {8/9})T, t = (1 - {7/9})T, … t = (1 -{1/9}) T, where T is the time taken for the shock to reach 1 AU. Note particularly the hardening of the spectrum with increasing time for the perpendicular shock example.

Observations

Perpendicular shock

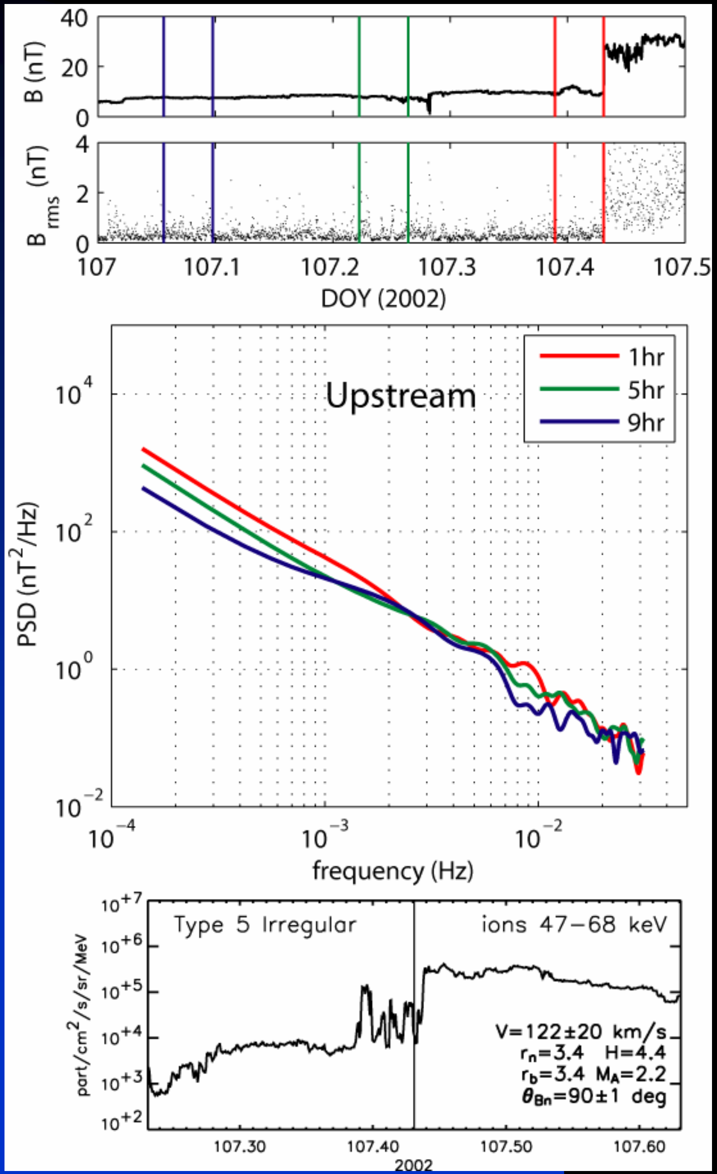

Quasi-perp shock

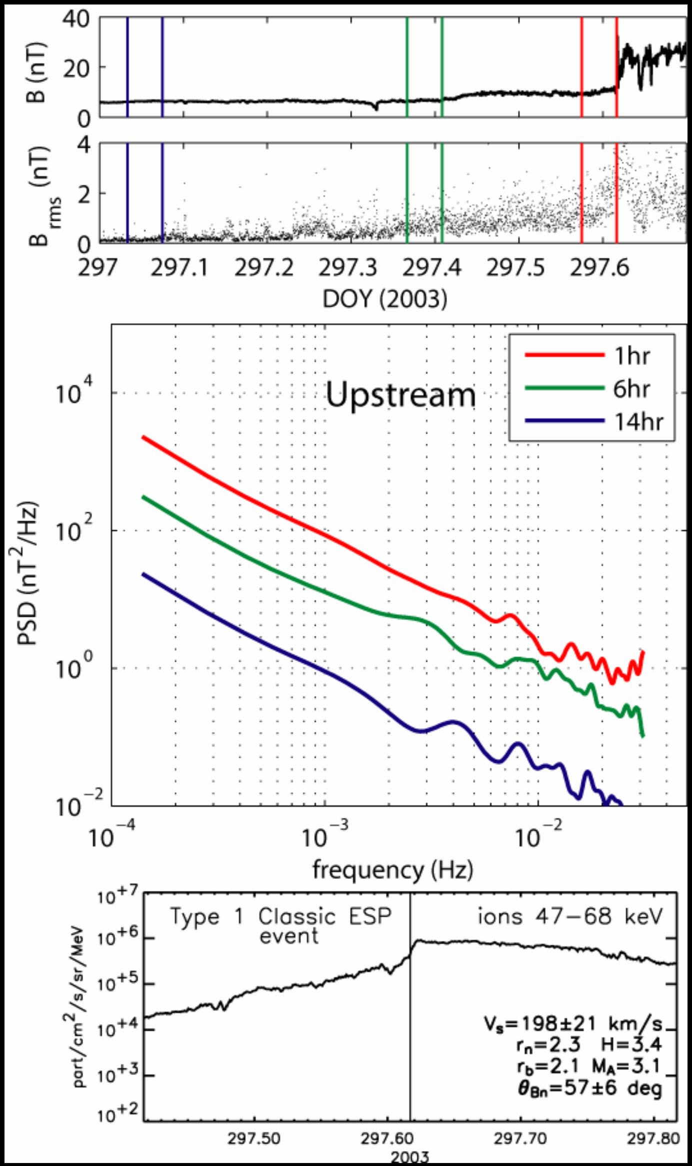

CONCLUDING REMARKS FOR PERPENDICULAR SHOCKS

- Developed basic theory for particle acceleration at highly perpendicular shocks based on convection of in situ solar wind turbulence into shock.
- Highest injection energies needed for quasi-perp shocks and not for pure perpendicular shock. 90 degree shock “singular” example.
- Determination of K_perp based on Nonlinear Guiding Center Theory
- Maximum energies at quasi-perp shocks less than at quasi-par shocks near sun. Further from sun, reverse is true.
- Injection energy threshold much higher for quasi-perp shocks than for quasi-parallel shocks and therefore can expect distinctive compositional signatures for two cases.
- Observations support notion of particle acceleration at shocks in absence of stimulated wave activity.

Summary of quasi-parallel modeling

- A time-dependent model of shock wave propagation (1- and 2-D), local particle injection, Fermi acceleration at the shock, and non-diffusive transport in the IP medium does remarkably well in describing observed SEP events: This includes spectra, intensity profiles, anisotropies.
- We can similarly model heavy ion acceleration and transport in gradual events, even understanding differences in Fe / O ratios, for example.
- We have begun to model mixed events to explore the consequences of a pre-accelerated particle population (from flares, for example) and have also related this to the timing of flare – CME events.